ADDIS ABABA UNIVERSITY
ADDIS ABABA INSTITUTE OF TECHNOLOGY
SCHOOL OF MECHANICAL AND INDUSTRIAL ENGINEERING

PERFORMANCE ANALYSIS OF CENTRIFUGAL PUMP OPERATING AS TURBINE FOR IDENTIFIED MICRO/PICO HYDRO SITE OF ETHIOPIA

By

Bazin Tsegaye

A Thesis Submitted to the School of Graduate Studies of
Addis Ababa University
In Partial Fulfillment of the Requirement for the Degree of
Masters of Science in Mechanical Engineering
(With Specialization in Thermal and Energy Conversion stream)

Advisor: **Dr. -Ing. Edessa Dribssa**

Co - Advisor: **Ato Tilahun Nigussie (PhD Candidate)**

June, 2015

ADDIS ABABA UNIVERSITY

INSITITUTE OF TECHNOLOGY

SCHOOL OF MECHANICAL AND INDUSTRIAL ENGINEERING

"PERFORMANCE ANALYSIS OF CENTRIFUGAL PUMP OPERATING AS TURBINE FOR IDENTIFIED MICRO/PICO HYDRO SITE OF ETHIOPIA"

By

Bazin Tsegaye

Approved by Board of Examiners	Date	Signature
Dr. Daniel Tilahun Dean of School	_____	_____
Dr.-Ing Edessa Dribssa Advisor	_____	_____
Ato Tilahun Nigussie Co-Advisor	_____	_____
Dr. -Ing Demiss Alemu Internal Examiner	_____	_____
Dr. Tesfaye Dama External Examiner	_____	_____

Declaration

I hereby declare that the work which is presented in this thesis entitled "**Performance Analysis of Centrifugal Pump Operating as Turbine for Identified Micro/Pico Hydro Site in Ethiopia**" is original work of my own, has not been presented for a degree in any other university and that all sources of material used for the thesis have been duly acknowledged.

Bazin Tsegaye — Date

This is to certify that the above declaration made by the author is correct to the best of my knowledge.

Dr.-Ing Edessa Dribssa — Date

(Thesis Advisor)

Ato Tilahun Nigussie — Date

(Thesis Co-Advisor)

Acknowledgement

First and for most I would like to thank almighty God for giving me the courage and strength to complete my work successfully. After that i would like to give my deepest appreciation to my advisor Dr. - Ing. Edessa Dribssa for his continuous guidance from the very beginning of selecting the title up to final thesis write-up. And I would also like to thank Ato Tilahun Nigussie, who guided and supported me by providing helpful research papers, journals, and ideas throughout the thesis work. And this research work would not have been possible without the valuable assistance of Deutsche Gesellschaft für Internationale Zusammenarbeit (GIZ) GmbH Energy Coordination Office (ECO), who provided me flow rate and head data of micro/pico hydro sites.

I would also like to thank specially Ato Kamil and Ato Sema Baye for giving me information about pumps and other important data's. Last but not list I also want to thank department of Mechanical Engineering, Addis Ababa University for providing me industrial visitation letters.

Abstract

In many countries, the supply of electricity in rural areas has always been challenge due to the relative isolation from the national electricity grid. The single most important solution to overcome this problem is through the development of the Micro/Pico hydro power generation. By using a Pump as Turbine (PAT) on particular Micro/Pico hydro sites, the required electricity demand can be more or less fulfilled.

This thesis presents performance analysis of PAT for Dabis Hydro site which is located in West Shewa zone. The numerical study of a centrifugal pump running as turbine at different operation conditions was achieved using commercial CFD software Ansys CFX. 3D Navier–Stokes equations were solved using Ansys CFX. The standard $k-\varepsilon$ turbulence model was chosen for turbulence model. Using results from simulation, complete characteristic curves of the pump in normal and reverse modes were obtained. After that, the performance of PAT was estimated using various methods proposed by different researchers. The pump mode simulated results was in good agreement with the performance of centrifugal pump evaluated experimentally. The turbine mode performance of the pump was simulated and results showed that when the PAT is made to operate from low to high head condition, the required flow rate at the site increases. And the simulation result of the PAT at best efficiency point (BEP) was compared with results obtained using published empirical formulas and the prediction method proposed by **Stephanoff [15]** showed acceptable result.

In this thesis, the pump was also simulated in reverse modes to evaluate the effect of impeller tip rounding. The result shows that the efficiency of the pump is greatly improved beyond the BEP when the impeller tips is made round. The effects of PAT speed were also studied considering constant flow rate/head conditions and the results indicate that as the impeller speed increase, impeller torque decreases. Whereas as the rotational speed of the PAT increases, the power output as well as the efficiency of the PAT increases till the impeller speed reaches 1400 RPM. Lastly, the effect of draft tube on PAT was simulated and studied. The results show that the PAT head increase when draft tube is added to the system. The result also shows that the system efficiency of the PAT with draft tube drops down due to the increase in head.

Nomenclature

U	Absolute velocity, m/s
V	Control volume
C	Conversion factor
Δn_j	Discrete outward surface vector
n_s	Dimensionless specific speed
Q	Flow rate, m^3/s
g	Gravity, m/s^2
H	Head, m
P_{hy}	Hydraulic power/water power, Kw
D	Impeller diameter, m
R	Local radius vector, m
m	Mass flow rate, kg/s
S_m	Momentum source
P_{in}	Power input, Kw
P_b	Power output/Brake power, Kw
N	Rotational speed, RPM
N_s	Specific speed, (for turbine $kg^{1/2}/ m^{1/4}s^{5/2}$ and for pump $m^{3/4} / s^{3/2}$)
P	Static pressure, pa
t	Time, sec
Δt	Time step
T	Torque, Nm
TP	Total pressure, Pa
P_k	Turbulent kinetic energy due to the mean velocity gradients,
k	Turbulence kinetic energy m^2/s^2

Greek Letters

ω	Angular velocity, rad/s
ρ	Density, kg/m^3
η	Efficiency
Φ	Flow coefficient
∇	Grad
Ψ	Head coefficient
δ	Kronecker Delta function
Π	Power coefficient
ϖ	Rotational speed, rps
τ	Stress tensor
σ_k and σ_ε	Turbulence Prandtl numbers
ε	Turbulence eddy dissipation, m^2/s^3
μ	Viscosity, kg/m.s

Subscript

eff	Effective
Q	Flow rate
H	Head
ip	Integration point
max	Maximum
min	Minimum
n	Nominal
p	Pump
rel	Relative frame of reference
stn	Stationary frame of reference
s	Specific
t	Turbine
t	Turbulence

Superscript

o	old time level

Abbreviations

BEP	Best Efficiency Point
CFD	Computational Fluid Dynamics
EEPCo	Ethiopian Electricity and Power Corporation
EECMY	Ethiopian Evangelical Church Mekane Yesus
GIZ ECO	Gesellschaft für Internationale Zusammenarbeit Energy Coordination Office
GUI	Graphics User Interface
ICS	Interconnected System
MHP	Micro Hydro Power
PHP	Pico Hydro Power
PAT	Pump as Turbine
REF	Rural Electrification Fund

Table of Contents

List of Table

List of Figures

CHAPTER ONE

Introduction

1.1. Background of the Study

Water power can be utilized to provide sufficient amount of electricity. Depending on the end user energy demand, water can be used to produce electricity in small or large scale. Micro/Pico-hydro power is the small-scale extraction of energy from falling water from a local river to power a small village in rural areas using turbine. Micro and Pico hydro power generation has particularly become a major focus of Ethiopian electricity sector for off-grid rural electrification in order to improve sustainable energy [3]. Even if initial capital cost is relatively high, micro/pico-hydro power projects are the appropriate options for generating electricity since the running cost of such plants is low[18].

The energy of the water can be extracted by means of turbine. Hydraulic turbines convert kinetic and potential energies of the water into mechanical power. The main types of turbines are broadly classified in to impulse and reaction turbines. Pelton wheels are categorized under impulse turbine. A reaction turbine is usually well suited for low heads. Francis, Kaplan, Bulb and Darize turbine are common example of this type of turbine [5].

Centrifugal pumps are used to raise liquids from a lower to a higher level by creating the required pressure with the help of centrifugal action. But when the direction of flow is reversed, they can be made to operate in a turbine mode. The use of centrifugal pump as turbine for electricity power generation was inspired by several researchers [7, 9-14]. The problem aroused from the use of high cost convention turbine for micro-hydro projects can be successful solved by utilizing Pump as Turbine (PAT) as a solution [18].

In this research, centrifugal pump operating in turbine mode are simulated by taking commercial available pump using Ansys CFX and the data obtained from the performance simulation are also evaluated.

1.2. Problem Statement

The use of pump by flowing water in the reverse direction to operate as a turbine is alternative for power generation in micro hydro system. But selection of a proper pump as turbine (PAT) for a site has been major problem in installation of pump in micro and pico hydro systems since the characteristics curves of the pumps operating as turbine is not provided by the manufacturers.

Since pumps are relatively simple and easily available machines in all developed and developing countries, they can be made to operate in reverse direction as turbines and be useful to produce cheap energy in rural zones. In addition to that, they can provide a suitable energy source in areas having small water resources and that are not currently supplied by conventional means.

But this challenge in the use of Pump as a Turbine (PAT) is not only the case for Ethiopia, but also for all other countries that have growing demand for energy to sustain life. It could be a convenient choice, but a deep study of the machine in a given operating conditions is necessary in order to encourage the use.

Various concepts have been developed over the years to provide the basis for determining the performance characteristics of pump as a turbine [7, 9-12]. Experimental investigation of centrifugal pump has been carried out to study its characteristics in pump and turbine mode operation. But it would be costly and time consuming to set up the experiment to check all pump manufactured and designed by different manufactures. Several researchers presented some relations for predicting the performance of Pump as Turbine (PAT).In order to calculate the machine operating characteristics, a one-dimensional method were purposed but doesn’t indicate the 3D complex flow behavior associated to the PAT.

The Computational Fluid Dynamics (CFD) technique, using 3D flow simulation, could be a valid tool to overcome this lack in order to provide basic information to understand the interaction between the hydro- mechanical equipment and the flow field.

In order to accommodate the main challenge stated above, the effects of reverse operation of the centrifugal pump are considered in this research. And the potential of the pump behaving as the turbine will be investigate by computational fluid dynamics (CFD) technique. Not only analysis, recommending on the best alternative is also to be conducted.

1.3. Objectives of the Research

The general objectives of this research is

- To determine the performance characteristics of centrifugal pump operating in turbine mode using CFD.

The specific objectives of this research are, therefore,

- To select a centrifugal pump that can be used as a turbine for Dabis hydro site to generate power.
- To investigate how the pump performs as turbine when it operates at different flow rate conditions using CFD.
- To predict the performance of pump in turbine mode using published empirical formulas and compare the results with CFD simulation result.
- To study the effect of speed on Pump as Turbine (PAT) performance
- To evaluate the effect of blade tip rounding on performance of PAT
- To study the effect of draft tube on PAT performance

1.4. Significance of the Research

Ethiopia has several rivers that carry huge amount of water including many micro/pico hydro sites capable of producing electrical power .This research is one way of assessing a means to reduce the use of non-renewable sources of energy by making use of this water bodies. Availability of pump at less cost, short duration of installation and maintenance characteristics of pumps makes them attractive and encouraging for the user to use them as turbine.

Regarding to the research, the use pumps operating as turbines being an alternative technical and environmental available solution to produce energy, can be identified. Moreover, conducting this study will help in guarantying and supplying continues decentralized electrification to residential sectors of rural areas in Ethiopia using of pumps as turbine in micro hydro sites. It is also important to reduce the time and cost required to investigate the performance of the PAT system through conducting experimental setup.

1.5. Research Methodologies

Several techniques have been used to achieve the objectives of this research. The methods employed are:

1. **Literature review:**

A review of literature on the area Pump as Turbine system available on different case studies, journals, books and previous research works are surveyed in order to have a clear understanding of the subject matter.

2. **Data Collection**

The necessary data for the research is collected from different sources. The necessary data is:-

- For identified micro/pico hydro potential site based on secondary source relevant data like head and flow rate for the analysis is taken.

3. **Tools and Techniques**

Different commercially available softwares like CFturbo is used to model impeller and volute casing, and Catia is used to model draft tube. Ansys ICEM is used to generate mesh on draft tube, casing and impeller fluid volume. Ansys CFX is used to simulate the flow around the whole pump when it is used as a turbine.

4. **Analysis and Evaluation**

By making use of the CFD tools, performance of the PAT at the different values of flow rate are assessed in detail and then evaluated to identify operation characteristics.

5. Result and Discussion

Different graphical display results like contour, vector and streamline were used to discuss the flow behavior through the PAT fluid volume. And by using the numerical result, the performance PAT is predicted considering the original and other models.

6. Conclusion and Recommendation

By using the result obtained from the CFD analysis, the results of the solution is discussed in detail. After the necessary justification, conclusion and recommendation is done based on the result.

1.6. Thesis Outline

This thesis work is comprised of 5 different chapters that are categorized in the order of specific topics. **Chapter 2** provides important concepts related to micro/pico power generation and PAT. It presents a brief reviews on the theory of micro/pico hydropower, hydraulic behavior and characteristics of centrifugal PAT along with related previous work on this machine. It also includes the different basic governing equations, numerical discretization and solution method used in the commercial CFD code Ansys CFX to analyze the PAT. **Chapter 3** deals with the procedure used for modeling and simulating of centrifugal pump when it operates in reverse mode. Creation of geometry and meshing of different components of the PAT is included in this chapter. The next **chapter 4** deals with the simulation results of pump models operating in direct and reverse mode. This chapter also includes the study of the effect of impeller tip geometry and impeller rotational speed. And the effect of draft tube and different published prediction method used to estimate the performance of PAT are presented in this chapter. In the final **chapter 5**, conclusion was drawn according the results and recommendation was given regarding the overall thesis work.

CHAPTER TWO

Literature Review

This chapter provides an overview of micro/pico power generation potential of Ethiopia. Turbines being the major components in micro/pico power generation, the concept underlying on the theory of hydraulic behavior and characteristics of centrifugal pumps when used as turbine for power generation along with related previous work on this machine are reviewed. Lastly, the basic governing equations, numerical discretization and solution method used in the commercial CFD code Ansys CFX to analyze the PAT are discussed.

2.1. Hydropower in Ethiopia

Ethiopia has an estimated installable hydro power potential up to 45,000 MW which make it second highest in Africa in hydropower potential. Out of the 45000 MW potential, approximately 30,000 MW are estimated to be economically feasible which is equivalent to an electricity generation of 162 TWh [3]. Not more than 750 MW has been utilized so far thus leaving more than 98% of the potential unused [2]. Almost all of the power stations operating at present are big plants and meant to feed the national grid. The development of mini- and micro-hydro power, which is more suited to rural electrification, is not practiced yet. At present, there are only about ten small-scale hydroelectric plants (0.25-1MW capacity) in the entire country. The average annual potential (exploitable with small slope plants without reservoir) is estimated to be about 20 TWh/year.

Since Ethiopia uses a classification of hydropower systems which differs from other countries, the Ethiopian definitions as shown in Table 2.1 are used throughout this paper.

Table 2.1: Hydro power classification in Ethiopia [3]

Terminology	Capacity Limits (Mw)
Large	>30
Medium	10-30
Small	1-10
Mini	0.5-1
Micro	0.11- 0.5
Pico	≤ 0.01

The current production of 3.98 TWh thus equals an exploitation of only 2.5%. In general, Ethiopia's land is advantageous for hydropower projects. A vast potential is not just given for large hydropower projects but also for small scale schemes, particularly in remote areas, which are not connected to the national grid.

2.1.1. Micro Hydropower

The Ethiopian definition of hydropower schemes differ from the ones of other countries. A Micro hydropower (MHP) scheme is defined from a range between 11 – 500 kW (Table 2.1).

According to **K.Meder** [3], the specific yield of Ethiopian highlands with a moisture surplus of at least 300 mm/a is 500 W/km² (see Figure 2-1). Since the maximum of MHP schemes is defined with 500 kW, the largest catchment area for MHP development is thus 1,000 km². Subtracting the catchments >1,000 km² from the total of 315,000 km² with perennial flows and a respective moisture surplus, that leaves a land area of 200,000 km² suitable for MHP development. Thus the theoretical MHP potential becomes 100 MW.

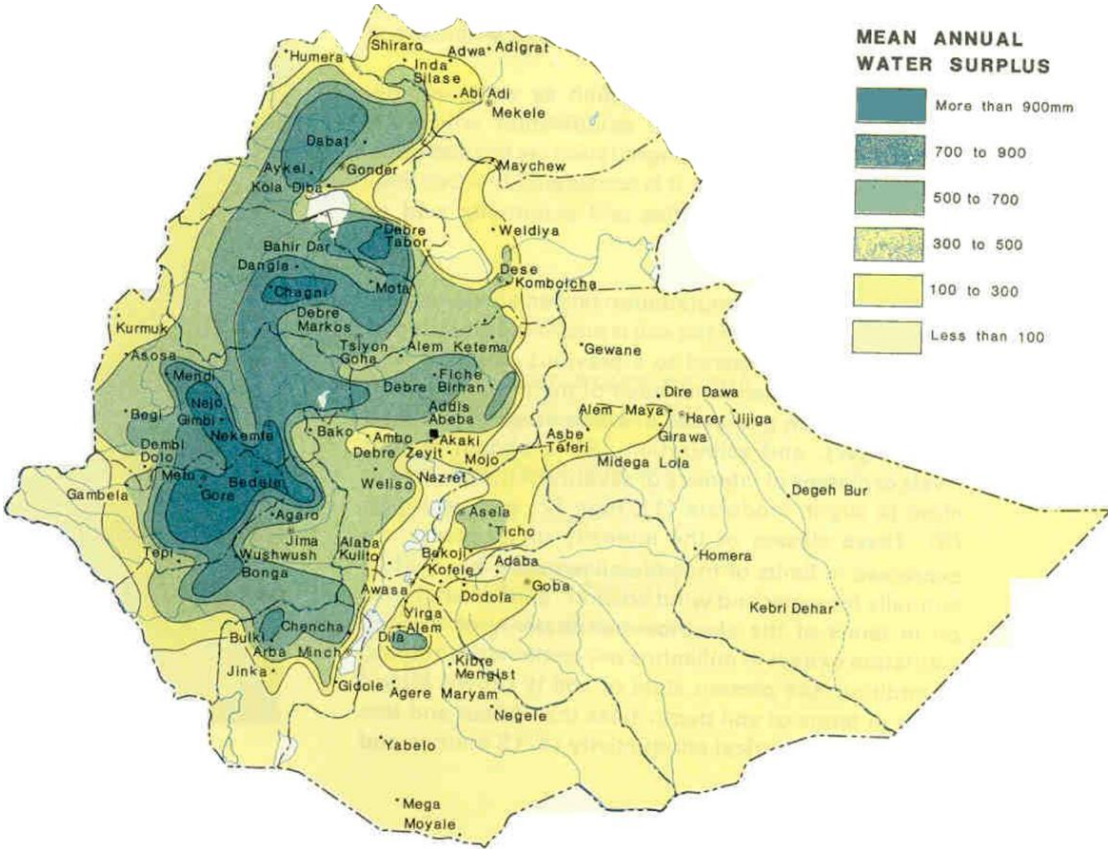

Figure 2-1: Mean annual water surplus Ethiopia [3]

Most promising sites can be found in the western part of the country, since suitable topographic conditions and constant flows are found most commonly. Several MHP schemes were installed with a total capacity of 1.5 MW. But all of them are not operational anymore: once the areas were connected to ICS (interconnected system), the MHP plants were shut down .However, some of the plants are still in good condition and it would be technically feasible to give maintenance services to make them operational again [3].

The Yaye MHP off grid plant, having 170kW capacity, was commissioned in 2002 by the Irish development Aid and the Sidama Development program already suffered from low river flow during the 2002/03 dry season. After only having operated for two years, EEPCo connected Yaye to its (ICS) and the MHP plant was shut down completely .Nevertheless 35 – 40% of those plants are not operational anymore due to a lack of water during dry season and management as well as technical problems. Ethiopian Evangelical Church Mekane Yesus (EECMY) and Rural Electrification Fund (REF) are planning the installation of further MHP plants such as 55 kw scheme on the Bege River and a 5.5 kw scheme in Sire .GIZ ECO Ethiopia has also identified several hydro sites that have the capacity to produce power for off grid application. But no feasibility studies have been carried out. It is also currently implementing four pilot MHP sites in the Sidama Zone/SNNPR with a capacity of 7 kw, 30 kw, 33 kw and 55 kw respectively [3].

2.1.2. Pico Hydropower

Typically **Pico hydropower (PHP)** plants are characterized by having a capacity up to 10 kW (Table 2.1). They are mainly used in remote location when there's an absence of a distribution grid and to supply energy to one or two households. Since the limited amount of production of electricity from the plant, two households with one injera cooker each fully absorb the plant's capacity [3].

2.2. Hydraulic Turbine

In micro/pico hydro system, power is produced through the interaction of water and turbine. In a power house, the mechanical power obtained from turbine is used to drive a generator so that electricity can be produced and supplied to a local village for domestic lighting or other uses.

In a hydraulic turbine, water is used as the source of energy. As the water flows continuous through the turbine, it expands to a lower pressure which causes the turbine to produce mechanical power. Thus water turbines convert kinetic and potential energies of the water into mechanical power. The main types of turbines are categorized into impulse and reaction turbine [5].

- **Impulse Turbines**

Impulse turbine uses a jet under atmospheric pressure that strikes on only one or two vanes at a time in which the pressure is the same for the entering and exiting flows .In impulse rotor, the water, under a high station head, has its pressure energy converted into kinetic energy in a nozzle. Therefore, work done by the fluid on the rotor is due to a change in kinetic energy, which represents an impulse function. Impulse turbines, such as Pelton and Turgo are used in high and medium head plants, whereas the cross-flow turbine covers from low to medium head ranges [5].

- **Reaction Turbines**

In reaction turbine, water from the reservoir enters the turbine casing through penstocks. Work done by the fluid, under elevated head, on the rotor is due to reaction from the pressure drop. In contrast to the impulse turbine, where a jet under atmospheric pressure strikes on only one or two vanes at a time, flow in a reaction turbine is under pressure and reacts on all vanes of the impeller turbine simultaneously. The reaction turbine is further subdivided into Francis, Kaplan, Propeller and Pump as Turbine (PAT) [5].

2.2.1. Pump As Turbine

The use of pump to transfer fluid from lower pressure to higher pressure in industrial and other areas has been applicable for several decades [5].Recently; however the use of pump-as-turbine (PAT) systems has become popular. In such a system a pump is operated in reverse so that it functions as a turbine.

According to **Chapallaz [6],** PATs are practically applicable in the areas of power generation. Pump-turbines have been used for several decades with power ratings of several megawatts. Standard pumps are now more and more used in MHP/PHP schemes (5 to 500 kW). For pumped storage scheme, pump-turbines are specifically used to operate in both modes; pumping water into an elevated storage lake overnight at low tariff electricity and during the day, generating peak demand electricity through the same machine operating in turbine mode.

The application of PAT for power generation requires the use of either a synchronous generator or induction generator (motor as generator) coupled directly to the rotating shaft of the PAT. For this reason, a nominal speed corresponding to one of the synchronous speeds of the generator (e.g. 750, 1000, 1500 or 3000 rpm) should be chosen [6].

The appropriate operating range of a reversible pump-turbine depends on the available head and flow rate on a hydro site. **Chapallaz [6]** presented a selection chart based on more than 80 test results of pump working in turbine mode. Figure 2-2 shows the range of head and flow rate for various types of PAT. From the Figure, it can be observed that centrifugal pumps can be used in turbine mode for head range 10 - 150 m and up to 0.5 m^3/s flow rate.

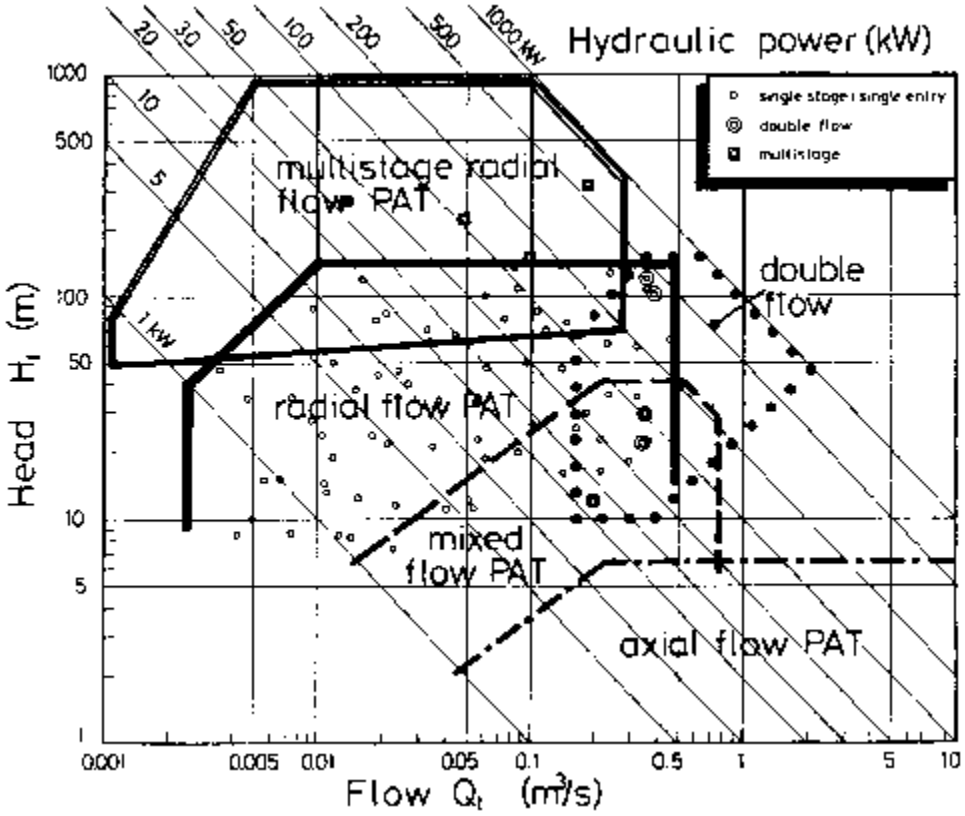

Figure 2-2: General range of application of different PAT types [6]

2.2.2. Flow Zone in Centrifugal PAT

A centrifugal pump consists of two major components. These components are used to impart kinetic energy on the fluid and change this energy in to pressure energy. The rotating part responsible for imparting kinetic energy to the fluid is called impeller. The other component used for converting the kinetic energy to pressure is called volute. Figure 2-3 shows how fluid flow through a centrifugal pump.

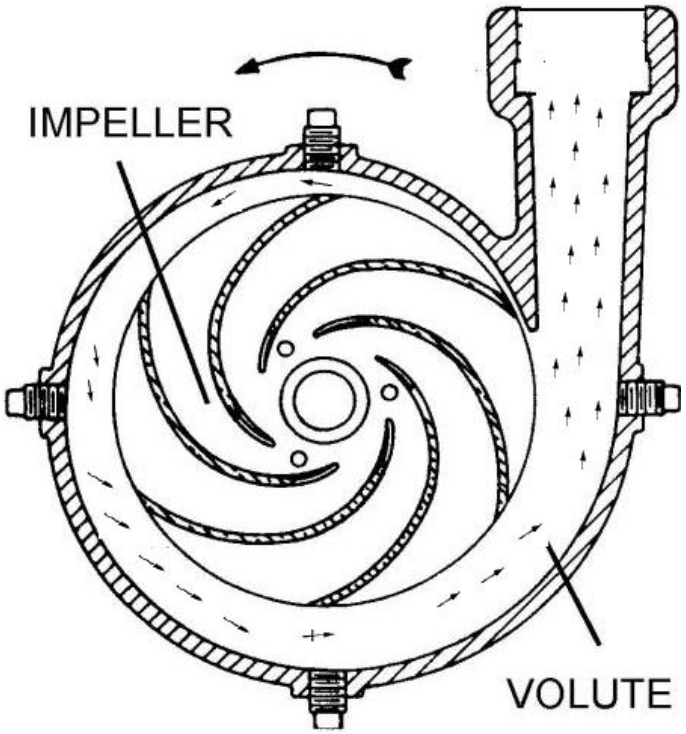

Figure 2-3: Flow through centrifugal pump in normal operation

When the direction of flow is reversed, the centrifugal pump operates in different manner. Like any other turbine, the basic principle behind the flow through the PAT is a complex 3D flow and is comprised of several zones.

Figure 2-4 indicates the flow of fluid through a pump when the flow direction is reversed. First the fluid flows from the enclosure provided in the inlet plane (outlet in pump mode) till the tongue cross-section (known as throat) and it flows throughout the semi-enclosed spiral path of the volute that ends back at the tongue (I).

Then it leads it way from the casing mouth and extends in radial direction in the outer impeller interface (impeller inlet in turbine mode) (II). After that it goes through the zone between the stationary volute and rotating impeller through which the main flow region of the impeller consisting of the flow passage within the blades is defined (III & IV). Ending the flow through impeller eye of the pump (V), the fluid will enter the draft tube where it exposes itself to atmospheric conditions. The draft tube constitutes of straight sections, bends and diffuser

sections. The mechanical shaft power obtained from the rotating pump impeller can be used to drive an electricity generator or induction motor to produce electrical energy [7].

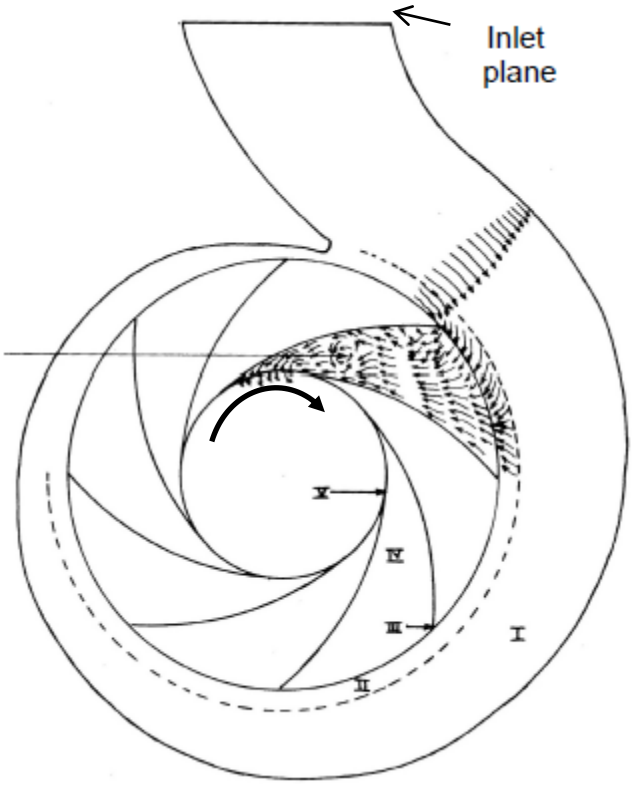

Figure 2-4: Fluid zone in PAT control volume [7]

2.2.3. Characteristics of PAT in Pump and Turbine Mode

The performance of a pump or a turbine is usually presented in head versus flow diagrams. Pump and turbine mode performance can be plotted in a single diagram by extending the flow axis (Q) into negative values representing the reverse operation of the pump, viz. the turbine mode performance. These diagrams are usually referred to as complete or total characteristics of a machine [6]. Figure 2-5 shows basic characteristic curves for a pump operating in pump and turbine mode.

With reference to Figure 2-5, the head is inversely proportional to the flow rate for pump mode (right side) while in turbine mode (left side), the head increase as the flow rate increases. The figure also indicates that in both pump and turbine mode, increasing the flow rate will increase efficiency until the flow rate reaches certain value at which the efficiency becomes maximum.

The flow rate at that point is called nominal flow rate and the efficiency is called Best Efficiency Point (BEP). Further increasing beyond the nominal flow rate will result in efficiency decrement.

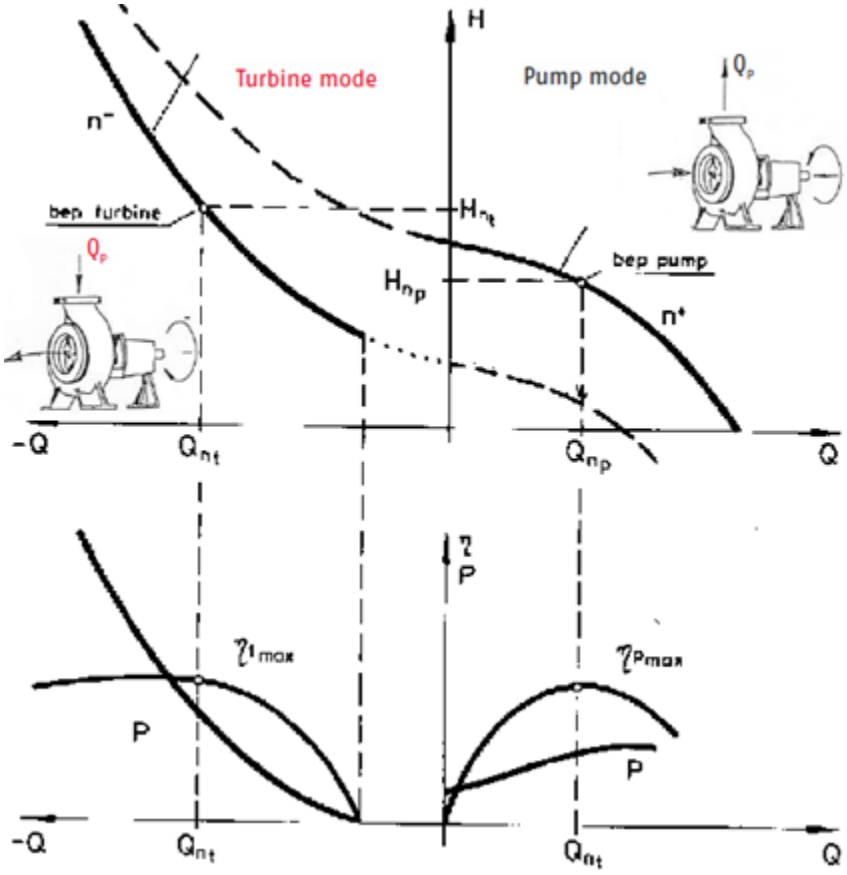

Figure 2-5: Complete pump-turbine characteristics at constant speed [6]

The efficiency of PAT is defined as the ratio of the brake power (output power) to water power and it can be expressed as:

$$\eta_t = \frac{P_b}{P_{hy}} \qquad 2.1$$

While the efficiency of pump is the ratio of water power to shaft input power and can be written as:

$$\eta_p = \frac{P_{hy}}{P_{in}} \qquad 2.2$$

For pump operating as turbine at constant speed, the power output of the shaft increases as the head and flow rate increases (see Figure 2-5). And the power delivered by the PAT is given as:

$$P_b = T \times \omega \qquad 2.3$$

Hydraulic power (water power), P_{hy} is defined as the power that can be obtained for a potential site regarding the available flow rate and head. It is given as:

$$P_{hy} = \rho g H Q \qquad 2.4$$

The performance or operating conditions of a turbine handling a particular fluid is function of **rotation speed**, turbine **power output** and **head**. It is important to know the range of these operating parameters covered by a machine of a particular shape. For this reason, dimensional parameter called **Specific Speed** is defined.

Specific Speed for turbine represents the speed of a member of the same homogenous turbine series as the actual turbine, so reduced in size as to generate unit power under a unit head of the fluid. It is expressed as:

$$N_{s_T} = \frac{N_t P^{0.5}}{H^{1.25}} \qquad 2.5$$

In dimensionless form, specific speed can be written as:

$$n_{s_T} = \frac{N_t \left(\frac{P}{\rho}\right)^{0.5}}{(gH)^{1.25}} \qquad 2.6$$

There are also other dimensionless parameters that are important to determine the performance characteristics of a turbine. This parameter include **head** , **flow** and **power coefficient** .What makes all these parameters similar is that the variables with the respective coefficient are made dimensionless through normalizing with diameter (D) and rotation speed (N) .With the exception of flow coefficient , former and latter parameters require one additional variable to normalize. The variables are gravity and density respectively.

Head coefficient is given by:

$$\psi = \frac{gH}{\varpi^2 D^2} \quad 2.7$$

Flow coefficient is expressed as:

$$\phi = \frac{Q}{\varpi D^3} \quad 2.8$$

Power coefficient is given as:

$$\pi = \frac{P}{\rho \varpi^3 D^5} \quad 2.9$$

2.2.4. Advantages of PAT

Using Pump as Turbine has the following advantages over a conventional turbine [6].

- **Availability**: In developing country, the availability of pumps is far better than turbine. Due to their widespread application, standard pumps with spare parts are readily available. In addition to that manufacturers and their representatives are world-wide present.
- **Construction**: Due to simple construction of pumps, they can be used as turbines more appropriate for developing countries than sophisticated turbines.
- **Maintenance**: Pumps are simple and do not require special equipment and highly qualified mechanics for maintenance
- **Economics**: The investment costs of PATs may be less than 50 percent of those of a comparable turbine (especially for small units below 50 Kw).

2.2.5. Disadvantages of PAT

Some of the limitations when using Pump as Turbine instead of conventional turbine in reference to [6] are discussed below.

Lack of Hydraulic Control Device:

- A control valve must be incorporated in the penstock line to start and stop the PAT. Hydraulic losses and cost of the installation will increase due to introduction of valve.

Peak Efficiency:

- Efficiency of PAT is lower than sophisticated turbines of the medium to high output range. PATs reach efficiency not more than to locally manufactured Cross flow or Pelton turbines.

Lower Efficiency at Part Load:

- If PATs are operated at other than the design flow (i.e. below their BEP), a relatively rapid drop of efficiency will occur.

2.2.6. Selection of PAT

According to **S.Derakhshan [10]**, the selection of pump for use in turbine mode has become a difficult task since pump manufacturers do not normally provide characteristic curves of their pumps working as turbines. This makes difficulty to select an appropriate pump to run as a turbine for a specific operating condition. While this draw backs holds for the use of PAT, different method have been proposed to choose a pump for a PAT system based on the required turbine mode characteristics. In this thesis, two methods of selection of PAT are discussed, used and the results obtained from the calculation are compared with each other. These methods are based on relations found by different researchers by experimental testing of several centrifugal pumps in reverse. The methods are illustrated as below.

2.2.6.1. Method 1

Chapallaz [6] has presented a selection charts based on more than 80 experimentally tested pump results operating in turbine mode. In his method, first turbine mode specific speed is calculated using nominal turbine flow Q_n (from flow-duration curve) and H_{nt} net turbine head in equation 2.10.

$$n_{qt} = N_t \frac{Q_{nt}^{0.5}}{H_{nt}^{0.75}} \qquad 2.10$$

The PAT to be selected should run under these head and flow conditions near its best efficiency point. Then by using turbine mode specific speed, the pump-mode specific speed is calculating using equation 2.11.

$$n_{qp} = \frac{n_{qt}}{0.89} \qquad 2.11$$

Where n_{qp} is pump-mode specific speed

The efficiency of the pump can be obtained using the graph in Figure D-1; pump efficiency as function of specific speed n_{qp} and flow Q_{np}. This figure indicates the maximum pump efficiency which can be attained by standard pumps for given head / flow conditions. For preliminary analysis, the nominal pump mode flow rate Q_{np} can be obtained using the available flow Q_{nt} divided by 1.3.

By using pump specific speed and efficiency, turbine design conditions are converted into pump design conditions using conversion factors. These conversion factors are indicated on appendix D. The conversion factors for head, C_H, can be obtained using Figure D-2 and conversion factor for flow rate, C_Q, can be read using Figure D-3.

Applying the conversion factors C_H and C_Q on the design head and flow in turbine mode to determine pump performance parameters at pump best efficiency point $(BEP)_p$ at the proposed turbine speed is the next step. The nominal pump head and flow rate at turbine speed N_t can be obtained using equation 2.12 and 2.13.

$$H_{np}(N_t) = \frac{H_{nt}}{C_H} \quad 2.12$$

$$Q_{np}(N_t) = \frac{Q_{nt}}{C_Q} \quad 2.13$$

Lastly, converting pump design conditions at turbine rated speed into pump rated speed using the similarity laws. The general selection charts in pump manufacturers' brochures indicate the type of pump and its rated speed which would probably accommodate the required head/flow conditions for the installation. However, the rated pump speed N_p does in most cases not correspond to the proposed turbine speed N_t. Therefore, the head/flow values must be transformed into new head/flow conditions valid for nominal pump speed N_p by applying the affinity laws.

The pump mode head and flow rate at pump rated speed can be calculated using equation 2.14 and 2.15 respectively.

$$H_{np}(N_p) = H_{np}(N_t)\left[\frac{N_t}{N_p}\right]^2 \quad 2.14$$

$$Q_{np}(N_p) = Q_{np}(N_t)\left[\frac{N_t}{N_p}\right] \quad 2.15$$

By using the rated pump head and flow rate, the required pump can be selected for the use in turbine mode.

2.2.6.2. Method 2

The second procedure for selecting proper PAT is proposed by **S.Derakhshan [10]**. In this procedure, the first step is to calculate pump specific speed in its operating point, N_{sp} by using equation 2.16.

$$N_{sp} = 0.3705\ N_{st} + 5.083 \quad 2.16$$

Where N_{sp} (m, m^3/s) and N_{st} (m,kW) and are the pump and turbine specific speeds in their rated points, respectively.

The second step is to calculate the specific speed in dimensionless form using equation 2.17.

$$\alpha_p = \frac{N_{sp}}{g^{0.75}} \qquad 2.17$$

The third step is to calculate the gamma (γ) parameter by inserting equation 2.17 in 2.18.

$$\gamma = 0.0233\ \alpha_p + 0.6464 \qquad 2.18$$

After finding the dimensionless parameter gamma (γ), the head ratio (the head ratio of pump to turbine mode) is obtained using equation 2.19.

$$h = \left[\frac{N_p}{N_t}\gamma\right]^{-2} \qquad 2.19$$

Where N_p - is pump mode rated speed

N_t - is turbine mode rated speed

Then the pump head at the rated (nominal) point, H_{pr}, is obtained using the head ratio in equation 2.19 and becomes:

$$H_{np} = \frac{H_{nt}}{h} \qquad 2.20$$

Where H_{tr} is the available head for the PAT

The rated (nominal) flow rate of pump, Q_{np}, can be obtained using N_{sp} and H_{pr} while choosing rated speed of pump, $N_{p.}$ The proper PAT can be easily selected when the rated head H_{pr}, flow rate Q_{pr} and speed N_p are known. These define the design point at which a pump should work in order to function at its best efficiency point as a turbine.

2.2.7. Published Performance Prediction Methods of PAT

Many researchers have tried to predict the performance of PAT from pump characteristic curves. Some of the relations presented for predicting the performance of pump as turbine were based upon either pump efficiency or specific speed. But deviation between experimental and predicted

reverse operation of standard pumps have been found to be more than 20% [16]. The objective of the estimation was to calculate the best efficiency point (BEP) of pump for turbine mode by using the pump operation data provided by the manufacturer. Some of the prediction methods considered in this thesis to estimate the PAT performance are summarized below.

A researcher called **Williams [17]** has proposed an estimation method that is used to predict PAT performance. In his method, the head and flow at the maximum pump efficiency point is used to estimate the head and flow rate at the best efficiency point of PAT .The proposed equation are as follows:

$$\left(\frac{H_t}{H_p}\right)_{bep} = \eta_p^{-1.2} \qquad 2.21$$

$$\left(\frac{Q_t}{Q_p}\right)_{bep} = \eta_p^{-0.8} \qquad 2.22$$

$$\eta_t = \eta_p \qquad 2.23$$

An estimation method cited on reference **[15]** and **[17]**, i.e. based on theoretical consideration, is proposed by **Stepanoff**. In his method, the turbine mode performance of PAT at the constant speed is calculated using two relations. Like **Williams [17]** method, the best efficiency point of PAT is considered equal to the pump best efficiency point.

$$\frac{H_t}{H_p} = \eta_p^{-0.5} \qquad 2.24$$

$$\frac{Q_t}{Q_p} = \frac{1}{\eta_p} \qquad 2.25$$

Another simple method cited on reference **[15]** is proposed by **Child**. He also assumed that the best efficiency point for pump and turbine are equal. The relation used to estimate the turbine head and flow rate are:

$$\frac{H_t}{H_p} = \frac{1}{\eta_p} \quad 2.26$$

$$\frac{Q_t}{Q_p} = \frac{1}{\eta_p} \quad 2.27$$

By using experimental testing of several centrifugal pump when operate in reverse (turbine mode), a prediction method has been proposed by **Derakhshan & Nourbakhsh [10]**. In their method, first the dimensionless pump and turbine specific speed of the pump in direct operation mode are calculated using equation 2.28 and 2.29 respectively.

$$\alpha_p = \frac{N_p Q_p^{0.5}}{(g H_p)^{0.75}} \quad 2.28$$

$$\beta_p = \frac{N_p P_p^{0.5}}{\rho^{0.5} (g H_p)^{1.25}} \quad 2.29$$

Then by inserting the value from equation 2.28 into equation 2.30 and 2.31 while the result from equation 2.29 into equation 2.32, the values of gamma (γ), alpha (α_t) and beta (β_t) with subscript 't' are solved. Finally turbine mode best efficiency point values of head, flow rate and power output can be obtained with the use of equation 2.20, 2.33 and 2.34 respectively.

$$\gamma = 0.0233\ \alpha_p + 0.6464 \quad 2.30$$

$$\alpha_t = 0.9413\ \alpha_p - 0.6045 \quad 2.31$$

$$\beta_t = 0.849\ \beta_p - 1.2376 \quad 2.32$$

$$\alpha_t = \frac{N_t Q_t^{0.5}}{(g H_t)^{0.75}} \quad 2.33$$

$$\beta_t = \frac{N_t P_t^{0.5}}{\rho^{0.5} (g H_t)^{1.25}} \quad 2.34$$

The rated (nominal) flow rate of pump, Q_{np}, can be obtained using N_{sp} and H_{pr} while choosing rated speed of pump, N_p. The proper PAT can be easily selected when the rated head H_{pr}, flow

rate Q_{pr} and speed N_p are known. These define the design point at which a pump should work in order to function at its best efficiency point as a turbine.

The BUTU (PAT in Spanish) method of **Alatorre-Frenk [15]** was first developed in Mexico and refined in Great Britain. The proposed empirical formulae were simply found by mathematical curve-fitting of experimental data for pump and turbine mode performance of standard pumps. The errors involved using this method is reported to be around 10% and more. The empirical formulas using BUTU method for prediction turbine-mode performance are as follows:

$$\left(\frac{H_t}{H_p}\right)_{bep} = \frac{1}{0.85\eta_p^{\,5} + 0.385} \qquad 2.35$$

$$\left(\frac{Q_t}{Q_p}\right)_{bep} = \frac{0.85\eta_p^{\,5} + 0.385}{2.00\eta_p^{\,9.5} + 0.205} \qquad 2.36$$

$$\eta_t = \eta_p - 0.03 \qquad 2.37$$

In order to determine the operating flow/head of a given PAT at the best efficiency point, a prediction method presented by **Chapallaz [6]** is used. This method involves the use of charts developed based on measured test results of over 80 machines performance data for the prediction of a PAT performance. This method calculates turbine BEP from the pump BEP which is usually known for a pump.

In this method, the conversion factors C_H and C_Q are read from the diagrams in Figure D-2 and D-3 in Appendix D using the maximum efficiency of the pump. Then using the correlation from equation 2.38 to 2.41, the maximum and minimum conversion factor for the head and flow rate can be determined.

$$C_{H\max} = 1.1C_H \quad (2.38)$$

$$C_{H\min} = 0.9C_H \quad (2.39)$$

$$C_{Q\max} = 1.075\,C_Q \quad (2.40)$$

$$C_{Q\min} = 0.925\,C_Q \quad (2.41)$$

After the max and min conversion factors for the head and flow rate are determined, the max. and min. operating point at the best efficiency head and flow rate of the turbine can be calculated using equation 2.42 up to 2.45 by substituting the appropriate factors together with to the head and flow rate value at maximum efficiency of the pump. The resulting values can be used to provide a good estimate of the performance of the pump in turbine operating mode.

$$H_{t\max} = C_{H\ \max} * H_p \quad (2.42)$$

$$H_{t\min} = C_{H\ \min} * H_p \quad (2.43)$$

$$Q_{t\max} = C_{Q\max} * Q_p \quad (2.44)$$

$$Q_{t\min} = C_{Q\min} * Q_p \quad (2.45)$$

The maximum efficiency point for turbine mode considered by **Chapallaz [6]** is the same as the BUTU method.

2.3. Previous Works on PAT

The section below summarized the review made on different literatures on the area Pump as Turbine system flow prediction. It is comprised of numerical investigation of pump when it operates in reverse direction (in turbine mode) with corresponding experimental validation of numerical result obtained from CFD analysis.

A four blade mixed flow pump having specific speed of 4883 in Us units was investigated by **Rawal S. [9]** with an objective of operating the pump in turbine mode by changing direction of

flow and hence the direction of rotation. Computational Fluid Dynamics (CFD) analysis using computer software Ansys CFX was carried out on mixed flow pump. Results were compared with data available form experimental test for parameters like head number, power number and efficiency versus the discharge number. The pump with impeller diameter 236 mm and eye diameter 190 mm has the best efficiency flow 0.1 m^3/sec at 8.3 m head at 1450 RPM. The numerical modal of Pump in turbine mode has exhibited very good characteristics with a maximum operating efficiency of 83.10 percent at a flow rate 0.127 m^3/s and 12.48 m head while operating at a speed of 1450 rpm. In the numerical simulation of the pump in turbine mode the author analyzed the accuracy of the CFD model using the experimental data as standard. The similarity between experimental and numerical results was satisfactory.

S.Derakhshan [10] investigated turbine mode performance of four industrial centrifugal pumps with specific speeds ranging from 14 - 56 (m, m^3/s) using experiments setup. These selected pumps had input power, head and flow rate up to 30 kW, 25 m and 0.15 m^3/s respectively. To test the Turbine mode, a feed pump, several pipes, an orifice, a generator and some ballast loads were used and installed in the test rig. The positions of barometers were defined individually for each test, depending on pump's and turbine's inlet and outlet pipes. After measuring all parameters, head, flow rate, output power and efficiency of PATs were calculated. A first-order uncertainty analysis was performed using constant odds combination method, based on a 95% confidence level. Using experimental data, some relations were obtained to calculate the BEP of the PAT based on the BEP of the pump mode. The prediction observed by the authors with this method was in good coincidence with the experimental data. They concluded that the relations are only valid for low-specific speed centrifugal pumps) with Ns < 60 (m, m^3/s) .They have also estimated off-design PAT operating condition using second and third order polynomials. Thus estimating the complete characteristic curves of a PAT based on its BEP. Lastly, they provided a practical procedure to select the proper PAT for a specific small hydropower stations using the rated point of pump (in Turbine mode) for turbine specific speed N_{st} < 150 (m, kW).

In another research, **S.Derakhshan [11]** made a numerical, experimental and theoretical study and investigation of hydraulic behavior of centrifugal pump with specific speed 23.5 (m, m^3/s) for testing as turbine. This pump has the maximum input shaft power, head and discharge of 20 kW, 25 m and 120 l/s respectively. In the Numerical study, 3D model of the whole impeller and

the volute was generated. A total grid size of 700,000 cells was generated using IGG 5.5 and Auto grid5 software for the volute and impeller respectively. Fine Turbo V.7 flow solver software was used to simulate the flow characteristic in turbine mode. Using numerical results; complete characteristic curves of the pump in reverse mode were obtained. In a theoretical analysis, the best efficiency point in turbine mode was achieved using hydraulic components of direct (pump) mode. For experimental verification of theoretical and numerical results, the pump was tested as a turbine in a test rig. All required parameters were measured to achieve characteristic curves of the reverse pump. The theoretical and numerical results were compared with experimental data. The observation made on CFD results were in acceptable level with experimental data for pump mode at BEP. But numerical results in part-load and over-load zones were not in acceptable coincidence with experimental data for turbine mode. Turbine head and power values achieved by CFD were lower than experimental data at same discharges. A theoretical method presented was slightly lower than experimental data to calculate BEP of reverse pump based on pumping mode characteristics (geometric and hydraulic).

R. Barrio [12] made numerical investigation on the performance of a commercial centrifugal pump with specific speed 0.42 operating in direct and reverse mode. The impeller has an eye diameter of 52 mm, outer diameter of 200 mm and seven blades. The width at the outlet of the impeller is 0.0169 m and the blade outlet angle is 29 ^{o}. The numerical calculations were carried out with FLUENT. This software was used to solve the full unsteady Reynolds averaged Navier-Stokes equations together with the standard k-epsilon model plus standard wall functions to simulate turbulent effects. The model was developed for a conventional centrifugal pump with volute casing. The mesh is unstructured and constituted by tetrahedral cells in the impeller and volute and by prismatic cells in the inlet and outlet duct. A total number of 800000 cells were used. The predictions were validated with laboratory tests, which showed a good agreement between the experimental and numerical flow-head characteristic.

2.4. Introduction to Computational Fluid Dynamics

Computational Fluid Dynamics (CFD) is field of fluid mechanics in which fluid flow problems are solved and analyzed using computational methods and numerical algorithms. In CFD method, it is concerned with the solution of equations of motion of the fluid as well as the

interaction of the fluid with solid bodies which is helpful to understand the physical events that occur in the flow of fluids around and within designated objects.

ANSYS CFX is general purpose CFD software that combines an advanced solver with powerful pre- and post-processing capabilities. It is suited for full integration of problem definition, analysis, and results presentation. It is capable of modeling Steady-state turbulent flows in multiple frames of reference [14].

2.4.1 Application of CFD

In recent years, CFD has become an important tool in different area application. The field of computational fluid dynamics has a broad range of applicability. Some of the application areas according to [13] include:

- CFD is used to model the aerodynamic effects of a fluid over automotive, planes and space shuttles bodies.
- CFD is used to study the flow through various types of turbo machineries like Pumps, Turbines, Compressors, Fans and Blower.
- CFD is applied in the study of thermal equipment like heat exchanger, boilers, etc.
- CFD has gained application in food industries. It is used in the analysis of refrigeration system, mixing process, etc.

2.4.2. Basic Flow Modeling in PAT

As discussed under the section: **Flow Zone in Centrifugal PATs**, the flow through PATs is characterized by a complex 3D rotation flow. These characteristics of flow are used to specify the closing physical models for the CFD analysis of the PATs in Ansys CFX. The commercial CFD codes Ansys CFX uses finite elements (cell vertex numerics) to discretize the domain and uses coupled algebraic multi-grid method to solve the governing equations of motion. Therefore, the flow through the PAT can be summarized and customized to the CFD simulation capabilities of Ansys CFX software as:

- 3D, Steady state flow
- Turbulent flow,
- Incompressible flow,
- Stationary and Rotating reference frame

The approaches used to solve flow variables in multiple frames of reference and model the turbulence are discussed below with reference to [14].

2.4.2.1. Fundamental Governing Equations

The governing equations of viscous flow are based on the three laws of conservation for physical systems:

1. Conservation of mass (continuity)

2. Conservation of momentum (Newton's second law)

3. Conservation of energy (first law of thermodynamics)

The temperature effects of flow through PATs will not be taken into account which means that the energy equation can be left out.

2.4.2.1.1. The Mass Conservation Equation

A continuity equation in physics is an equation that describes the transport of a conserved quantity. It is the mathematical way to express that any matter that exists in face of universe can neither be created nor destroyed; only it can only be moved by a continuous flow. The instantaneous equations of mass conservation in a stationary frame can be written as follows:

$$\frac{\partial(\rho U)}{\partial t} + \nabla.(\rho U) = 0 \qquad 2.46$$

This equation is the general form to solve any problem involving compressible or incompressible and steady or transient flow. For steady incompressible flow, since density, ρ is constant, it can be left out and the first expression on the left becomes zero. Thus equation 2.46 becomes:

$$\nabla U = 0 \qquad 2.47$$

Where

$$\nabla = \frac{\partial}{\partial x_i}\hat{i} + \frac{\partial}{\partial x_j}\hat{j} + \frac{\partial}{\partial x_k}\hat{k} \qquad 2.48$$

And $U = u_i\hat{i} + u_j\hat{j} + u_k\hat{k}$ 2.49

2.4.2.1.2. The Momentum Equation

The instantaneous equation of momentum conservation in stationary frame is described as:

$$\frac{\partial(\rho U)}{\partial t} + \nabla.(\rho U \otimes U) = -\nabla P + \nabla.\tau + S_m \qquad 2.50$$

The stress tensor, τ is given by

$$\tau = \mu\left(\nabla U + (\nabla U)^T - \frac{2}{3}\delta \nabla U\right) \qquad 2.51$$

The scalar form of Eq. 2.50 is also known as the Navier-Stokes equations (x, y and z direction). The fluid flow that is going to be analyzed numerically in this thesis can be considered incompressible, i.e. the density is constant. Momentum source term can be used to model isotropic losses in porous regions, directional losses in porous regions, or other processes but it has no significance for this particular analysis thus can be ignored. The steady state momentum equation becomes:

$$\nabla.(\rho U \otimes U) = -\nabla P + \nabla.\tau \qquad 2.52$$

2.4.2.2. Turbulence Models

Turbulence is the time-dependent chaotic behavior seen in many fluid flows. It occurs when the inertia forces in the fluid become significant compared to viscous forces, and is characterized by a high Reynolds number. It can have a significant effect on the characteristics of the flow. It is a complex process, mainly because it is three dimensional, unsteady and consists of many scales.

In principle, the Navier-Stokes equations describe both laminar and turbulent flows without the need for additional information. However, turbulent flows at realistic Reynolds numbers span a large range of turbulent length and time scales, and would generally involve length scales much smaller than the smallest finite volume mesh, which can be practically used in a numerical analysis.

To enable the effects of turbulence to be predicted, a large amount of CFD research has concentrated on methods which make use of turbulence models. Turbulence models have been specifically developed to account for the effects of turbulence without recourse to a prohibitively fine mesh and direct numerical simulation. Some of the turbulence models that are used to describe turbulence in a flow are described below.

1. The k-epsilon Model
2. The Renormalization Group (RNG) k-epsilon Model
3. The k-omega and Shear-Stress-Transport SST Models
4. The Reynolds Stress Model

2.4.2.2.1. The k-epsilon Model

Within CFX, $k-\varepsilon$ model provides good predictions for many flows of engineering interest. It is the most well know turbulence model that has been used in most general purpose CFD codes and is considered as a standard model. It has proven to be stable and numerically robust and has a well-established regime of predictive capability. For general purpose simulations, this model offers a good compromise in terms of accuracy and robustness.

$k-\varepsilon$ model is appropriate choices for modeling turbulence in liquid pumps and turbines. But this model is not suitable for modeling flows with boundary layer separation, in rotating fluids and flow over curved surfaces.

The $k-\varepsilon$ model in ANSYS CFX, turbulence kinetic energy, k is defined as the variance of the fluctuations in velocity. And turbulence eddy dissipation, ε is the rate at which the velocity fluctuations dissipate.

The $k-\varepsilon$ model introduces two new variables into the system of equations. The continuity equation is then:

$$\frac{\partial(\rho U)}{\partial t}+\frac{\partial .}{\partial x_j}(\rho U_j)=0 \qquad 2.53$$

And the momentum equation becomes:

$$\frac{\partial(\rho U_i)}{\partial t}+\frac{\partial}{\partial x_j}(\rho U_i U_j)=-\frac{\partial P'}{\partial x_i}+\frac{\partial}{\partial x_j}\left(\mu_{eff}\left(\frac{\partial U_i}{\partial x_j}+\frac{\partial U_j}{\partial x_i}\right)\right)+S_m \qquad 2.54$$

The $k-\varepsilon$ model is based on the eddy viscosity concept, so that:

$$\mu_{eff}=\mu+\mu_t \qquad 2.55$$

The $k-\varepsilon$ model assumes that the turbulence viscosity is linked to the turbulence kinetic energy and dissipation via the relation:

$$\mu_t=C_{\mu'}\rho\frac{k^2}{\varepsilon} \qquad 2.56$$

Where

$C_{\mu'}$ is constant equal to 0.09

The values of k and ε come directly from the differential transport equations for the turbulence kinetic energy and turbulence dissipation rate:

$$\frac{\partial(\rho k)}{\partial t}+\frac{\partial}{\partial x_j}(\rho U_j k)=\frac{\partial}{\partial x_j}\left(\left(\mu+\frac{\mu_t}{\sigma_k}\right)\frac{\partial k}{\partial x_j}\right)+P_k-\rho\varepsilon+P_{kb} \qquad 2.57$$

$$\frac{\partial(\rho\varepsilon)}{\partial t}+\frac{\partial}{\partial x_j}(\rho U_i\varepsilon)=\frac{\partial}{\partial x_j}\left(\left(\mu+\frac{\mu_t}{\sigma_\varepsilon}\right)\frac{\partial\varepsilon}{\partial xj}\right)+\frac{\varepsilon}{k}\left(C_{\varepsilon 1}P_k-C_{\varepsilon 2}\rho\varepsilon+C_{\varepsilon 1}P_{\varepsilon b}\right) \qquad 2.58$$

Where $C_{\varepsilon 1}=1.45; C_{\varepsilon 2}=1.9; \sigma_\varepsilon=1.3; \sigma_k=1.0$

P_{kb} and $P_{\varepsilon b}$ represent the influence of Buoyancy forces. For flow through the PAT, P_{kb} and $P_{\varepsilon b}$ are ignored.

2.4.2.3. Rotating Frames of Reference (RFR)

Rotating Frames of Reference (RFR) are useful for rotating fluid machinery applications, such as pump impeller or turbine blade problems. CFX enables user to specify a domain that is rotating about an axis. When a Rotating Frame of Reference is specified, angular velocity input is required.

The velocity in the rotating frame of reference is defined as:

$$U_{rel} = U_{stn} - \omega \times R \qquad 2.59$$

2.4.2.4. Interface Characteristics and Modeling

Domain interfaces provide a way of connecting meshes or domains together. There are many uses of them. They are always required when multiple assemblies are used within a domain or when multiple domains are created within a single assembly. If the required domain interfaces is not create, the required variables at the interface cannot be solved. Depending on the type of domains defined, the different model connection across the interface is used. Type of interface may be categorized into Fluid-Fluid, Solid-Solid, Porous-Porous, Fluid-Solid, Fluid-Porous and Solid-Porous.

Domain interface are used in the following situations:

- Domains can be connected together with a domain interface. This is often useful for connecting static domains together with non-matching grids.
- A domain may contain multiple mesh blocks. Non-matching interfaces can be connected together using a domain interface.
- Domains that have a change in the reference frame (such as rotor-stator) can be connected together.

- If the flow field is repeated in multiple identical regions, then only one region needs to be solved, but the boundaries are specified as periodic.

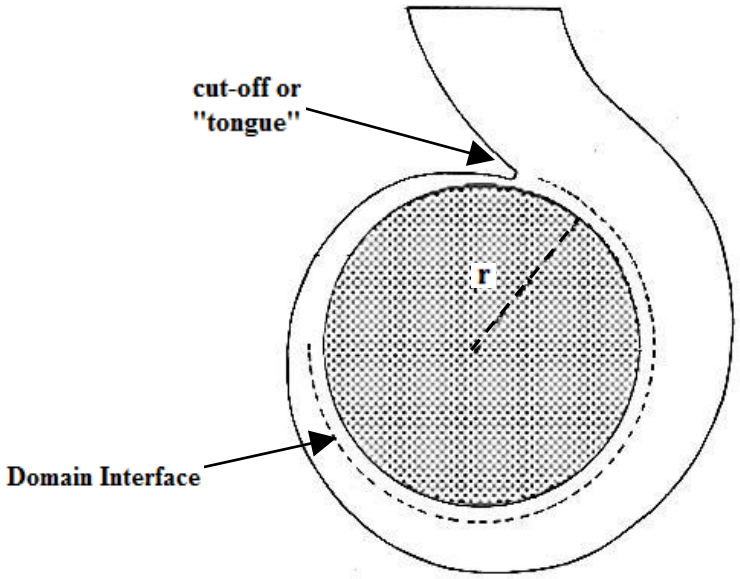

Figure 2-6: Volute and impeller interface [14]

Figure 2-6 shows the interface that exists when modeling flow through PAT fluid domains. The interface model defines the way the solver models flow physics across the interface. The models include:-

- Periodic Interface Model
- General Connection

2.4.2.4.1. Periodic Interface Model

The periodic condition is most common for fluid-fluid interface that allows a simplified geometry to be used if the full problem has multiple identical regions .It ensures that the flow out of one side of the interface automatically appears on the other side. The two types of periodic interface model in Ansys CFX:-

- Rotational Periodicity
- Translational Periodicity

Translation periodicity is often useful to model periodic flow through; for example in tube banks of heat exchangers or periodic duct flow. Since it has no significance for modeling the interface in PAT, it will not be discussed.

2.4.2.4.1.1. Rotational Periodicity

Rotational periodicity is the most common case of periodic interface which is used to model a single flow passage for domain having identical flow passage in the domain; for example the analysis of a centrifugal pump impeller. Since the blade passage on the impeller is identical circumferentially, a single passage can be used to mimic as if the complete blade are taken for analysis .In this interface model, the two sides of the periodic interface can be mapped by a single rotational transformation about an axis. For the analysis of PAT, a single impeller passage is used for simulating the flow pattern with in the impeller.

2.4.2.4.2. General Grid Interface (GGI)

General Grid Interface (GGI) connections refer to the class of grid connections where the grid on either side of the two connected surfaces does not match. In general, GGI connections permit non-matching of node location, element type, surface extent, surface shape and even non-matching of the flow physics across the connection. Any number of GGI connection conditions is possible within a computational domain. The interface is applicable to incompressible, subsonic flow conditions and all model options within CFX including turbulence models support the use of GGI connections. The General Connection option is necessary when the frame of reference or pitch changes across the interface. It is used in the following cases:

- One side is in a stationary frame of reference and the other side is in a rotating frame of reference
- Both sides are in a rotating frame of reference but each with a different rate of rotation
- Both sides are in the same frame of reference but have unequal pitches. In this situation, the flows through the interface must account for pitch change.

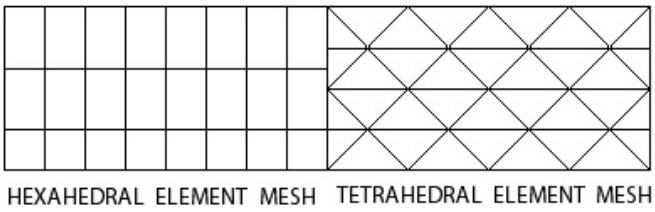

Figure 2-7: General Grid Interface (GGI) connection [14]

Multiple Frames of Reference (MFR) allows the analysis of situations involving domains that are rotating relative to one another. For CFX, this feature focuses on the investigation of stationary and rotating part interaction for rotating machinery.

The General Connection interface model is a powerful way to connect regions together. When a general connection is used, the following details need to be specified:

- A frame change at the interface between a rotating and stationary component
- Connection type (pitch change) between non-matching grids

2.4.2.4.2.1. Frame Change/Mixing Model

There are three types of frame change/mixing models available in ANSYS CFX:

- Frozen Rotor
- Stage
- Transient Rotor-Stator

The Transient Rotor-Stator model is used any time it is important to account for transient interaction between components on each side of the GGI connection is simulated. Since the flow regime through the PAT is considered to be steady, this model would not be discussed.

2.4.2.4.2.1.1. Frozen Rotor

Frozen Rotor analysis is most useful when the circumferential variation of the flow is large relative to the component pitch. This model assumes the frame of reference and/or pitch is changed but the relative orientation of the components across the interface is fixed. The two frames of reference connect in such a way that they each have a fixed relative position throughout the calculation.

This model produces a steady state solution to the multiple frame of reference problems, with some account of the interaction between the two frames. This model requires the least amount of computational effort of the three frame change models.

2.4.2.4.2.1.2. Stage

The Stage model is an alternative to the Frozen Rotor model for modeling frame change. Instead of assuming a fixed relative position of the components, the stage model performs a circumferential averaging of the fluxes through bands on the interface. Steady state solutions are then obtained in each reference frame.

Stage analysis is most appropriate when the circumferential variation of the flow is of the order of the component pitch. Stage analysis is not appropriate when the circumferential variation of the flow is significant relative to the component pitch (for example, a pump and volute combination at off-design conditions).

The Stage model usually requires more computational effort than the Frozen Rotor model to converge. To obtain best results, it is required to obtain an approximate solution using a Frozen Rotor interface and then restart with a Stage interface.

2.4.3.4.2.2. Pitch Change

To connect dissimilar meshes, an intersection algorithm is used to find the overlapping parts of each mesh face at the interface; Pitch change can be applied. It is used; for example, a domain interface can connect a stator domain with a rotor domain where the number of stator blades is not equal to the number of rotor blades, even if the mesh contains only one blade from each side. This way the pitch for each domain component must be specified.

For this research, different computational fluid domains of the PAT can be meshed using different element and GGI can be used to make a connection at the interfaces between the stationary and rotating domains. The volute and the draft tube are assumed to be stationary and the impeller is considered as a rotating domain. To reduce the computation time and resource, the number of blade passage in the impeller fluid domain is considered to be one, thus the pitch angle on impeller side and volute side fluid- fluid interface as well as the pitch angle on impeller side and draft tube domain side interface is specified.

2.4.3. Discretization and Solution Theory

ANSYS CFX uses an element-based finite volume method, which first involves discretizing the spatial domain using a mesh. The mesh is used to construct finite volumes, which are used to conserve relevant quantities such as mass, momentum, and energy.

Figure 2-9 shows a typical two-dimensional mesh. All solution variables and fluid properties are stored at the nodes (mesh vertices). A control volume (the shaded area) is constructed around each mesh node using the median dual (defined by lines joining the centers of the edges and element centers surrounding the node).

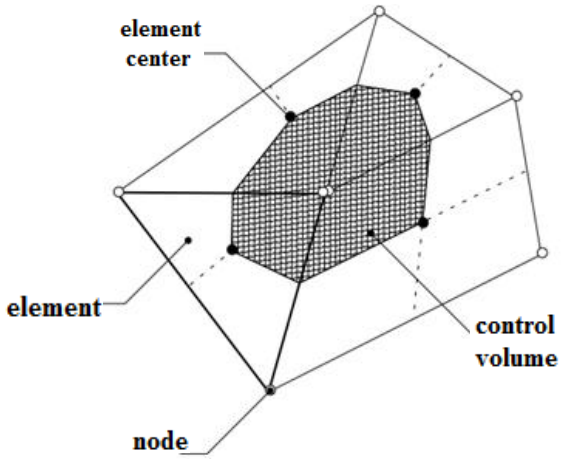

Figure 2-8: Control volume definition [14]

To illustrate the finite volume methodology, consider the conservation equations for mass, and momentum, in equation 2.60 and 2.61 respectively expressed in Cartesian coordinates

These equations are integrated over each control volume, and Gauss' Divergence Theorem is applied to convert volume integrals involving divergence and gradient operators to surface integrals. If control volumes do not deform in time, then the time derivatives can be moved outside of the volume integrals and the integrated equations become:

$$\frac{d}{dt}\int_V \rho dV + \int_S \rho U_j dn_j = 0 \qquad 2.60$$

$$\frac{d}{dt}\int_V \rho U_i dV + \int_S \rho U_j U_i dn_j = -\int_S P dn_j + \int_S \left(\mu_{eff} \left(\frac{\partial U_i}{\partial x_j} + \frac{\partial U_j}{\partial x_i} \right) \right) dn_j + \int_V S_{Ui} dV \qquad 2.61$$

Where V and s respectively denote volume and surface regions of integration, and

dn_j are the differential Cartesian components of the outward normal surface vector.

The volume integrals represent source or accumulation terms, and the surface integrals represent the summation of the fluxes.

The next step in the numerical algorithm is to discretize the volume and surface integrals. To illustrate this step, consider a single element like the one shown below.

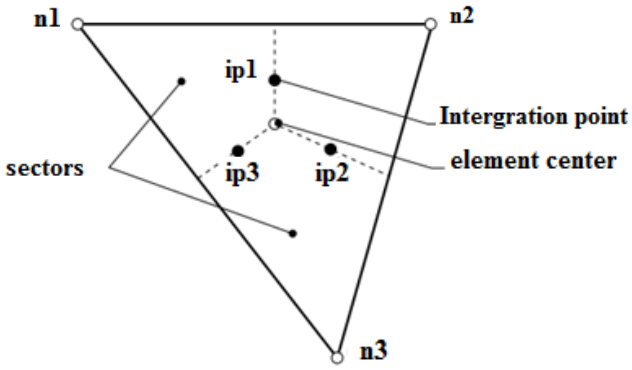

Figure 2-9: Mesh element [14]

Volume integrals are discretized within each element sector and accumulated to the control volume to which the sector belongs. Surface integrals are discretized at the integration points (ipn) located at the center of each surface segment within an element and then distributed to the adjacent control volumes. Because the surface integrals are equal and opposite for control volumes adjacent to the integration points, the surface integrals are guaranteed to be locally conservative.

After discretizing the volume and surface integrals, the integral equations become:

$$V\left(\frac{\rho - \rho^o}{\Delta t} \right) + \sum_{ip} \dot{m}_{ip} = 0 \qquad 2.62$$

$$V\left(\frac{\rho U_i - \rho^o U_i{}^0}{\Delta t}\right) + \sum_{ip} \dot{m}_{ip}(U_i)_{ip} = \sum_{ip}(P\Delta n_i)_{ip} + \sum_{ip}\left(\mu_{eff}\left(\frac{\partial U_i}{\partial x_j} + \frac{\partial U_j}{\partial x_i}\right)\Delta n_j\right)_{ip} + \overline{S_{Ui}}V \qquad 2.63$$

Where $\dot{m}_{ip}$ is the discrete mass flow through a surface of the control volume and is given by:

$$\dot{m}_{ip} = (\rho U_j \Delta n_j)_{ip} \qquad 2.64$$

The subscript **'ip'** denotes evaluation at an integration point; summations are over all the integration points of the control volume.

2.4.4. General Solution Strategy

ANSYS CFX uses a coupled solver, which solves the hydrodynamic equations (for u, v, w, and p) as a single system. This solution approach uses a fully implicit discretization of the equations at any given time step. For steady state problems, the time-step behaves like an 'acceleration parameter', to guide the approximate solutions in a physically based manner to a steady-state solution. This reduces the number of iterations required for convergence to a steady state.

The flow chart in Figure 2-11 shows a solution approach used to solve each set of field equations consisting numerically intensive operations. When solving fields for steady state analyses in CFX-Solver, the outer (or time step) iteration is controlled by the physical time scale and only one inner (linearization) iteration is performed per outer iteration. The linear equations are solved using an Algebraic Multigrid method.

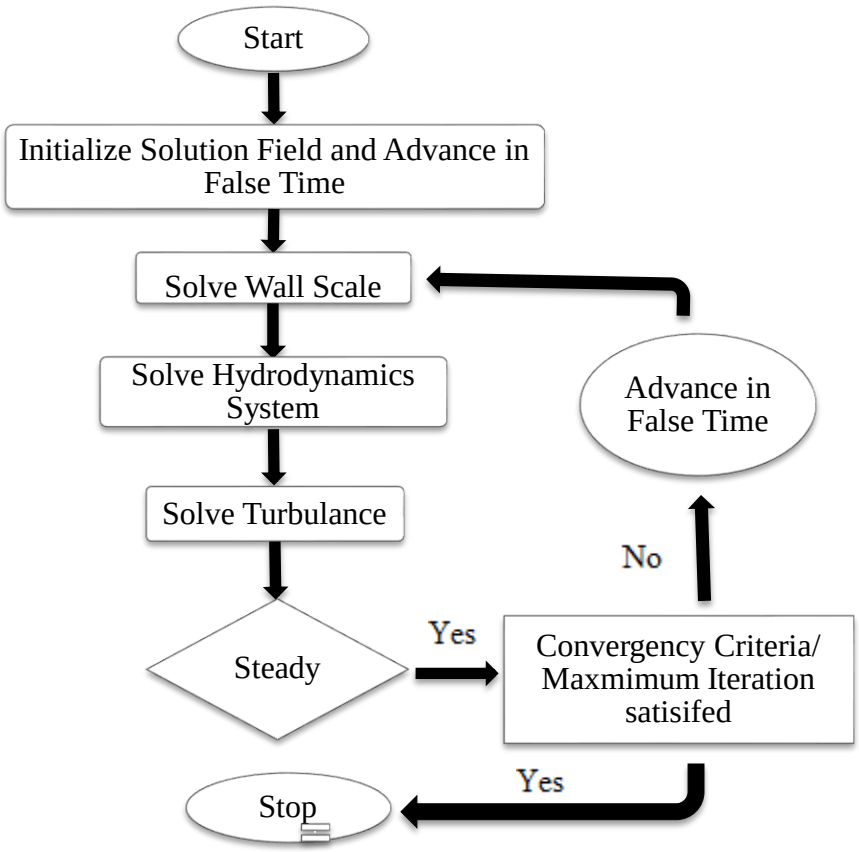

Figure 2-10: Solution process for PAT [14]

2.4.5. Linear Equation Solution

ANSYS CFX uses a Multi-grid (MG) accelerated Incomplete Lower Upper (ILU) factorization technique for solving the discrete system of linearized equations. It is an iterative solver whereby the exact solution of the equations is approached during the course of several iterations.

The linearized system of discrete equations described above can be written in the general matrix form:

$$[A][\varphi] = [b] \qquad 2.65$$

Where $[A]$ is the coefficient matrix,

$[\varphi]$ – the solution vector and

$[b]$ – the right hand side.

The above equation can be solved iteratively by starting with an approximate solution, φ^n , that is to be improved by a correction, φ' , to yield a better solution, φ^{n+1} , that is:

$$\varphi^{n+1} = \varphi^n + \varphi' \qquad 2.66$$

Where φ' is a solution of:

$$A\varphi' = r^n \qquad 2.67$$

And r^n is residual and can be obtained from:

$$r^n = b - A\varphi^n \qquad 2.68$$

Repeated application of this algorithm will yield a solution of the desired accuracy. By themselves, iterative solvers such as ILU tend to rapidly decrease in performance as the number of computational mesh elements increases.

2.4.6. The Coupled System of Equations

The linear set of equations that arise by applying the finite volume method to all elements in the domain are discrete conservation equations. The system of equations can be written in the form:

$$\sum_{nb_i} a_i^{nb} \varphi_i^{nb} = b_i \qquad 2.69$$

Where $[A][\varphi] = [b]$ is the solution

a - The coefficients of the equation

b - The right hand side,

i - is the identifying number of the control volume or node in question, and

nb - means “neighbor”, but also includes the central coefficient multiplying the solution at the ith location.

The node may have any number of such neighbors, so that the method is equally applicable to both structured and unstructured meshes. The set of these, for all control volumes constitutes the whole linear equation system. For a scalar equation (for example turbulent kinetic energy), and bi are each single numbers. For the coupled, 3D mass-momentum equation set, they are a (4 x 4) matrix or a (4 x 1) vector, which can be expressed as:

$$a_i^{nb} = \begin{bmatrix} a_{uu} & a_{uv} & a_{uw} & a_{up} \\ a_{vu} & a_{vv} & a_{vw} & a_{vp} \\ a_{wu} & a_{wv} & a_{ww} & a_{wp} \\ a_{pu} & a_{pv} & a_{pw} & a_{pp} \end{bmatrix}_i^{nb} \qquad \varphi_i^{nb} = \begin{bmatrix} u \\ v \\ w \\ p \end{bmatrix}_i^{nb} \qquad b_i = \begin{bmatrix} b_u \\ b_v \\ b_w \\ b_p \end{bmatrix}$$

CHAPTER THREE

Selection and Computational Modeling of PAT for Performance Analysis

This chapter provides a brief description of potential site found in Oromia region. The procedure used to select the required pump that is used to operate as PAT for this potential hydro site is also discussed on the basis of concepts on the previous chapter. Lastly, the pre and post processing steps undertaken to simulate the selected PAT using Ansys CFX is discussed in detail.

3.1. Site Description

The hydro potential site selected for this research, on which a pump is used as turbine, is called Dabis River. The hydro site is located 148 km from Addis Ababa in the Oromia regional state in West Shewa zone at an elevation of about 2411 m above sea level. The Dabis River is found under small Woreda Dadi Gelan and Bejiro Kebele located at 8°52'38.97" N latitude and 37°47'04.95" E longitude.

According to secondary source data, the site is characterized by a minimum flow rate of 0.025 m^3/s from flow duration curve and a gross head of 17m.The estimated output power for this site is 2.70 kW.

Figure 3-1: Location of Dabis river hydro site in the West Shewa zone / Ethiopia.

3.2. PAT Selection for Dabis Hydro Site

It is required that the pump to be selected should operate in turbine mode under given site head/flow rate conditions to delivers shaft power output for power generation. And the PAT nominal speed must be chosen in such a way that the available machine should operates near its best efficiency point under the given site conditions. The generator speed decides the nominal speed of PAT since it can only take a distinct value according to the number of poles; that is 750 ,1000 ,1500, 3000 RPM [17]. Generally, as the number of poles in the generator increases, the synchronous speed decreases. This causes the generator to be costly. So compromise between the cost and synchronous speed, 1500 RPM is often used. Thus for this research, a nominal speed of 1500 RPM is selected and used.

Thus the appropriate pump to be used in turbine on Dabis hydro site can be selected using the methods presented in **Section 2.2.6**. The first method used to select pump is based on the **Chapallaz [6]** approach while the second pump selection procedure used is according to **S.Derakhshan [10]** method. Equations in **Section 2.26** are inserted in Matlab GUI to calculate the required pump head and flow rate at BEP. The Matlab codes used for calculation are presented on Appendix C. Table 3.1 shows the summery of calculated Pump head and flow rate at best efficiency point (BEP) using the two stated methods that is required to perform as turbine on Dabis site .

The result in Table 3.1 can be summarized as:-

- The method proposed by **Chapallaz [6]** predicted higher values of Pump head and flow rate at BEP in contrast to **S.Derakhshan [10].**
- Pump specific speeds calculated with both methods are very close in value.

Table 3.1: Operating characteristics of required pump at Best Efficiency Point (BEP) to operate in turbine mode at hydro site

	Calculated pump specification at BEP		
Researchers	Pump specific speed (m, m^3/s)	Pump head (m)	Pump flow rate (m^3/s)
Chapallaz [6]	31.83	47.2222	0.0397
S.Derakhshan [10]	31.59	41.28	0.0294

In order to choose between the two methods, the approach used by the researchers to develop the selection procedure should be evaluated based on the number of experiment carried out. **Chapallaz [6]** experimentally tested about 80 pumps to determine turbine mode characteristics and develop selection procedure of appropriate pump to use it as turbine. On the other hand, number of pumps used to propose the selection procedure by **S.Derakhshan [10]** is much lower than **Chapallaz [6].**This makes **Chapallaz [6]** method more reliable to use.

Therefore for this thesis, a pump having performance characteristics at BEP closer to calculated pump characteristics using **Chapallaz [6]** approach is selected. Thus specification of the proposed centrifugal pump to operate in turbine on Dabis River is tabulated in Table 3.2.

Table 3.2: Specification of selected pump

Manufacturer	Erocole Marelli & C.S.P.A
Type	702/46
Nominal head (m)	48.42
Nominal flow rate (m^3/s)	0.025
Specific Speed (m, m^3/s)	25.5
Motor	Asynchronous 3 Phase,50 cycle,380 Volts, 38.1 Ampere: 2960 RPM
Impeller	5 Blade, 200 mm diameter

3.3. Principal Steps of CFD Simulation of PAT

Computational Fluid Dynamics (CFD) is a useful technique that's used to perform fluid flow analysis once a model and finite volume grid on the model is generated. The general steps undertaken for problem analysis using CFD include defining boundary conditions, fluid properties, executing the solution and displaying the result.

The steps undertaken to perform a CFD analysis of Pump as Turbine (PAT) are summarized in the flow chart below.

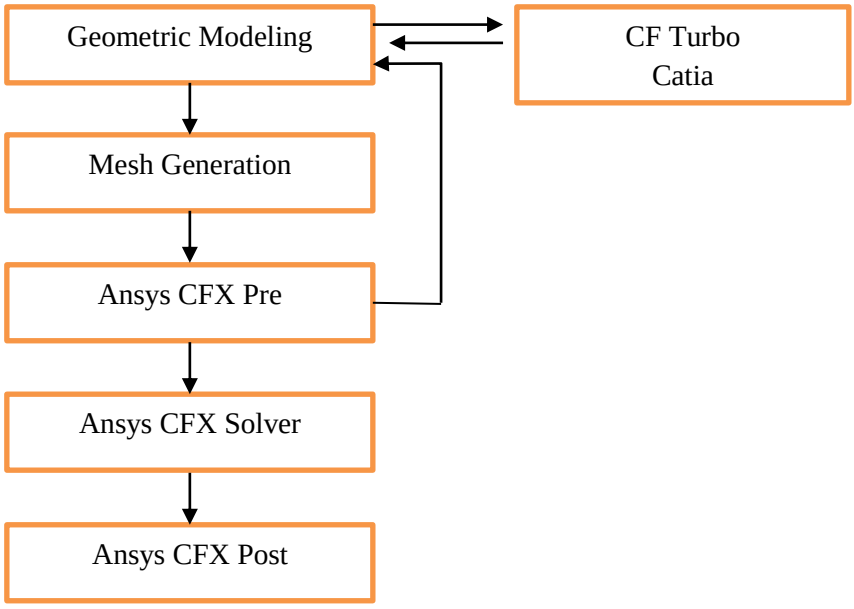

Figure 3-2: Flow chart for simulation of PAT

The preprocessing software packages used to generate the geometry models of the PAT and draft tube are CF turbo and Catia respectively. After the geometry models are created, the models are discretized into control volume using Ansys ICEM.After all the necessary problem specification generated in Ansys CFX-pre; the CFX-solver solves all the solution variables for the simulation. Lastly, the results obtained from the solution are displayed using Ansys CFX post. This chapter briefly describes the steps followed starting from generating geometry model up to post processing.

3.3.1. Geometric Modeling

Modeling of the geometry of a centrifugal pump running in turbine mode involves defining the impeller and volute components. Geometric modeling of draft tube is also considered since it is one of the major component in PAT system.

3.3.1.1. Impeller and Volute

The volute and the impeller are generated using CF turbo. CFturbo is software package used to model and design turbo machineries like pumps, ventilators, compressors, turbines interactively. The software is easy to use and does enable quick generation and variation of impeller and volute geometries. Several models can be displayed, compared and modified simultaneously.

Therefore the dimensions of impeller of selected pump to operate in turbine mode are tabulated in Table 3.3.

Table 3.3: Centrifugal pump impeller specification

Impeller Geometry Parameter	Inlet	Outlet
No. of Blades	5	
Eye Diameter	44 mm	
Impeller Diameter	101.5 mm	200 mm
Blade width	32 mm	20 mm
Blade angle	18^{o}	40^{o}
Blade thickness	2.4 mm	4.2 mm

Using CFturbo graphics user interface (GUI), two components of the pump; namely the impeller and volute casing are modeled. Due to the periodic nature of the impeller geometry, only a single blade passage of the complete impeller model of the original pump is considered, thus minimizing the computer resources required to obtain a solution.

Figure 3-3 and 3-4 depicts the complete and segment (one fifth) fluid volume extracted from impeller model and the fluid domain within the pump volute casing respectively. A complete workflow of the CAD modeling is presented in Appendix A.1.

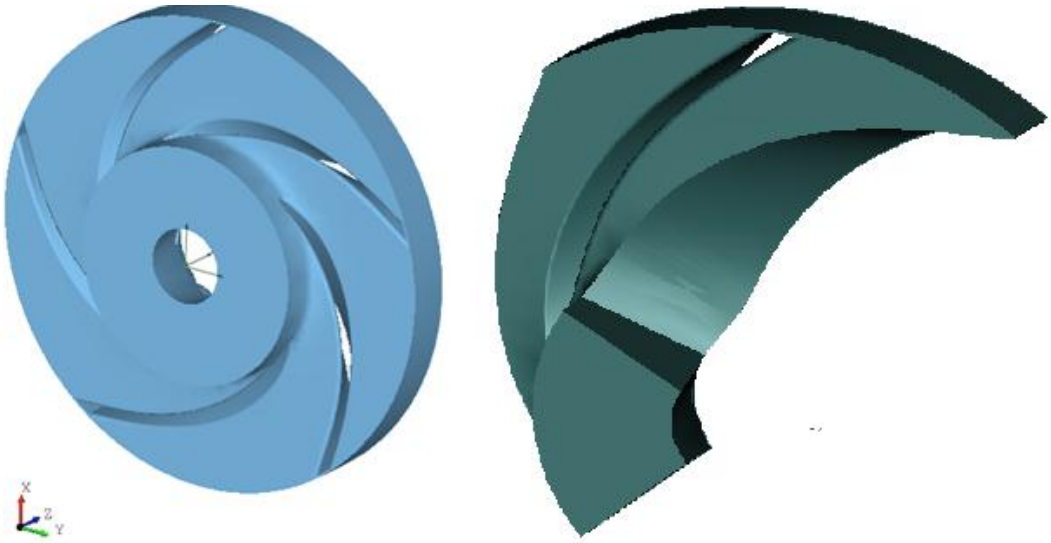

Figure 3-3: Complete and segment 3D CFD fluid domain of centrifugal pump impeller model.

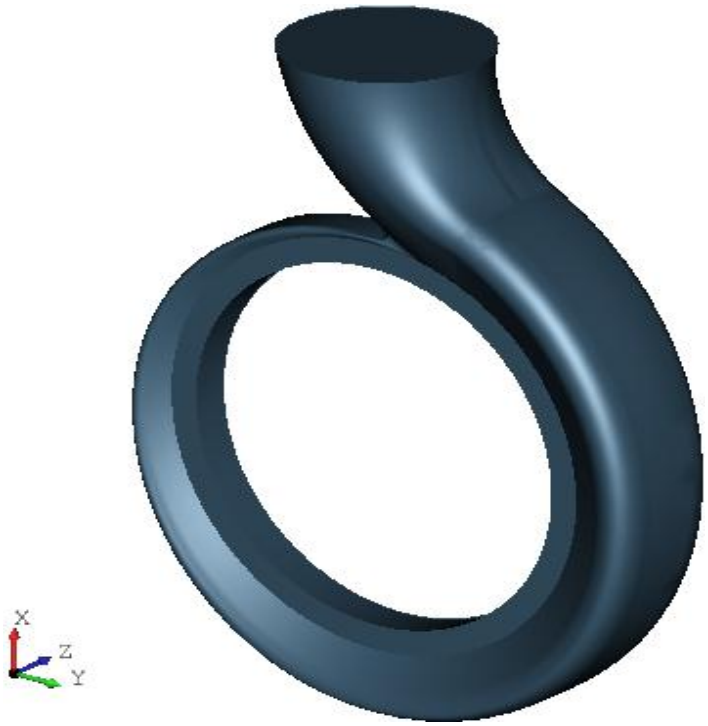

Figure 3-4: 3D model of a centrifugal pump volute fluid volume

3.3.1.2. Draft tube

Draft tubes are usually used on PAT to partially regain the velocity energy at the diffusor throat of the PAT outlet (pump inlet). Due to gradual expansion of area toward the outlet section of the draft tube, the kinetic energy of the water then can be transformed into pressure which will increase the net turbine head of the installation.

Figure 3-5 shows a typical design used to size draft tube for PATs. The dimensions of the draft tube are calculated according to Figure 3-5. Since centrifugal pumps are usually mounted with their impeller axis being horizontal and parallel to the ground and since the outlet of the draft tube must be submerged to be operational, the elbow – type draft tube design shown on right hand side of Figure 3-5 is selected. By making use of the dimension, the draft tube fluid domain is modeled. Figure 3-6 shows the fluid volume within the draft tube. From the figure, it can be seen that to make the flow through PAT more realistic, the fluid domain that exists within pump diffusor throat is added at the right end of draft tube domain. The procedure used to create fluid domain model is clearly presented in Appendix A.2.

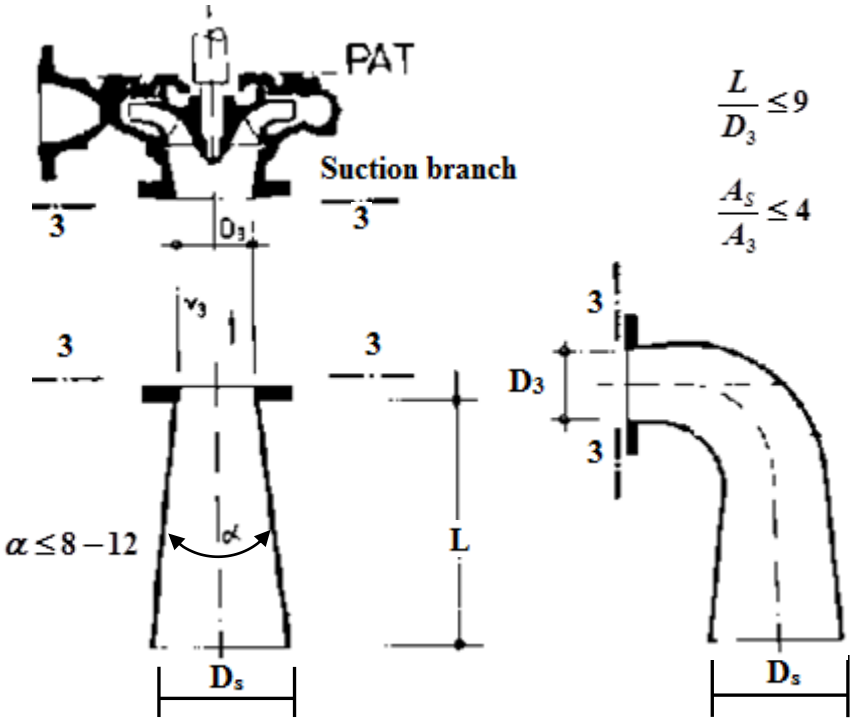

Figure 3-5: Typical draft tube design and main dimensions (according to Lein) [6]

.

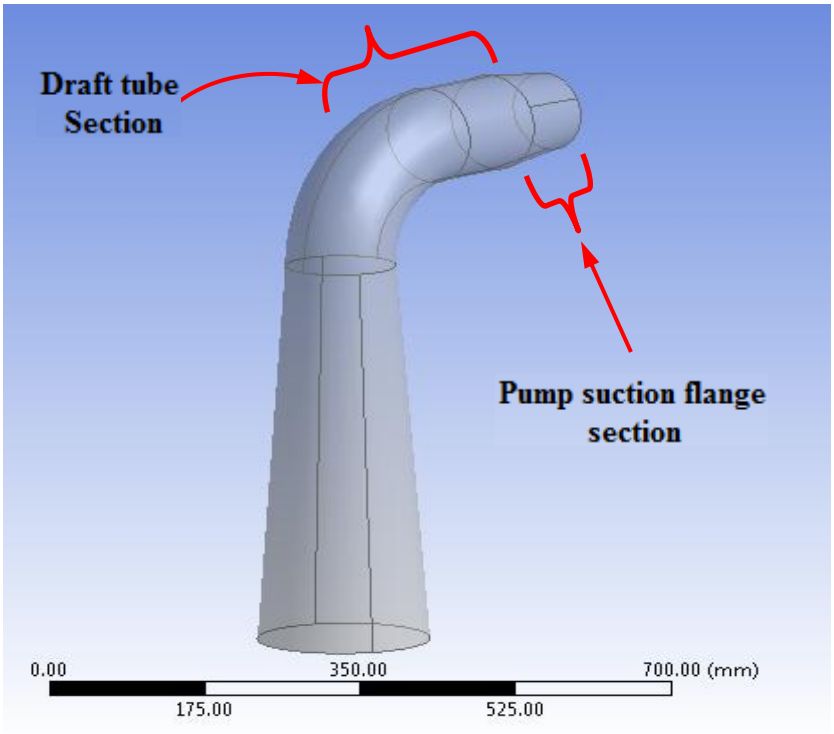

Figure 3-6: Draft tube fluid volume

3.3.2. Mesh Generation

Meshing is the process of discretizing of a region under consideration in to a set of control volume. Mesh for different components of the PAT system like volute casing, impeller and draft tube fluid volumes are generated in Ansys ICEM.After modeling of the geometry of impeller and volute is finished, the two components were exported to design modeler in Ansys workbench using '.stp' format. As it can be seen from the workflow diagram in Figure 3-9, since the volute casing and impeller are imported together, they are meshed in a single meshing cell, while the draft tubed is meshed using a separate meshing cell.

When the ANSYS meshing application is launched from the ANSYS workbench project schematic, the physics preference will be set based on the type of system being edited. In this case CFD is selected in the physics preference.

There are basically two ways of making a computational mesh; one is to use the software that produces an unstructured mesh automatically and the other is to use structured mesh through manual input. The advantage of the unstructured mesh is that it is quick to make but on the other hand, many elements may have sharp corners and the size difference between neighboring

elements may be large which is bad with respect to numerical error. A structured mesh is assumed to be better with respect to numerical error but is on the other hand tedious to make.

Since the preparation of structured grid is very time consuming task, unstructured grid with tetrahedral elements has been used to discretize and generated all components of PAT fluid domains. The automatic meshing method used in Ansys mesh is sweep/patch conforming method. These methods are useful to mesh multi-body part at the same time but when the mesh does not need to be conformal.

The Global settings are categorized into the different groups and are available through drop-down menus. Advanced size function is set to 'Proximity and Curvature' to capture the small curvature surrounding, the impeller. The next step is to define the relevance center to allow control over the fineness of the mesh for the entire model. The finer the mesh, the more accurate the result but more time consuming and the coarser the mesh, the less accurate the result becomes. So compromise between the two should be made to get good result in short duration of time. Thus medium is selected. Table 3.2 shows the mesh statistics of PAT with 5 blade impeller and draft tube model. After domains are meshed in to control volumes, boundaries of the domains are selected and named so that the region on which boundary conditions are applied can be searched easier and faster.

Table 3.4: Mesh statistics of different components of PAT system

	Tetrahedral elements	
Component	**Number of Elements**	**Number of Nodes**
Impeller	325878	8258
Volute Casing	138437	73301
Draft tube	83571	33732
Total	547886	117303

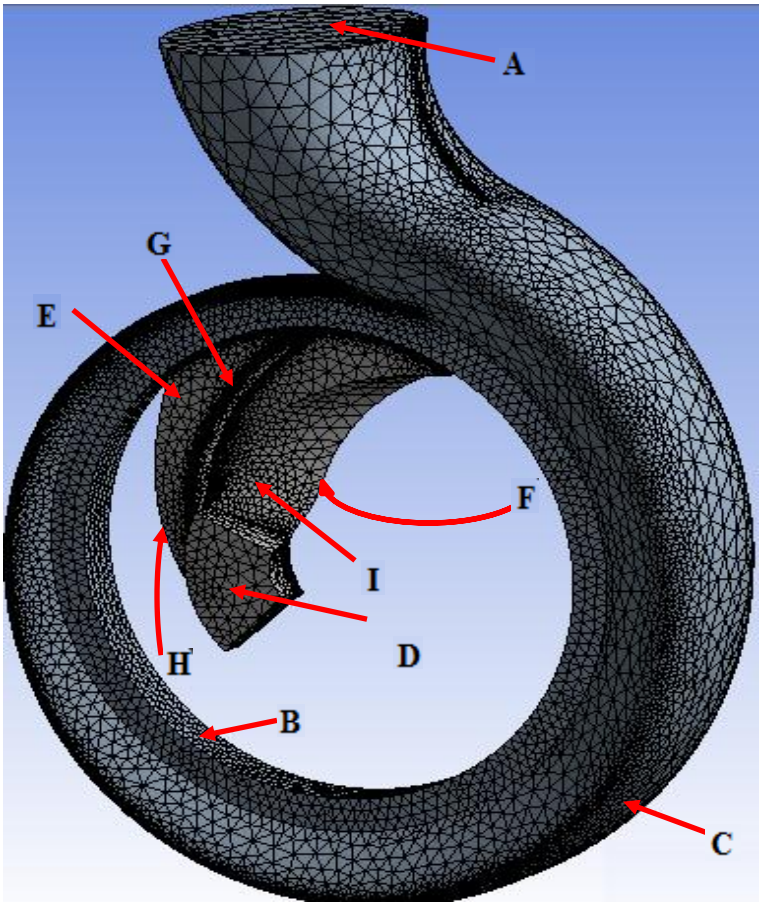

Boundary Names

A - Volute casing inlet

B - Volute casing wall

C - Volute interface

D - Impeller outlet

E - Impeller hub

F - Impeller shroud

G - Impeller blade

H - Impeller periodic surface 1

I - Impeller periodic surface 2

Figure 3-7: Meshed volute and impeller fluid domains with PAT boundary names

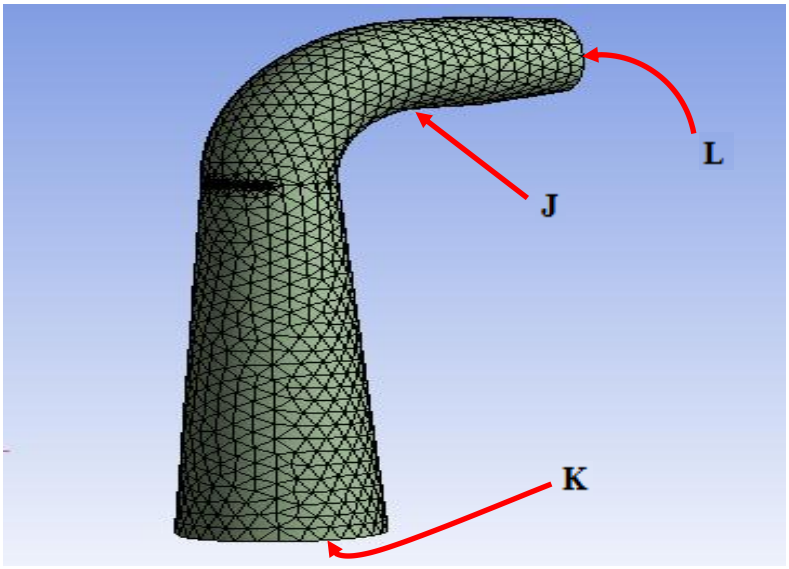

Boundary Names

J - Draft tube wall

K - Draft tube outlet

L - Draft tube interface

Figure 3-8: Meshed draft tube fluid domain with PAT boundary names

3.3.3. Pre-processing in ANSYS CFx

The pre-processing is made using ANSYS CFX .After the volute and impeller components are meshed, mesh cell displays a 'right mark' to show meshing has completed. Then the mesh files are automatically transferred to the setup cell of the project scheme. When simulation includes draft tube, the draft tube mesh file is transferred by dragging the mesh cell in which the draft tube mesh generated to the PAT setup cell of the workbench project scheme. Figure 3-9 shows the work flow used to simulate the PAT and draft tube. After the mesh file is transferred to the setup cell, preprocessing starts in Ansys CFX. The transferred mesh file contains information about the boundary name.

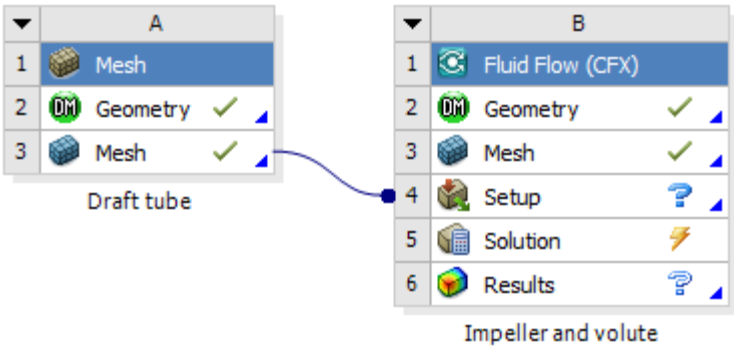

Figure 3-9: Overview of Ansys workbench workflow of PAT with draft tube simulation.

3.3.3.1. Analysis Type

In each "Flow Analysis" in ANSYS Pre there is a tab called "Analysis Type". This is where whether steady-state or transient simulation is defined, and Thus for PAT simulation case, the steady state option was chosen.

3.3.2.2. Domains Definition

For the simulation of the PAT alone, two fluid domains were created; one for the stationary volute and the other for the rotating impeller by clicking the '**domain**' icon on the toolbar. After clicking the domain icon, the domain details view appears in the workspace.

On basic setting tab in the workspace, the reference pressure, turbulence model, fluid type and domain motion are defined. The reference pressure in both domains was set to 1 *atm*. The k-ε

model is selected for turbulence model with scalable wall function. The fluid type for both domains is selected from the CFX data base. The fluid type used for the PAT simulation is summarized in Table 3.3.

Table 3.5: Material property of liquid water

Material	Reference temperature, ^{o}C	Molar mass, M Kg/Kmol	Density, ρ Kg/m^3	Specific Heat, C_p J/Kg-K	Dynamic viscosity, μ Kg/m-s
Water	25	18.02	997	4181.7	0.0008899

The domain motion for the volute domain is set to stationary while for the impeller domain, the domain motion is set to rotating and angular velocity is specified. The impeller domain is made to rotate at angular velocity 157.08 rad/s (1500 RPM). In this case the angular velocity is positive because the domain was modeled to rotate in the positive rotation direction about the z-axis.

3.4.3.3. Setting Boundary conditions

The stationary and the rotating component boundary conditions of the whole PAT domain are summarized in Table 3.4 according to the boundary names give in Figure 3-7 to 3-8. For boundary or region under consideration, boundary condition is set using the '**Boundary**' icon on the toolbar.

The inlet and outlet boundary condition were set by imposing a constant 0 Pa total pressure on the casing inlet surface and variable mass flow rate on the impeller outlet surface respectively. 5% medium turbulence intensity for the inlet conditions is considered. For the simulation where draft tube is involved, the boundary condition imposed on impeller outlet is used on draft tube outlet surface. Figure 3-10 shows the PAT model after all boundary conditions imposed on the fluid domains.

Table 3.6: Summary of boundary conditions for PAT model

Domain Name	Domain motion	Surfaces	Boundary Condition
Volute	Stationary	Volute casing wall	Smooth no slip wall
		Volute casing Inlet	Inlet
Impeller	Rotating	Impeller Hub	Smooth no slip wall
		Impeller Shroud	
		Impeller Blade	
		Impeller Outlet	Outlet
		Impeller Periodic surface 1	Periodic
		Impeller Periodic surface 2	
Draft tube	Stationary	Draft tube wall	Smooth no slip wall
		Draft tube outlet	Outlet

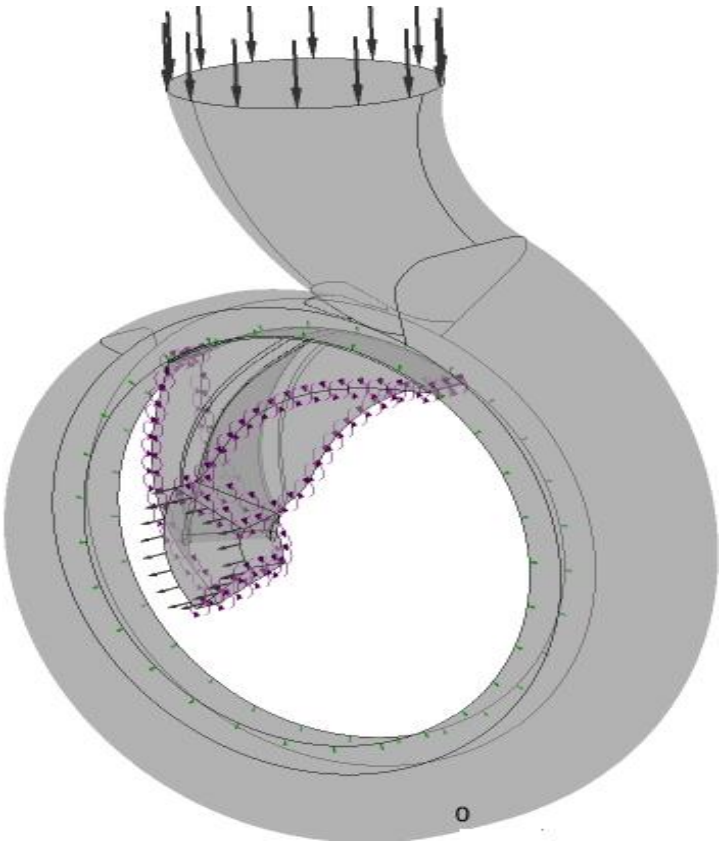

Figure 3-10: PAT model with boundary conditions

3.3.3.4. Setting Interface

There exists one interface between two domains when simulating a PAT model. The interface is found between the stationary volute and rotating impeller domain. When draft tube is included in the simulation, a second interface exists between stationary draft tube and rotating impeller domain. Interface between domains is created using the '**interface**' icon  on the toolbar.

Between volute and impeller domain, the interface is created first by defining the interface type between these domains .The interface type is set to fluid-fluid interface. The next step is to define the interface sides on which connection between the domains surface exists. This is done by selecting individual domain name and the location of both domains. For the first interface side the volute domain is selected and 'Volute interface' surface is selected as location whereas the 'impeller interface 1' surface on the impeller domain is selected for the second interface side.

The General Grid Interface (GGI) connection option is chosen as interface model to be used on the two separate individual rotating and stationary domains. Frozen rotor is used for the frame change/mixing model. The same technique is used to create the interface between draft tube and impeller domain.

3.3.3.5. Solver Control and Output

Setting solver control in Ansys CFX involves defining advection scheme, turbulence numeric and convergence criteria. The default advection scheme, high resolution, is chosen because it is recommended by ANSYS [14] for simulations involving liquid pumps and turbines.

First order upwind is used for turbulence numeric option since this setting gives the most robust performance of the CFX solver. The residual is the most important measure of convergence, as it relates directly to whether or not the equations have been solved. A residual level of 10^{-4} is considered as a relatively convergence criteria by ANSYS [14].

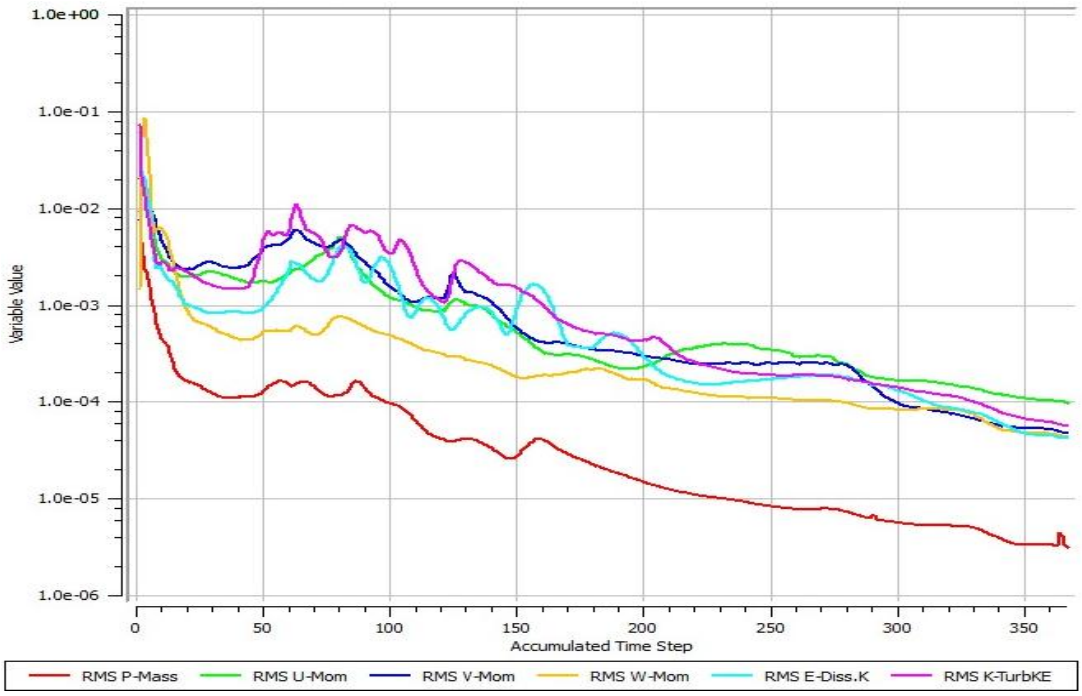

Figure 3-11: Convergence plot residual values for mass, momentum and turbulence

3.3.3.6. Solution Initialization

Initialization in Ansys CFX is done by providing initial guess values to solve the governing equation so that the flow field variables can be solved by iteration toward the solution. By clicking the '**Global Initialization**' icon on the toolbar, the initial values are specified. The default automatic initialization for the velocity and static pressure is used to provide a start point to the solution.

3.3.4. Processing in Ansys CFX Solver

After defining the required boundary condition and solution initialization on the PAT fluid domain, the preprocess stage in Ansys CFX is completed. In this case, setup cell displays a 'right mark' to show setup is finished. Then the setup files consisting of the necessary information to solve the PAT model is transferred to solution cell of the project scheme. When solution starts, plots of residual and other solution monitors are displayed on separate tab. One of the most important features of ANSYS CFX is, it uses a coupled solver in which all the hydrodynamic equations are solved as a single system. The coupled solver is faster thus less iteration is required to obtain a converged flow solution [14].

3.3.5. Post Processing in Ansys CFX Post

The CFD-Post for ANSYS CFX, is a flexible, state-of-the-art post-processor for CFD products. It is designed to allow easy visualization and quantitative analysis of the results of CFD simulations once the solution converged. It supports a variety of graphical objects and locator objects that are used to create post-processing plots and quantitative calculation.

The graphical objects that are helpful to visualize the flow pattern through the PAT include contour plots of velocity and pressure on a surface and velocity vector plots .The color bar in the legend indicates the magnitude these variables.

The quantitative results for PAT in Ansys CFX post can be obtained using the built- in function calculator. By setting the locations, function and variable to be calculated, the numerical value of the variable can be obtained.

The function that's used to calculate the **total pressure** on the surface is **massFlowAveAbs**. This function takes and calculates the average variable on any 2D region of the domain weighted by the mass flow at each point on the location in absolute frame of reference.

The Ansys CFX outputs used to evaluate the performance of PAT are:-

Total pressure at the inlet, TP_{in}
Total pressure at the outlet, TP_{out}
Impeller torque, T (about z-axis)

CHAPTER FOUR

Results and Discussions

4.1. Introduction

This chapter deals with the simulation results of the centrifugal pump operating in pump as well as turbine mode. After collecting all the information about PAT simulation results, the results were analyzed and discussions were made on the concept established on published previous literature works. Primarily, a description of the results of the selected pump with original geometry is made to show how it operates in normal operation mode (pump mode). Then the pump operating in reverse mode (turbine mode) is discussed. Then using the simulated result of the PAT at BEP, the deviation is discussed in contrast to predicted performance using published empirical formulas. After that, the effect PAT speed on performance is discussed. Lastly, the effect of adding draft tube on the discharge end of the PAT and impeller tip rounding on PAT performance is discussed in contrast to the original non - modified geometry based on obtained results.

4.2. Pump Mode Performance

In order to begin the investigation of the PAT performance, it is mandatory to check the pump mode performance of the model under consideration whether it coincides with the experimental data. For this reason, the simulation of the model operating in pump mode is performed at the design rotation speed of 2960 RPM (310 rad/s). By using these results obtained from the simulation, the data are reported in Table 4.1. Finally comparison where made between the experimental data and numerical result.

4.2.1. Pump Mode Graphical Display Results

In order examine the flow characteristics of centrifugal pump operating in normal mode, pressure and velocity contour plots and vectors are used. The streamlines of the 3D models are plotted at design point to examine the flow pattern within the centrifugal pump.

4.2.1.1. Static Pressure Distribution for Centrifugal Pump Model

Figure 4-1 shows the static pressure distribution of the 3D centrifugal pump model. From the figure, it can be observed that at the suction side of the pump, a minimum value of the static pressure is seen where the leading edge of the blades is located.

When kinetic energy is imparted to the fluid, as it flows from the inlet (leading edge) to outlet (trailing edge) of the impeller, the static pressure gradually increases. It is clearly seen in the figure that a high pressure region is observed on the pressure side while a low pressure region is seen on the suction side of the impeller at the same radial position.

As the fluid lead its way to volute casing, the static pressure further increases. This is due the conversion of the kinetic energy of the fluid to pressure energy as a result of increasing cross-sectional area of the volute casing. Finally as the fluid flows through the diffuser end of the pump volute, the fluid attains a maximum pressure at delivery side of the pump. In order to clarify how the fluid acts within the fluid volume, the 2D static pressure distribution on the mid plane of the centrifugal pump shown in Figure 4-2 is used.

Figure 4-3 shows graphical display of the static pressure distribution at different flow rate within the pump fluid domain. It can be seen from Figure 4-3 that, the static pressure decrease as flow rate changes from lower to higher values.

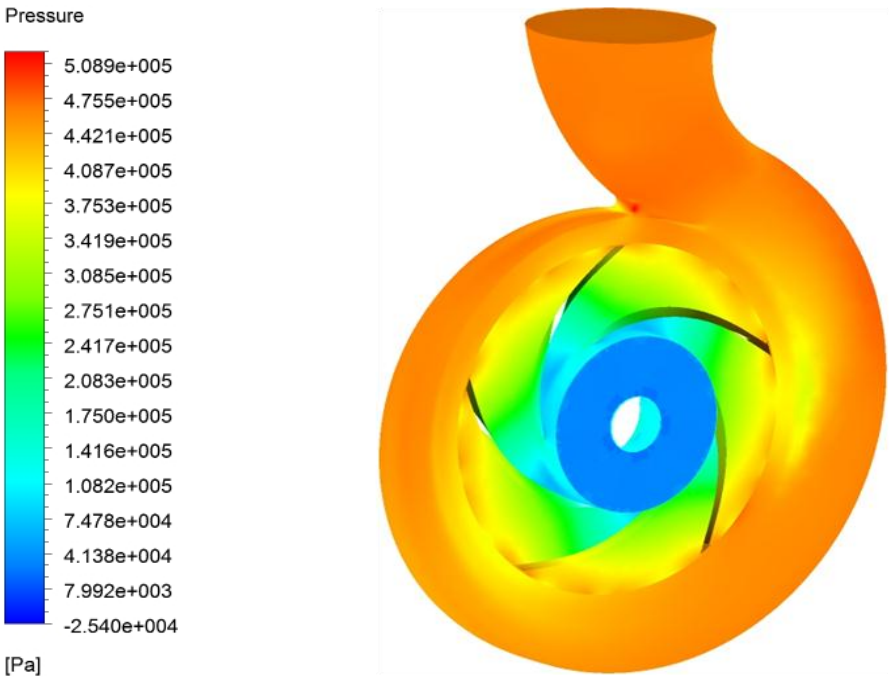

Figure 4-1: 3D Static pressure (gauge) distribution for selected centrifugal pump model at Q_p = 0.025m^3/s

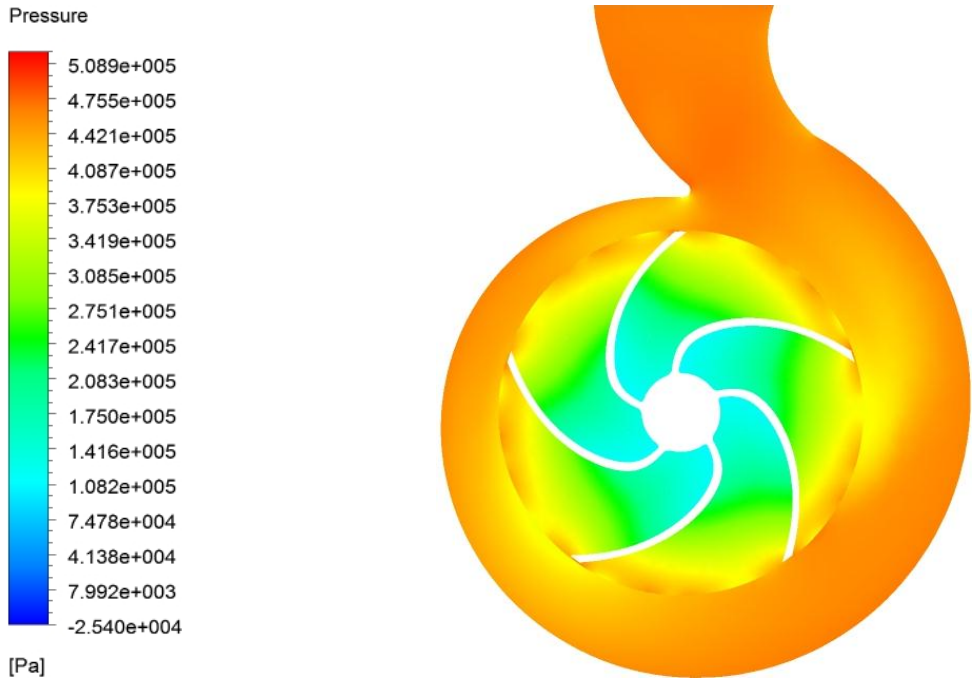

Figure 4-2: Static pressure (gauge) distribution for selected centrifugal pump model on mid impeller plane at Q_p = 0.025m^3/s

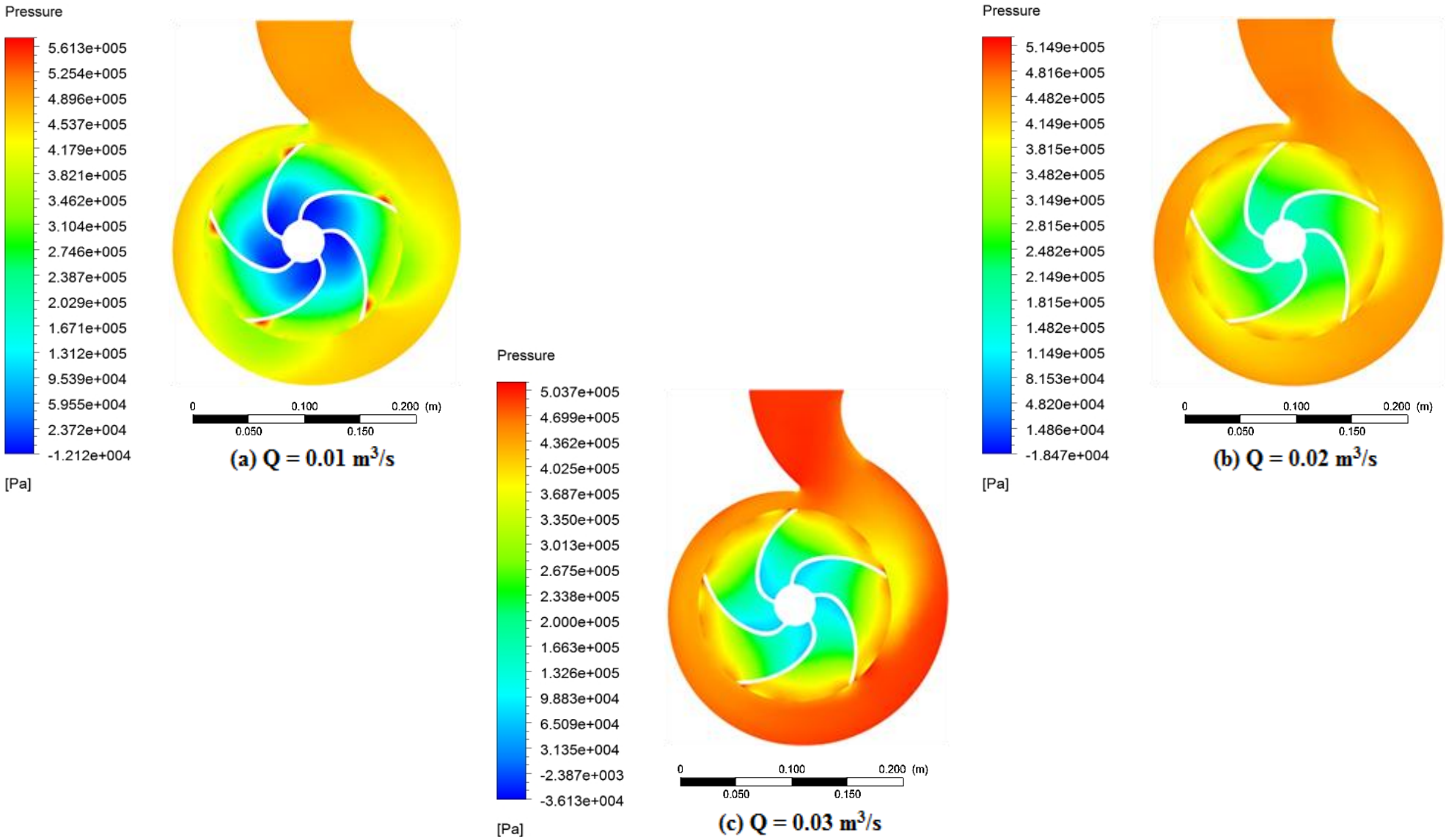

Figure 4-3: 2D Static pressure (gauge) distribution contour plot for selected pump model at different flow rates

4.2.1.2. Velocity Distribution for Centrifugal Pump

Figure 4-4 shows the stream-line in the centrifugal pump colored by absolute velocity distribution. It can be seen in the figure that, the absolute velocity of the fluid increases as the fluid flow within pump impeller.

To permit good visualization of flow within the impeller blade passage, the absolute velocity distribution in Figure 4-6 at different stream-wise locations of 35, 65 and 90 % is used. It can be seen from the figure that as the water flows in the passage while the impeller rotates, the absolute velocity continuously increases in the stream-wise direction from the leading edge to the trailing edge.

As the fluid progresses smoothly to volute casing and flows through the fluid domain, the absolute velocity gradually decreases. The absolute velocity decreases as a result of the increase in cross – sectional area of the volute in transverse direction. The absolute velocity distribution within the pump can be clearly represented using Figure 4-5.

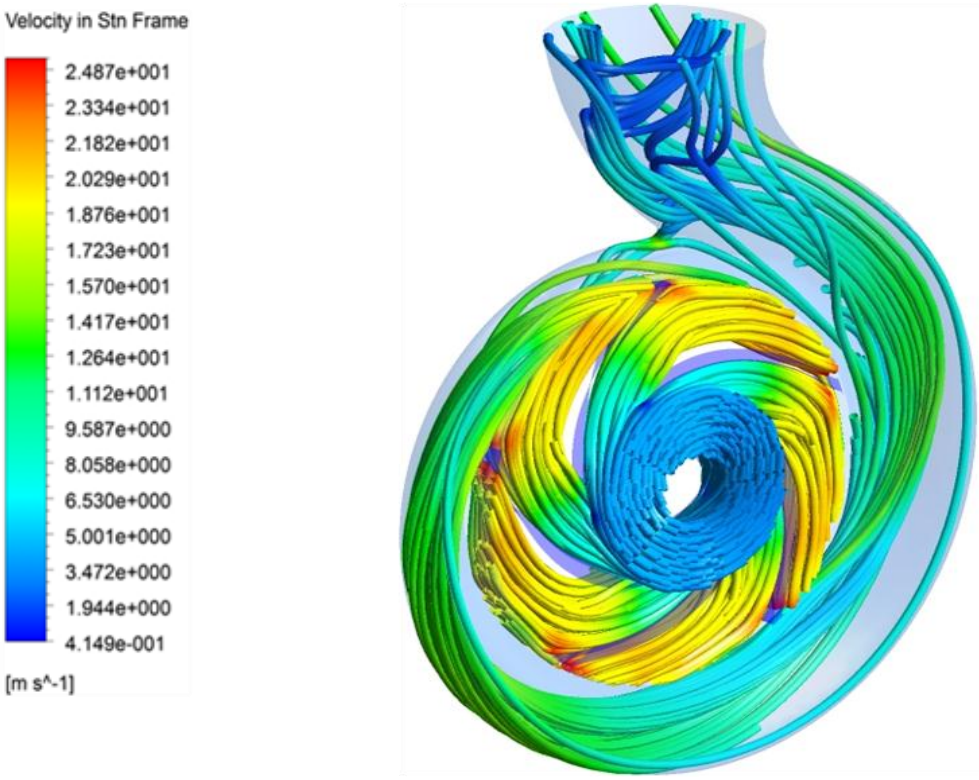

Figure 4-4: 3D stream - line plot colored by absolute velocity distribution for selected centrifugal pump model at Q = 0.025m^3/s and N_p = 2960 RPM

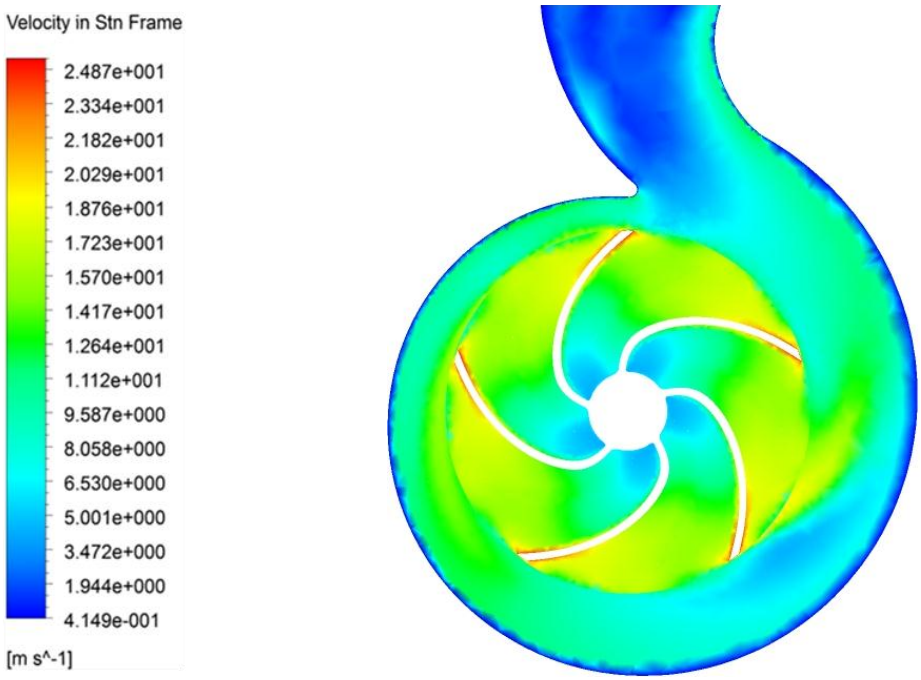

Figure 4-5: 2D Velocity contour colored by absolute velocity distribution for selected centrifugal pump model at Q_p = 0.025m^3/s and N_p = 2960 RPM

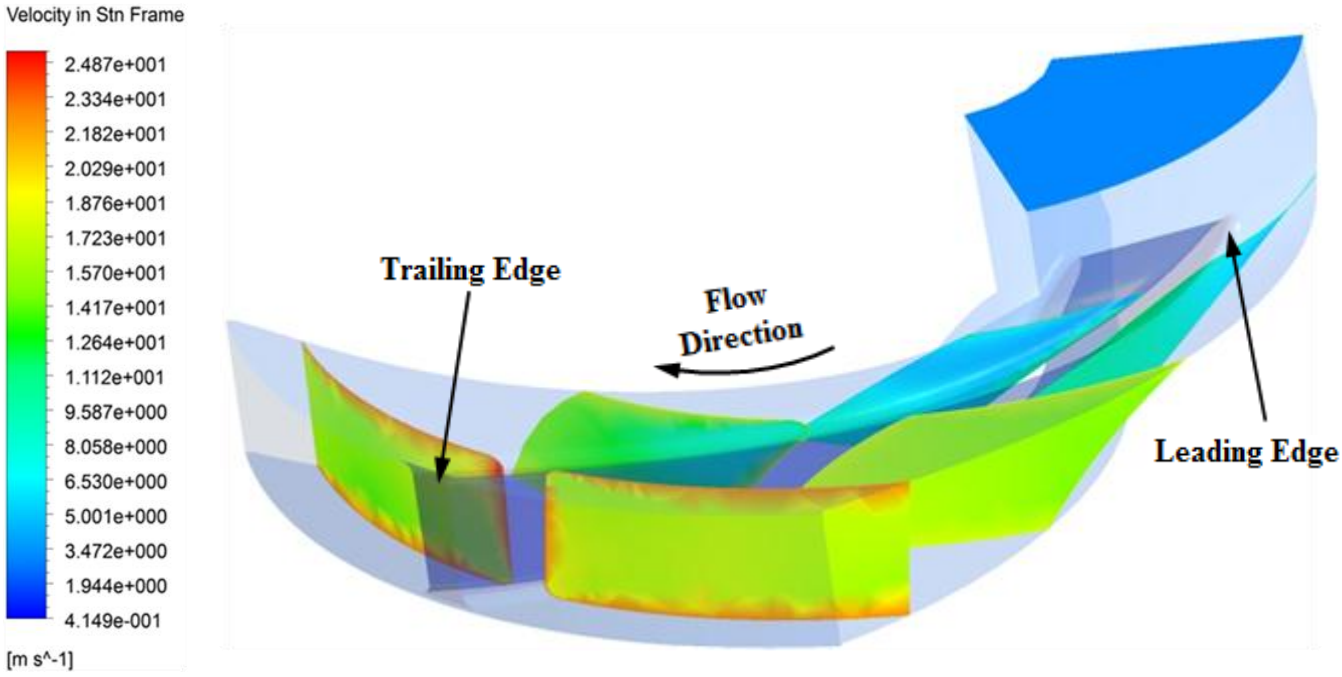

Figure 4-6: Absolute velocity distribution of centrifgual pump model through impeller blade passage at Q_p = 0.025 m^3/s and N_p = 2960 RPM

4.2.2. Pump Mode Performance Evaluation and Characteristic Curve

The overall pump mode performance characteristics curve of a pump consists of the relation b/n pump head and flow rate together with pump efficiency and flow rate. The flow rate data's are located on the x - axis while both head and efficiency on the y - axis of the performance curve.

To start with, the important parameters computed from the numerical simulations used for the calculation of head and efficiency are ***total pressure*** at the inlet and outlet of the pump and the ***torque*** exerted on the pump.

Simulations at different operation point are carried out to generate the characteristic curve of the pump. The values on Table 4.1, obtained from the numerical simulation together with experimental test, are plotted on Figure 4-7 and 4-8. The experimental data's is obtained through the tests conducted by Addis Ababa Institute of Technology; Mechanical engineering department.

Figure 4-7 shows the variation of flow rate with developed pump head. From the figure, it can be seen that the head developed by the pump decreases as the flow rate increases.

While Figure 4-8 shows the variation of flow rate with overall and hydraulic efficiency of pump for experimental and CFD results respectively. In the Figure, it can be observed that the efficiency of the pump increases when flow rate increases until it reaches peak value. At flow rate Q = 0.025 m^3/s, the pump attains a maximum efficiency.

In both Figure 4-7 and 4-8, the experiment results show that beyond the nominal flow rate of the pump, the head developed by the pump as well as the pump efficiency rapidly drops down.

This is because as the pump flow rate increases, the fluid pressure at the suction side of the pump becomes so lower that bubble will start to form. The formation of bubble within the fluid causes cavitation in the pump.

On Figures 4-7 and 4-8, slight variation between CFD and experiment result curves can be seen. In contrast to experiment test, CFD simulation does not consider mechanical and volumetric losses that exist within the real existing pump. As a result, slight deviation between the numerical and experiment result within reasonable range is observed.

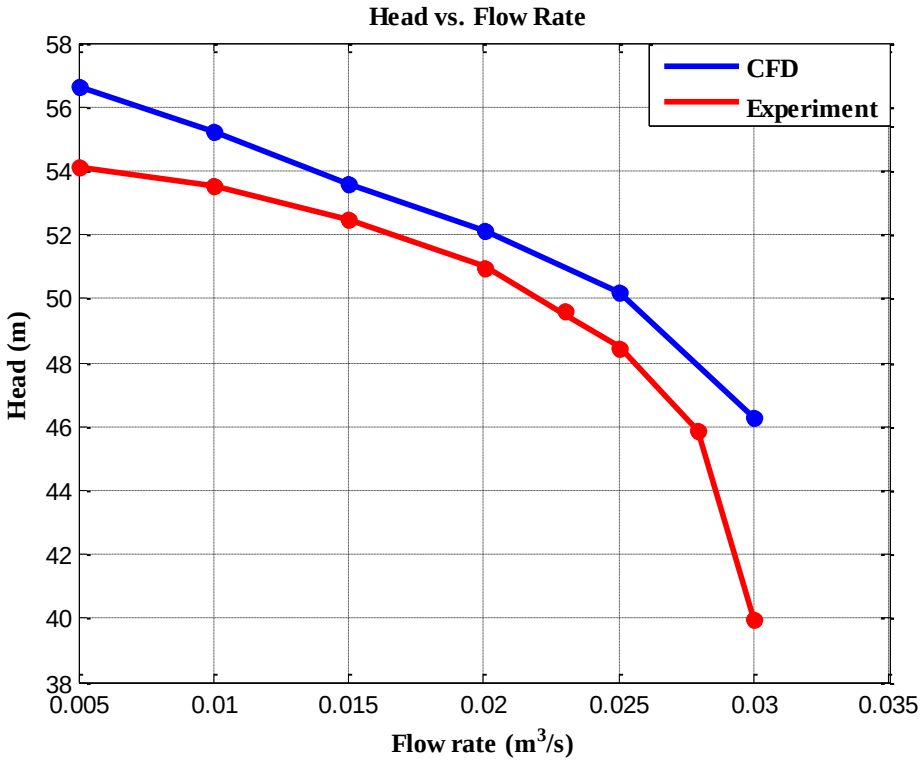

Figure 4-7: Pump head vs. flow rate characteristics curve of selected pump model at N_p = 2960 RPM

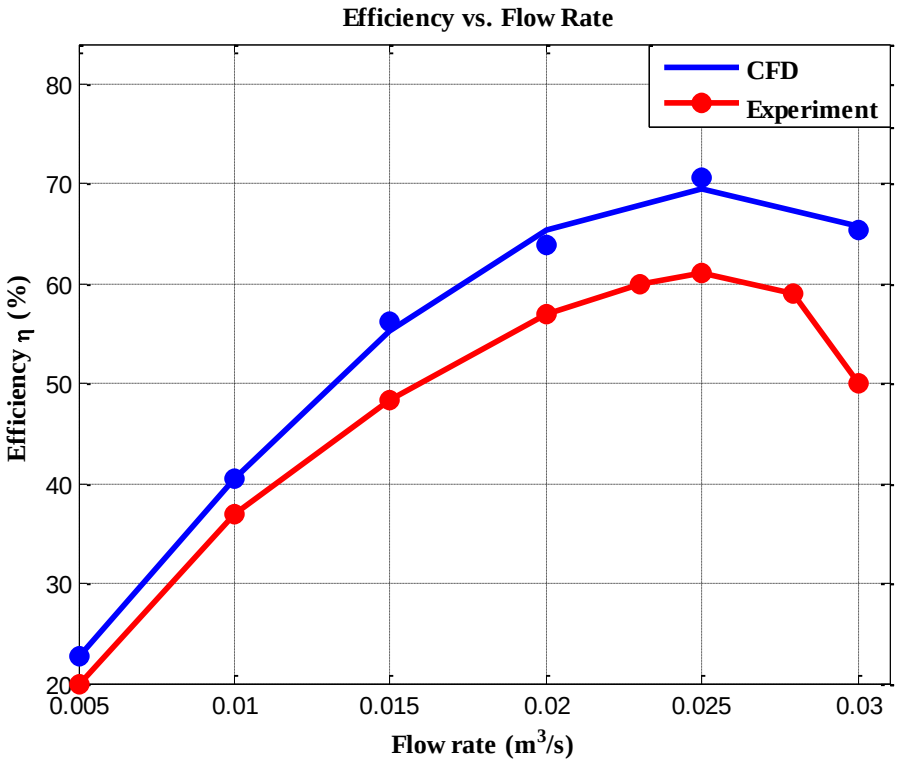

Figure 4-8: Pump efficiency vs. flow rate performance characteristics curve of selected pump model at N_p = 2960 RPM

Table 4.1: Pump mode CFD output and experimental data for selected pump model at 2960 RPM

CFD Output								Experiment Data (Source: AAIT thermal lab tested data) [19]		
Flow rate, Q (m^3/sec)	Total pressure at Inlet, TP_{in} (pa)	Total pressure at Outlet, TP_{out} (pa)	Head (m), H $\frac{TP_{out} - TP_{in}}{\rho g}$	Water Power, P_{hy}(W), $= \rho gHQ$	Torque (Nm)	Brake Power, P_b(w) $T \times \omega$	Efficiency **η**	Flow rate, Q (m^3/sec)	Head, H (m)	Efficiency **η**
0.005	100843	656129	56.604	2776.431	39.519	12249.723	0.2267	0.005	54.1284	0.20
								0.01	53.516	0.37
0.01	100951	642767	55.231	5418.1611	43.132	13369.647	0.4053	0.015	52.497	0.48442
0.015	101121	626721	53.578	7884.003	45.279	14035.153	0.5617	0.02	50.968	0.57
								0.023	49.592	0.60
0.02	101236	612543	52.121	10226.140	51.694	16023.614	0.6382	0.025	48.42	0.61
0.025	101260	593663	50.194	12310.079	56.221	17426.85	0.7064	0.0279	45.8716	0.59
0.03	101298	555393	46.289	13622.853	67.218	20835.595	0.6538	0.03	39.96	0.50

4.3. Predicted Performance of the PAT

After simulating the behavior of the pump operating in turbine mode at different flow rate values, the results obtained are graphically and numerically displayed. Based on the discussion made on the selection of PAT for Dabis Pico hydro site in **Section 3.2**, the PAT is simulated in accordance to the selected synchronous speed of a generator. Thus all the simulations of PAT were carried out at fixed rotational speed of 1500 RPM (157.08 rad/s) and with same procedure.

4.3.1. Graphical Display Results of PAT

The overall flow characteristics output of the PAT is displayed using pressure and velocity contour plots and vectors. The stream-lines as well as pressure fields of the 3D models are plotted at design and off – design flow rate values.

4.3.1.1. Static Pressure Distribution

Figure 4-9 shows the static pressure distribution of the PAT in 3D. As it can be seen from the figure, the static pressure decreased from the inlet to outlet of the PAT as the fluid flows within the domains. A high pressure region is noted at opening of the diffuser of the pump. As the flow progresses through the volute, the static pressure decreases due to increase in velocity as a result of gradual reduction of cross- sectional area of the volute casing. It is also observed that the static pressure decreases continuously along the impeller flow passage from the inner to the outer region as energy is transmitted to the blades. Figure 4-10 shows the 2D pressure distribution within the PAT at the mid plane of the impeller which permits good representation within the fluid volume.

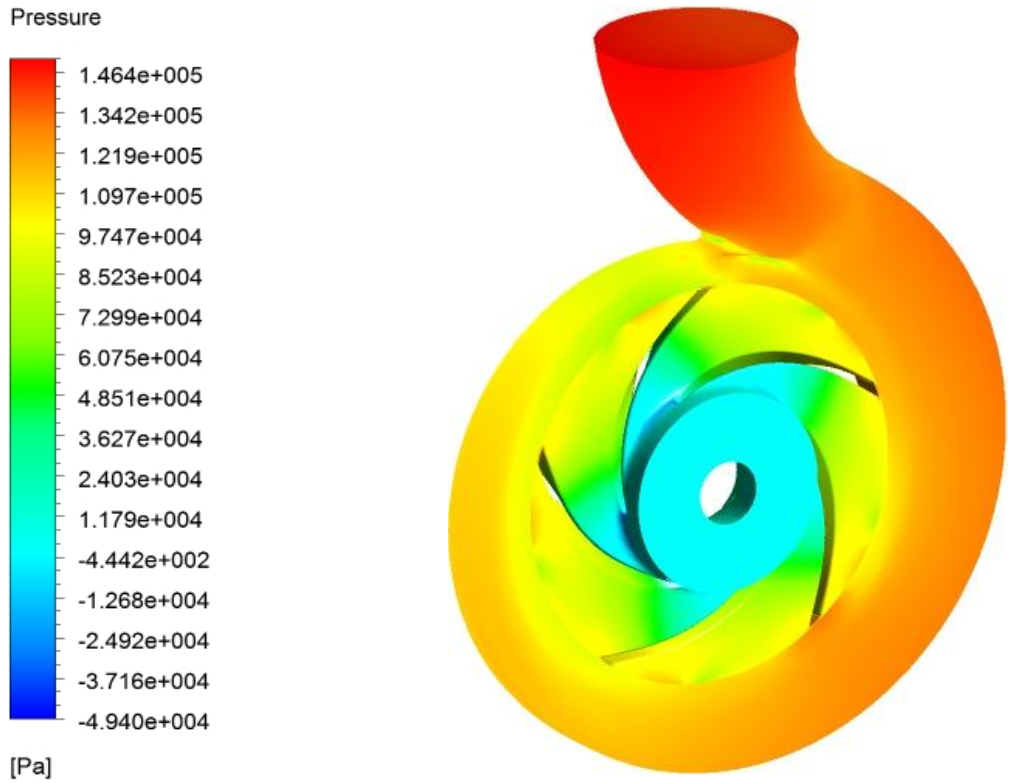

Figure 4-9: 3D Static pressure (gauge) distribution for selected PAT model at Q_t = 0.025m^3/s

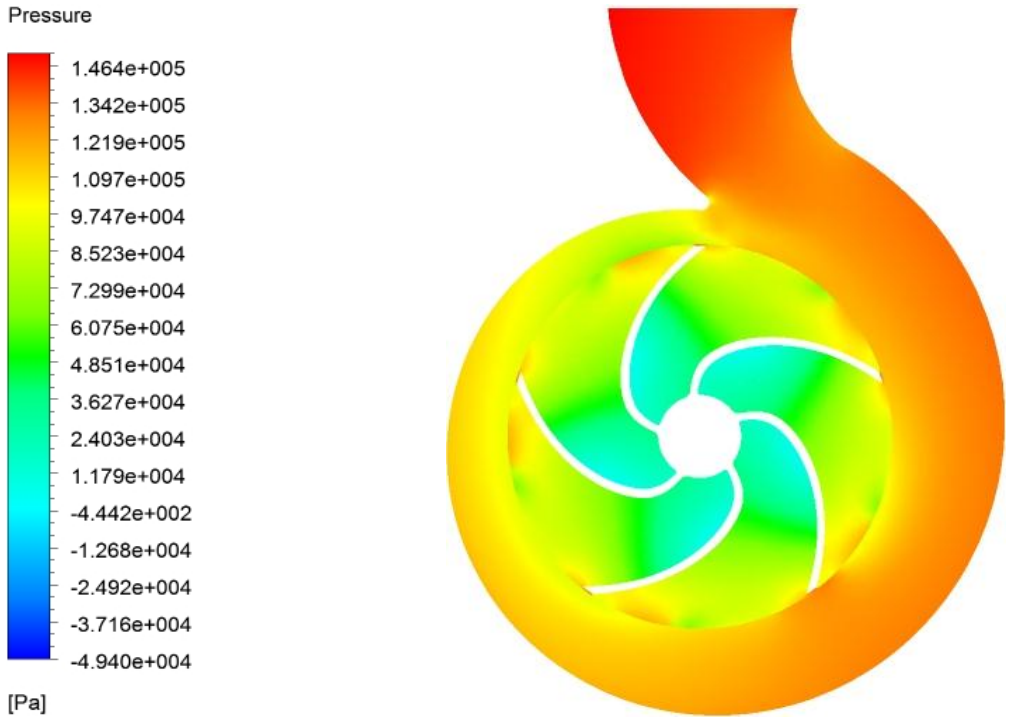

Figure 4-10: Static pressure (gauge) distribution for selected PAT model on impeller mid plane at Q_t = 0.025m^3/s

4.3.1.2. Velocity Distribution in PAT Model

Figure 4-11 shows the stream line in the PAT colored by relative velocity distribution. The velocity field indicates that according to the shape of the volute, velocity increases as the volute cross-section decreases because of the reduction of transversal area. The flow progresses smoothly through this volute region at nominal flow rate. It can also be observed that the velocity of the fluid retards after it strikes the trailing edge of the pump impeller blade. After that the relative velocity of the fluid tends to increase slightly ones again.

Figure 4-12 displays the relative velocity field with in the blade passage. It shows the velocity contour created at 20, 60, 100 % fractional stream-wise distance between the inlet and outlet in the blade passage. As the water enters in the passage way provided between the impeller blades, the relative velocity increases following the curvature of the blade in the stream wise direction since the passage narrows down gradually. Therefore, PAT as a reaction turbine, part of the work done by the fluid on the impeller is due to reaction from the pressure drop, and part is due to a change in kinetic energy.

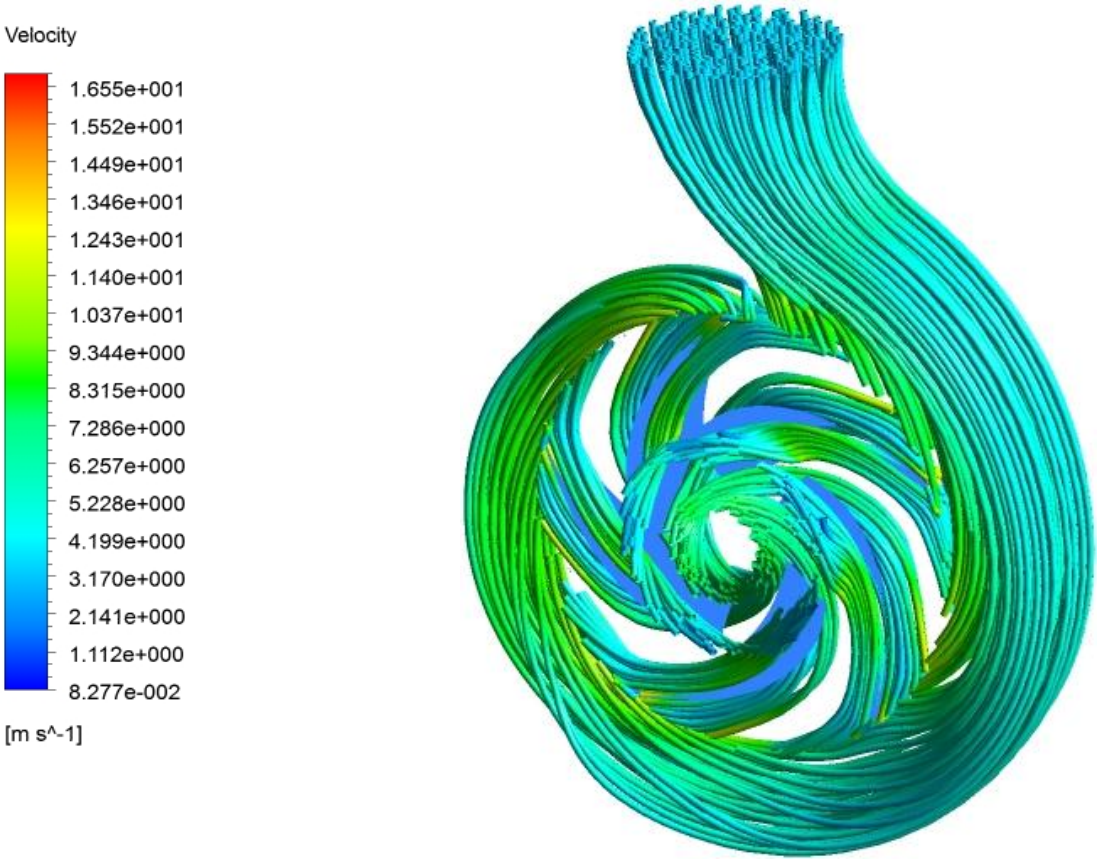

Figure 4-11: 3D stream line plot colored by relative velocity distribution for selected PAT model at Q_t = 0.025m^3/s at N_t = 1500 RPM

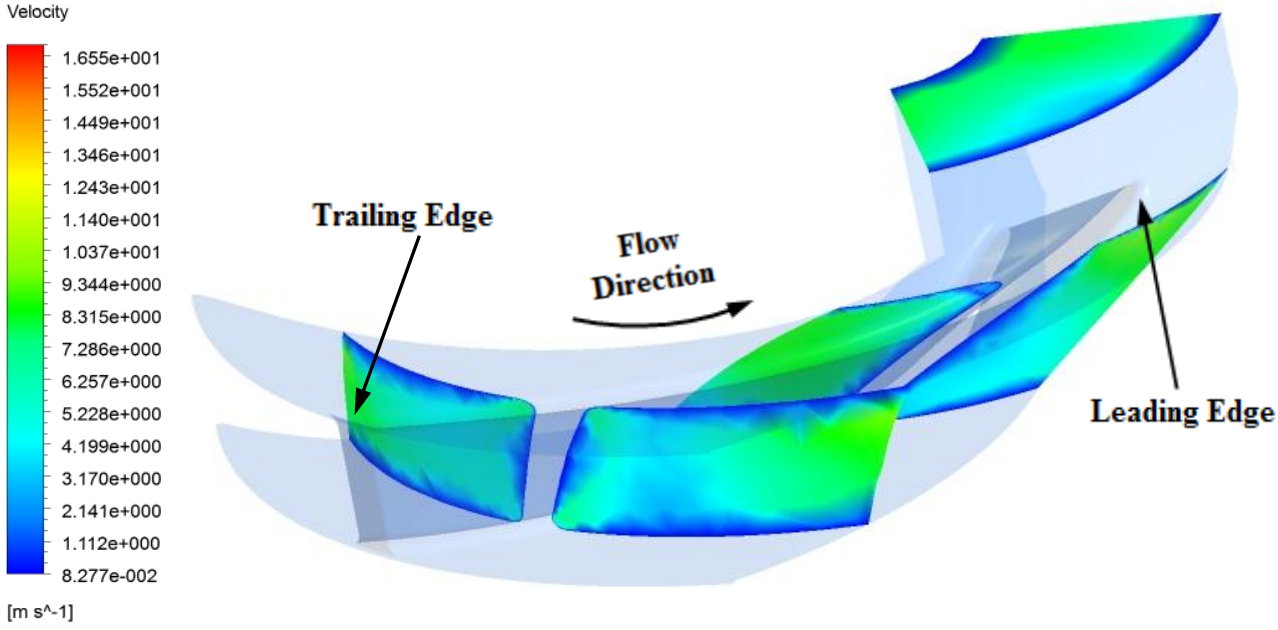

Figure 4-12: Relative velocity distribution of PAT through impeller blade passage at Q_t = 0.025 m^3/s

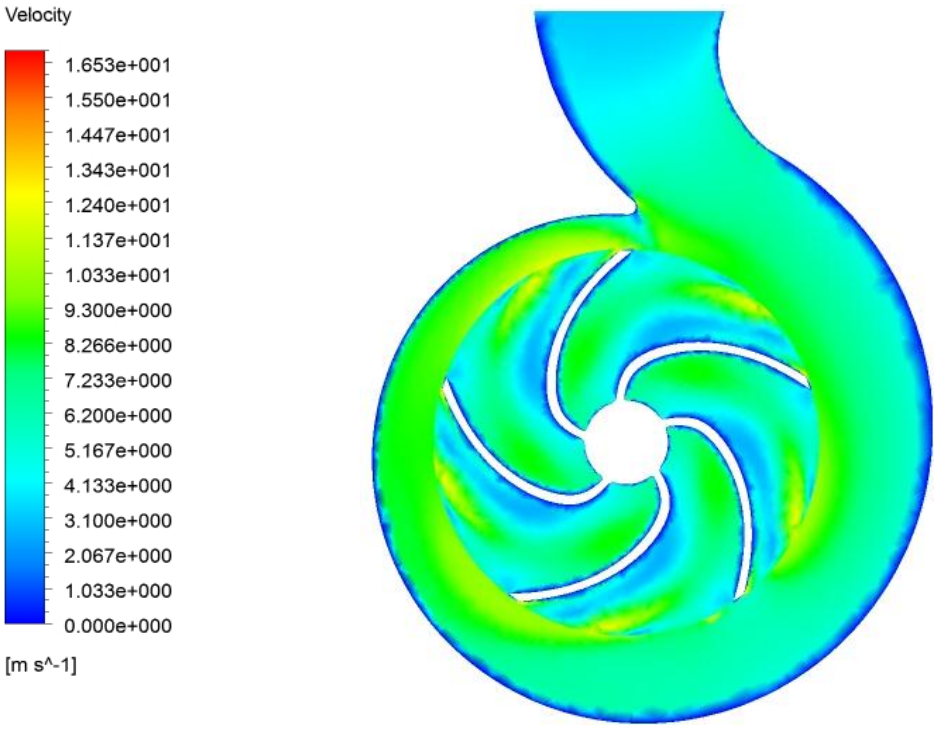

Figure 4-13: 2D Contour plot colored by relative velocity distribution for selected PAT model on impeller mid plane at Q_t = 0.025 m^3/s and N_t =1500 RPM

4.3.1.3. Static Pressure Distribution at Different Flow Rate

The static pressure distribution at different flow rate within the PAT fluid domain is graphically displayed in Figure 4-14. It can be seen from Figure 4-14 that, the static pressure decreases as flow rate reaches lowest values while increases with increasing flow rates. Comparing the three flow condition, at Q = 0.04 m^3/s, a low pressure region is seen at the volute cutwater. This region is located between the tongue and the impeller. In addition, as flow rate increases, the static pressure drop closer to the exit duct of the volute increases.

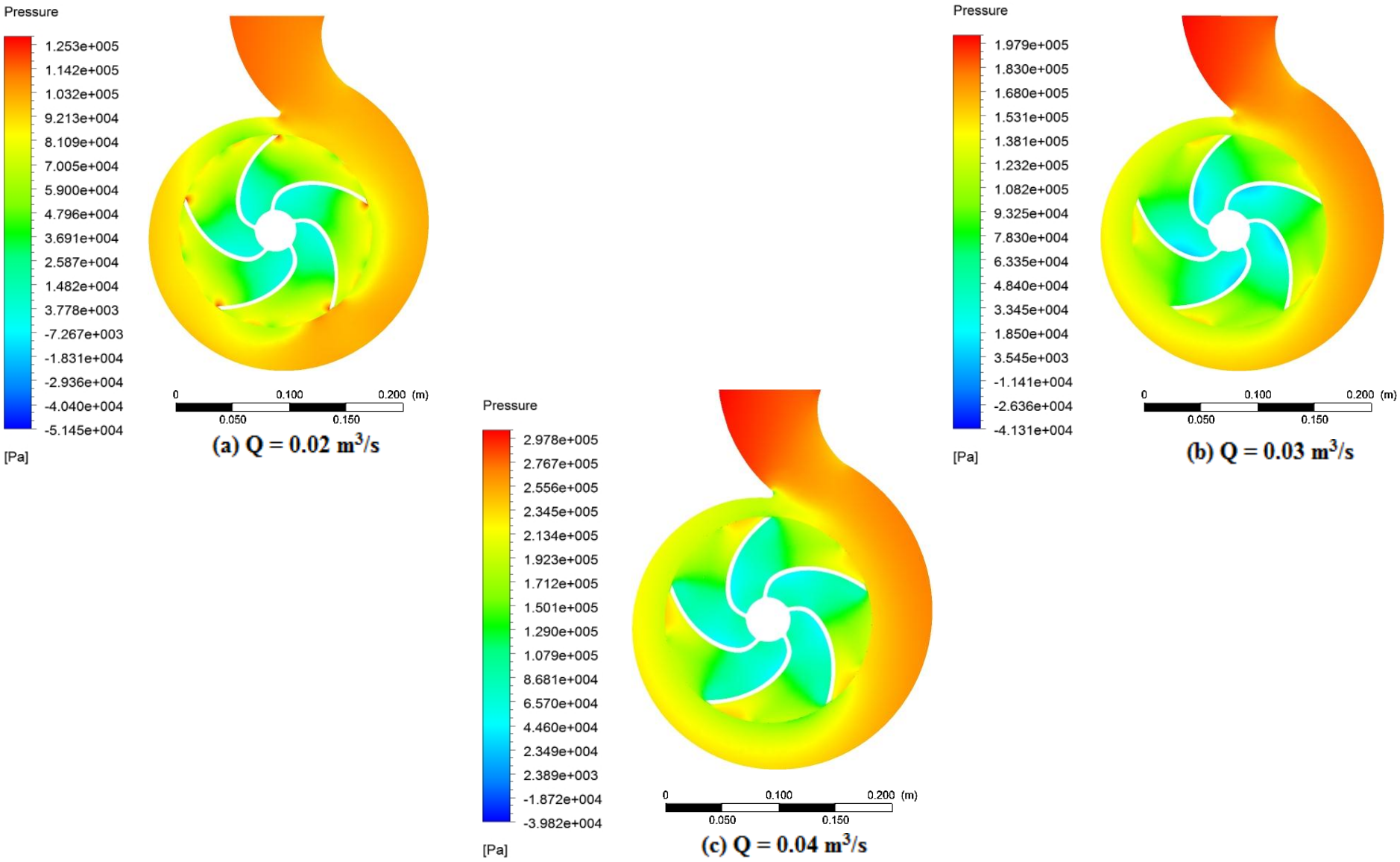

Figure 4-14: 2D Contour plot colored by static pressure (gauge) distribution for selected PAT model at different flow rates

4.3.2. Predicted Performance Curves of the PAT

The numerical results obtained from Ansys CFX are used to calculate the performance parameters of the PAT. These parameters are useful to identify the behavior of the PAT at different flow rate conditions. These parameters include the head, power, and the non-dimensionless coefficients like head, flow, and power coefficient. In the previous **Section 2.2.3**, the equation useful to calculate these parameters are clearly stated. Therefore using the output results like **torque** and **total pressure** at the inlet and outlet of PAT together with these equations, Table 4.2 is constructed. The Table shows the complete parameters used to define the performance characteristics curve of the PAT.

From Figure 4-15 up to 4-20, the effect of variation of flow rate with different performance variables of the selected PAT model are plotted and displayed. The result obtained for head and brake power variables were curve – fitted with a third degree polynomial function as a function flow rate while fourth degree polynomial function was used to show the relationship between efficiency and flow rate.

Figure 4-15 shows, the variation of flow rate versus head curve of PAT at 1500 RPM (157.08 rad/s). The figure shows the relationship that exists when the PAT is installed at different sites with available heads and the flow rate required by the PAT to operate at that particular site. It is observed that when the PAT is made to operate from low to high head condition, the required flow rate at the site increases. This implies that, if the PAT is required to operate at a site with a given head, it is required that the flow rate at that site should match the available head. And the relation between head and flow rate at 1500 RPM is shown at bottom of the Figure 4-15.

Figure 4-16 shows the flow rate-torque characteristics curve for the PAT model. It is clearly seen that, when the PAT is made to operate at different flow rate conditions with the corresponding head, the torque increases from the minimum value to maximum. But operating the PAT at hydro site having a flow rate of Q = 0.0111 m^3/s and head H= 6.67 m, will cause the impeller to stop imparting torque to the shaft thus no power output can be delivered. This point is called ’zero torque point’ and is indicated and labeled in Figure 4-16.

The relationship between the flow rate and the brake power/ power output of the PAT are indicated in Figure 4-17.The brake power of the PAT acts on the same manner with the torque as

indicated in Figure 4-17 due to the direct relationship involved with torque as shown in equation 2.3. Figure 4-18 shows the variation of flow rate with efficiency. The efficiency of the PAT increases until it reaches some flow rate value and then decrease beyond that critical operating point. This point is considered to be the ***Best Efficiency Point*** (***BEP***). The PAT operates at maximum efficiency of 66.92 % when the PAT is installed on a hydro site with 0.025 m^3/s flow rate and available head of 14.01 m.

The dimensionless coefficients are also plotted using the head and brake power results obtained from the PAT simulation. Figure 4-19 show the variation of head coefficient at different values of flow coefficient. It can be observed the head coefficient decreases as the flow coefficient increases. And Figure 4-20 shows the variation of flow coefficient with power coefficient. From the figure, it can be shown that the power coefficient acts in the similar manner with brake power of the PAT for different flow rate conditions. It is characterized by increasing in value as the flow coefficient increases.

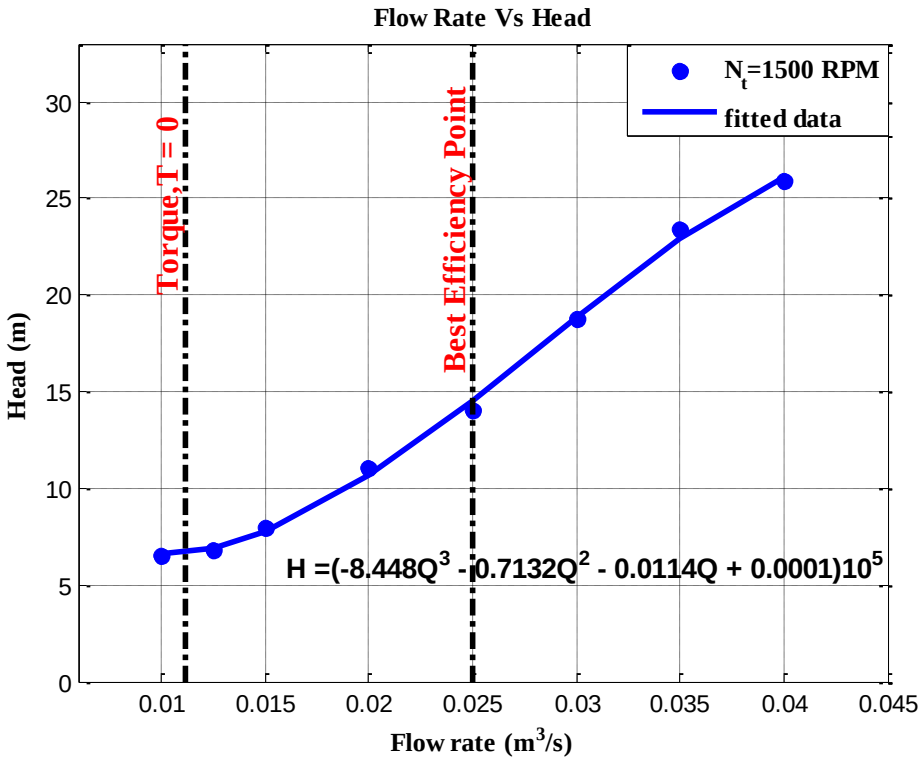

Figure 4-15: Head vs. flow rate characteristics curve for selected PAT model

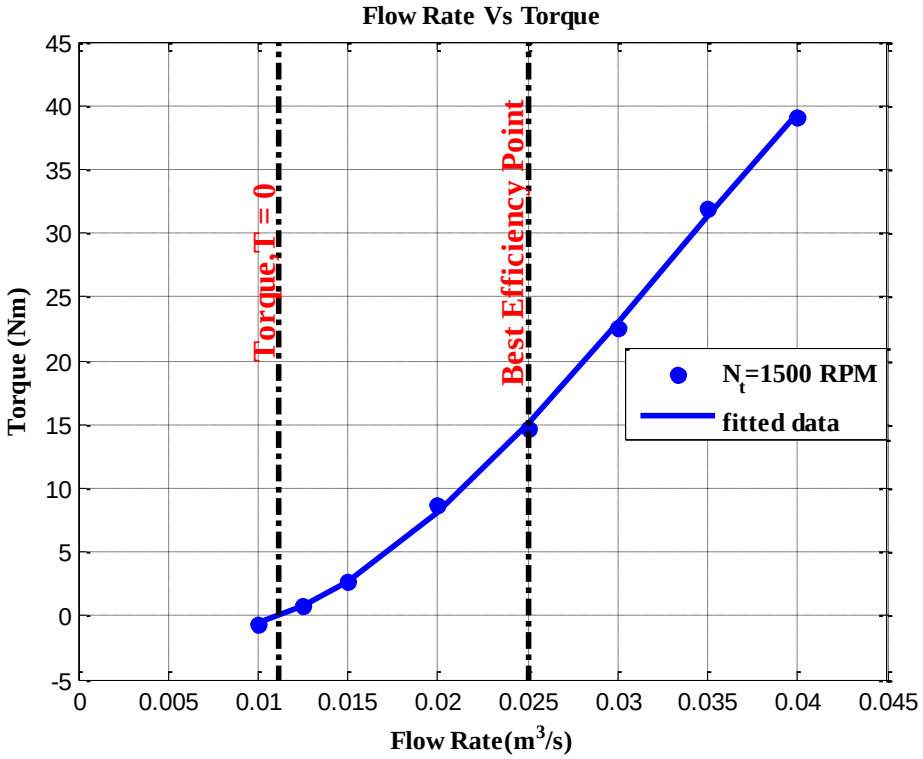

Figure 4-16: Torque vs. flow rate characteristics curve for selected PAT model

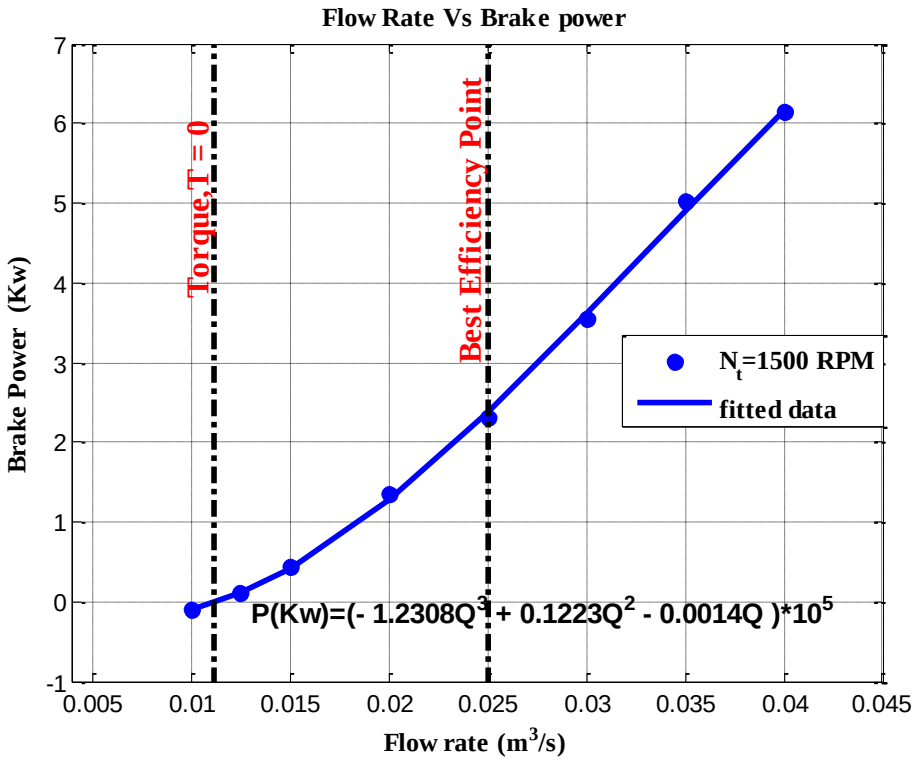

Figure 4-17: Brake power vs. flow rate for selected PAT model

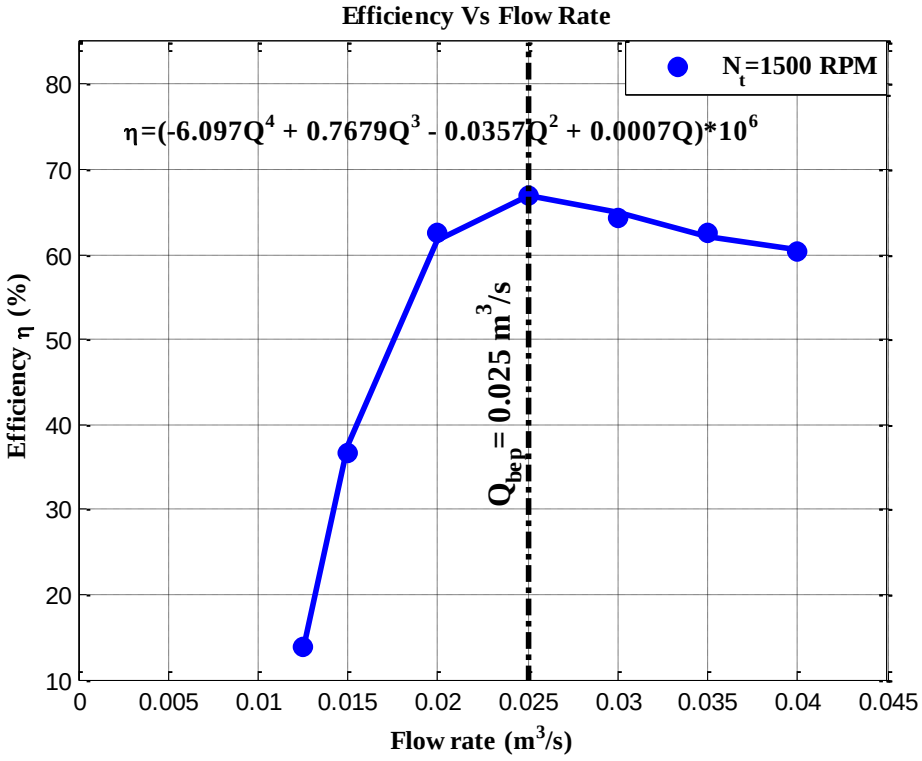

Figure 4-18: Efficiency vs. flow rate for selected PAT model

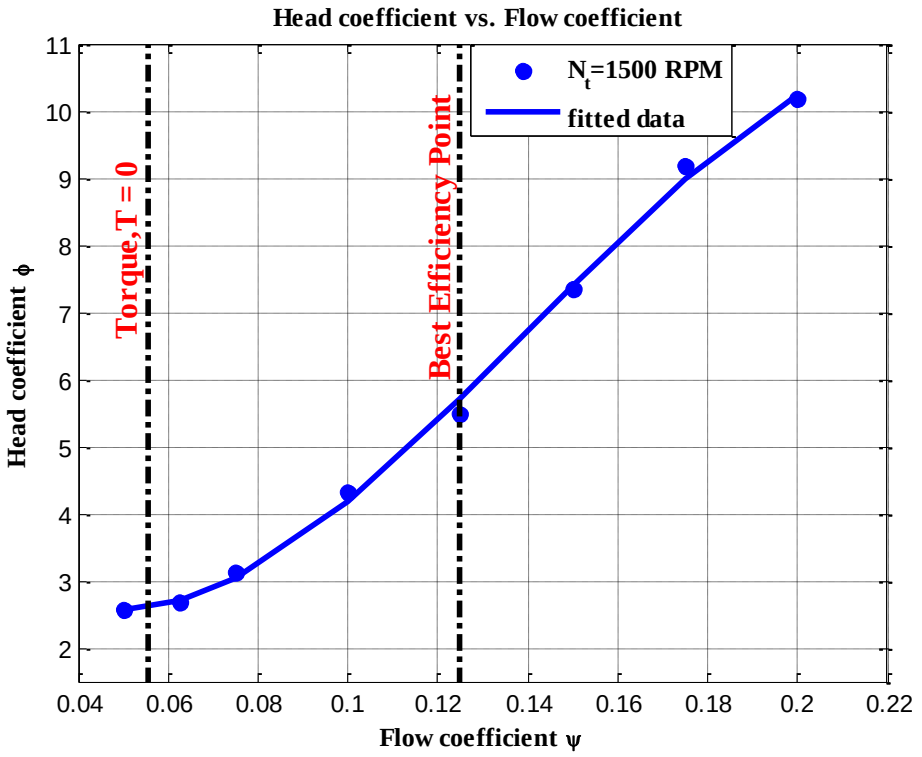

Figure 4-19: Head coefficient vs. flow coefficient curve for selected PAT model

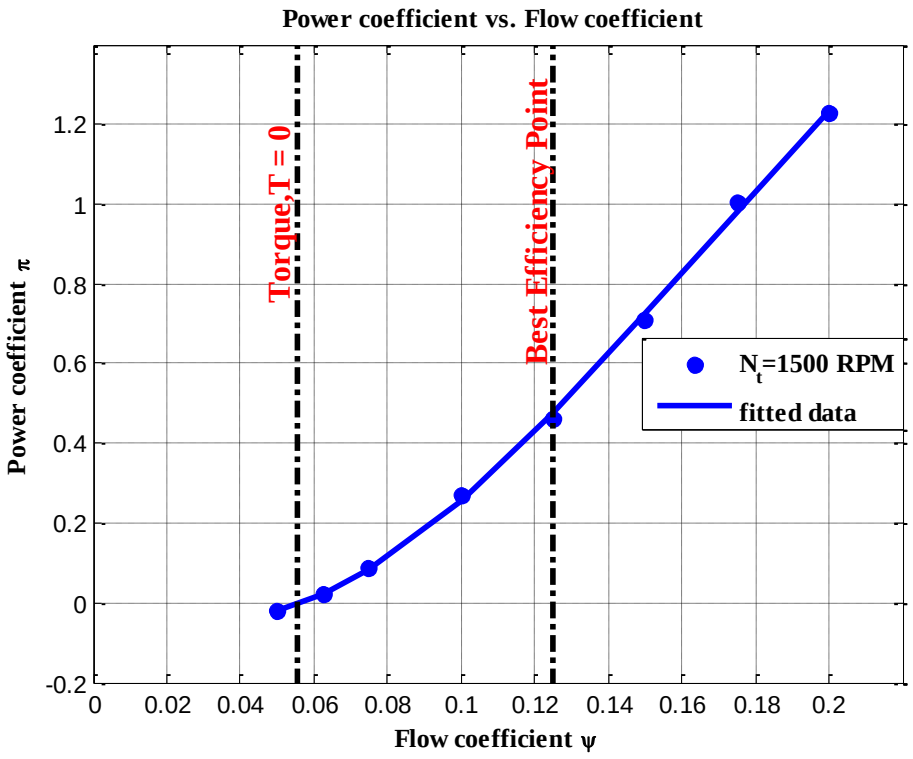

Figure 4-20: Power coefficient vs. flow coefficient curve for selected PAT model

Table 4.2: Numerical output result of a pump in turbine mode for selected pump model

Flow rate, Q (m^3/sec)	Total pressure at Inlet, TP_{in} (pa)	Total pressure at Outlet, TP_{out} (pa)	Head (m) H $\frac{TP_{in} - TP_{out}}{\rho g}$	Water Power, P_{hy}(W) $= \rho gHQ$	Torque (Nm)	Brake Power, P_b(W) $T \times \omega$	Efficiency **η**	Head Coefficient, **ψ**	Flow Coefficient, **ϕ**	Power Coefficient **π**
0.01	47872.1	111970.64	6.534	640.985	-0.6284	-98.709	-0.1540	2.564	0.05	-0.0197
0.0125	78117.1	11260.4785	6.815	835.708	0.738	115.957	0.1388	2.674	0.0625	0.0232
0.015	87055.7	8984.2865	7.958	1171.071	2.727	428.425	0.3658	3.123	0.075	0.0857
0.02	115768	7756.957	11.0103	2160.221	8.61	1352.156	0.6259	4.320	0.1	0.2704
0.025	149127	11737.95	14.01	3434.73	14.633	2298.546	0.6692	5.496	0.125	0.46
0.03	200909	16976.405	18.75	5517.98	22.572	3545.57	0.6425	7.357	0.15	0.709
0.035	258112	28827.775	23.373	8024.948	31.975	5022.606	0.62587	9.171	0.175	1.0045
0.04	301411	47107.351	25.923	10172.146	39.069	6136.991	0.6033	10.172	0.2	1.227

4.4. Performance of PAT Predicted Based on Pump Performance

As it is said before in **Section 2.2.7**, the turbine mode performance of a PAT can be predicted on the basis of pump mode data by using the Best Efficiency Point (BEP) of the pump. In doing so, these section will focus on determining the PAT performance using BEP of pump and comparing these predicted results with the result obtained from the CFD simulation .In order to predict the turbine mode performance, the performance parameters of a PAT operating in pump mode should be taken under considered. The well-known affinity laws are used to establish relationships between the performance parameters of similar machines operating under similar kinematic conditions. Equation 2.14 and 2.15 are used to determine the head and flow rate at different operating speed of the pump respectively.

Table 4.3: Experimental and converted data of selected pump at 2960 and 1500 RPM

Experimental Data			**Converted data using Similarity Law**		
At 2960 RPM			At 1500 RPM		
Flow rate, Q (m^3/sec)	Head, H (m)	Efficiency η	Flow rate, Q (m^3/sec)	Head, H (m)	Efficiency η
0.005	54.1284	0.2000	0.0025	13.9003	0.2000
0.01	53.5160	0.3700	0.0051	13.7430	0.3700
0.015	52.4970	0.4844	0.0076	13.4814	0.4844
0.02	50.968	0.5700	0.0101	13.0887	0.5700
0.025	48.42	0.6100	0.0127	12.4344	0.6100
0.030	39.96	0.5000	0.0152	10.2618	0.5000

To determine the operating characteristic of a PAT at 1500 RPM, the pump performance characteristics operating at 2960 RPM should be converted to 1500 RPM. Table 4.3 shows the pump mode performance characteristics of a pump when it operates at 2960 and 1500 RPM.

The **red rectangle** marks the best efficiency point of pump when it operates at 2960 and 1500 RPM.

So at right hand side of Table 4.3, it can be seen that

$$\text{At Best Efficiency Point (BEP)} \left.\begin{array}{l} Q_p = 0.0127 \ \ m^3/s \\ H_p = 12.4344 \ \ m \end{array}\right\} \text{at 1500 RPM}$$

The next step is to estimate the PAT performance from the pump BEP when it operates in same angular velocity as the pump i.e. 1500 RPM. Correlations presented in **Section 2.2.7** were used to calculate the PAT operating flow rate and head at BEP. The estimated results with their respective researcher name are tabulated in Table 4.4.

Table 4.4: Flow rate and head results of PAT at BEP using prediction and CFD method

	Researchers		**PAT** Flow rate, Q_t (m^3/sec)	**PAT** Head H_t (m)
Using published prediction methods	Stephanoff [15]	**At Best Efficiency Point (BEP)**	0.0208	15.9206
	Child [15]		0.0208	20.3843
	Williams[17]		0.0189	22.5024
	Alatorre-Frenk[15]		0.0260	27.2212
	S.Derakhshan[10]		0.0195	21.8887
	Chapallaz [6]		min 0.0172	17.9055
			max 0.0200	21.8845
Using CFD			0.0250	14.01

From Table 4.4, it can be seen that, the head at BEP obtained using CFD is in good agreement with the result predicted using **Stephanoff [15]** method while the BEP head using **Alatorre-Frenk [15]** method has estimated higher value from the CFD.On the other hand, the **Stephanoff [15]** method shows better result for flow rate at BEP while the **Williams [17]** method shows the least accurate result compared to numerical method.

4.5. Effect of Speed on PAT Performance

The speed of a turbine varies according to the load put on it. At constant flow rate and head, if a load which is higher than design load put on a turbine, the turbine speed reduces. Also as the load put on a turbine decreases, (while keeping the head and flow rate the same), the speed of the turbine increases [17]. When it comes to PAT operating at a given site at constant flow rate, the same principle applies and plays an important role in determining the performance characteristics of a machine. In this thesis, the performance of pump when used as a turbine with variable PAT impeller speed has been considered for CFD analysis assuming nominal flow rate/ head data of Dabis hydro sites. The analysis is made without changing the original pump design parameters of the selected PAT. The result from the CFD simulations are tabulated in Table 4.5 and plotted with their respective RPM values. Finally using the plotted results, the performance characteristics of PAT is discussed.

Figure 4-21 shows the variation of torque with respect to the PAT speed while keeping the flow rate at 0.025 m^3/s flow rate and 17 m head. It can be seen from the figure that, as the speed of the turbine increases, the torque supplied by PAT decreases. This is a clear indication that the two parameters are inversely related. As the load on the PAT is further reduced, the speed of the PAT reaches a maximum value that no torque can be delivered by the PAT. This speed is called ***runaway speed***. The runaway speed of the PAT is obtained to be approximately 2780 RPM (291.15 rad/s) and is indicated and labeled in Figure 4-21.

While Figure 4-22 shows the relationship between speed and brake power. It can be observed that as the speed of the PAT increases, the power output increases until it reaches 1400 RPM (146.61 rad/s).Beyond this speed value, the power output gradually decreases.

Finally, the variation of efficiency with PAT speed is shown in Figure 4-23.It is indicated in the figure that the PAT efficiency increases as the rotational speed of the impeller increases until it reaches 1400 RPM. But operating the PAT beyond 1400 RPM will cause the efficiency of the PAT to drop. These kind of operating characteristic turbines are mainly observed since the overall effect of reduction in torque offsets the increase in turbine speed. And when comparing Figure 4-22 with 4-23, the efficiency acts in the same manner as the power output of the PAT. Thus it can be concluded that best operating conditions of selected PAT can obtained when it operates at 1400 RPM.

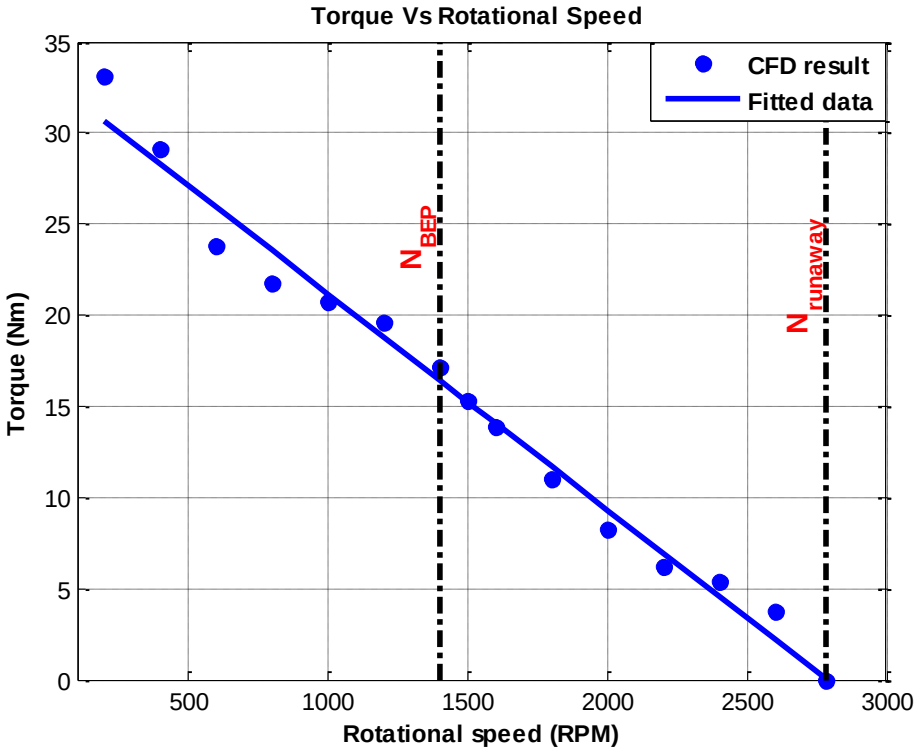

Figure 4-21: Torque vs. speed for selected PAT flow rate at Q_t = 0.025 m^3/s and H_t = 17 m

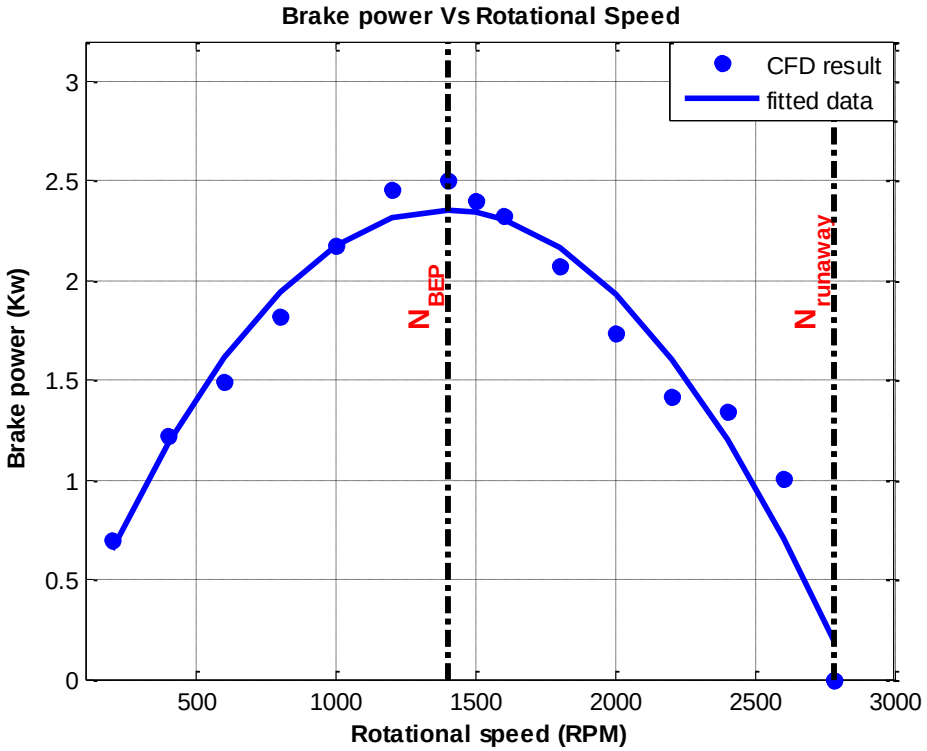

Figure 4-22: Brake power vs. speed for selected PAT at Q_t = 0.025 m^3/s and H_t = 17 m

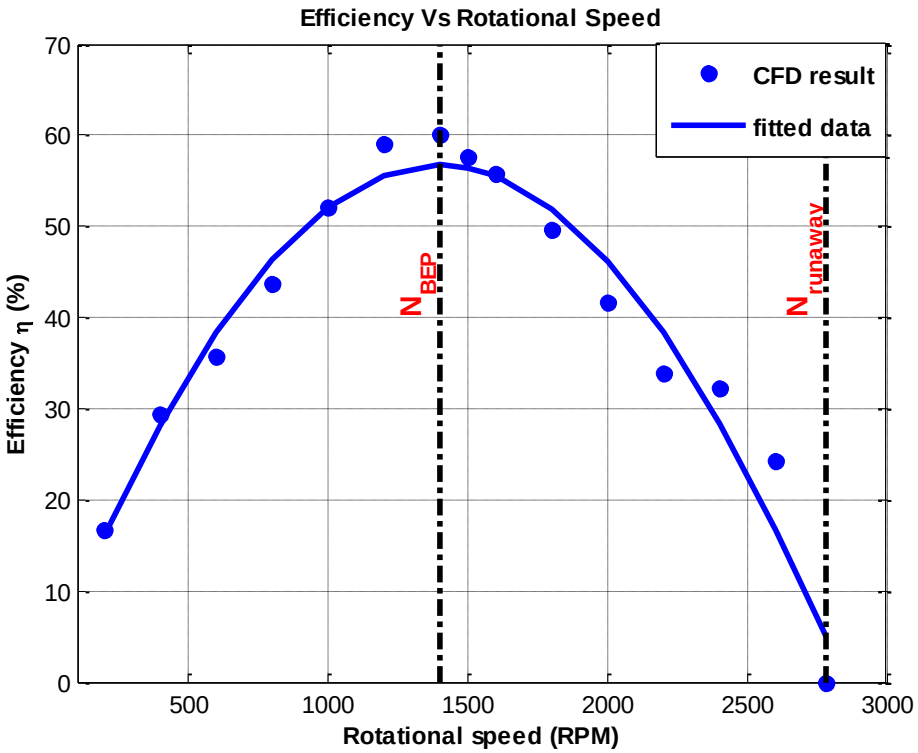

Figure 4-23: Efficiency vs. speed for selected PAT at Q_t = 0.025 m^3/s and H_t = 17 m

Table 4.5: Numerical output result of a pump in turbine mode for H_t = 17 m and Q_t =0.025 m^3/s

Rotational Speed N (RPM)	Angular velocity,(rad/s) $\omega = \frac{2\pi N}{60}$	Water Power, P_{hy}(W) $= \rho g H Q$	Torque (Nm)	Brake Power, P_b(W) $T \times \omega$	Efficiency **η**	Head coefficient **ψ**	Flow coefficient **ϕ**	Power coefficient **π**
200	20.944	4169.25	33.139	694.062	0.1665	375.233	0.9375	58.561
400	41.8879	4169.25	29.1641	1221.623	0.293	93.81	0.46875	12.884
600	62.8319	4169.25	23.7488	1492.18	0.3579	41.693	0.3125	4.663066
800	83.7758	4169.25	21.7388	1821.19	0.4368	23.452	0.234375	2.401
1000	104.72	4169.25	20.7691	2174.94	0.5217	15.009	0.1875	1.468
1200	125.664	4169.25	19.558	2457.73	0.5895	10.423	0.15625	0.96
1400	146.608	4169.25	17.101	2507.138	0.6013	7.658	0.1339286	0.617
1500	157.08	4169.25	15.266	2397.978	0.5752	6.671	0.125	0.48
1600	167.552	4169.25	13.9	2328.967	0.5586	5.863	0.1171875	0.384
1800	188.496	4169.25	10.997	2072.89	0.4972	4.633	0.1041667	0.24
2000	209.44	4169.25	8.2731	1732.714	0.4156	3.752	0.09375	0.146
2200	230.383	4169.25	6.1461	1415.96	0.3396	3.10	0.0852273	0.0898
2400	251.327	4169.25	5.3493	1344.426	0.3225	2.606	0.078125	0.0656
2600	272.271	4169.25	3.70784	1009.539	0.2421	2.22	0.0721154	0.0388
2800	293.215	4169.25	-0.4045	-118.606	-0.0284	1.914	0.0669643	-0.00364

4.6. Effect of Impeller Trailing Edge Rounding on Performance of PAT

Pump impellers are usually machined at outer periphery causing the vane tips to have sharp edge. These sharp edges may cause vortices and separation of flow when pump are used in reverse as turbine resulting decrease in efficiency [6].

Trailing edge rounding is a geometric alteration on an impeller tip that is used to reduce the flow separation loss component at blade profiles. It involves rounding of the trimmed or sharp blade trailing edges at both front and rear tip of blade. Figure 4-26 shows modification of a PAT by rounding the impeller vane tips. On the blade edge profile, the rounding radius 'R' is taken to be equal to half the blade thickness and care is taken to ensure that the overall diameter D_1 is not altered [7].So in this thesis, the effect of impeller tip rounding has been analyzed numerically by using the radius of the tip to be half of the outer blade thickness. And the numerical results obtained from the simulation are plotted using dimensionless coefficients. These results compared with the original trimmed blade profile results. The numerical result for the round blade profile is tabulated in table 4.6.

To visualize the separation phenomena more clearly, 2D velocity vector plot on the mid impeller plane at Q = 0.04 m^3/s is used. In Figure 4-24, it can be seen that the existence of separation around the tip trimmed of impeller blade. This region presents low velocity as a result of recirculation of flow. And this leads to low efficiency value of the PAT .On the other hand, Figure 4-25 shows the flow of fluid is much smoother at the round trailing edge of the impeller blade which enhances the transfer of energy from the fluid to the blade improving the efficiency of PAT.

From Figure 4-27 up to 4-29 indicate the performance result of trimmed and round edge PAT impeller model. It is clearly seen in Figure 4-18 that torque line for the rounded tip PAT impeller model has considerably lowered in contrast to the trimmed tip on 0.02 m^3/s and the torque increase when the PAT operated at and above 0.025 m^3/s.

The power coefficient characteristics for the round and trimmed blade tips are shown in Figure 4-29.It can be observed that the power coefficient for both trimmed and round tip that indicates power number as well as power output the of the PAT acts in the similar manner as the torque due the relationship involved between each other.

Also from the Figure 4-28, it can be observed that the head number line for the rounded tip model has considerably lowered compared to that for the trimmed blade tip. The reduction of head numbers is almost constant in the over-load region but the effect is magnified below the BEP in the part-load region.

Therefore the overall effect of reduction of head number and torque indicate that, the efficiency of the round tip impeller of PAT has increased from range of 1.6% at BEP up to 2.44 % in the overload region compared to trimmed tip impeller.

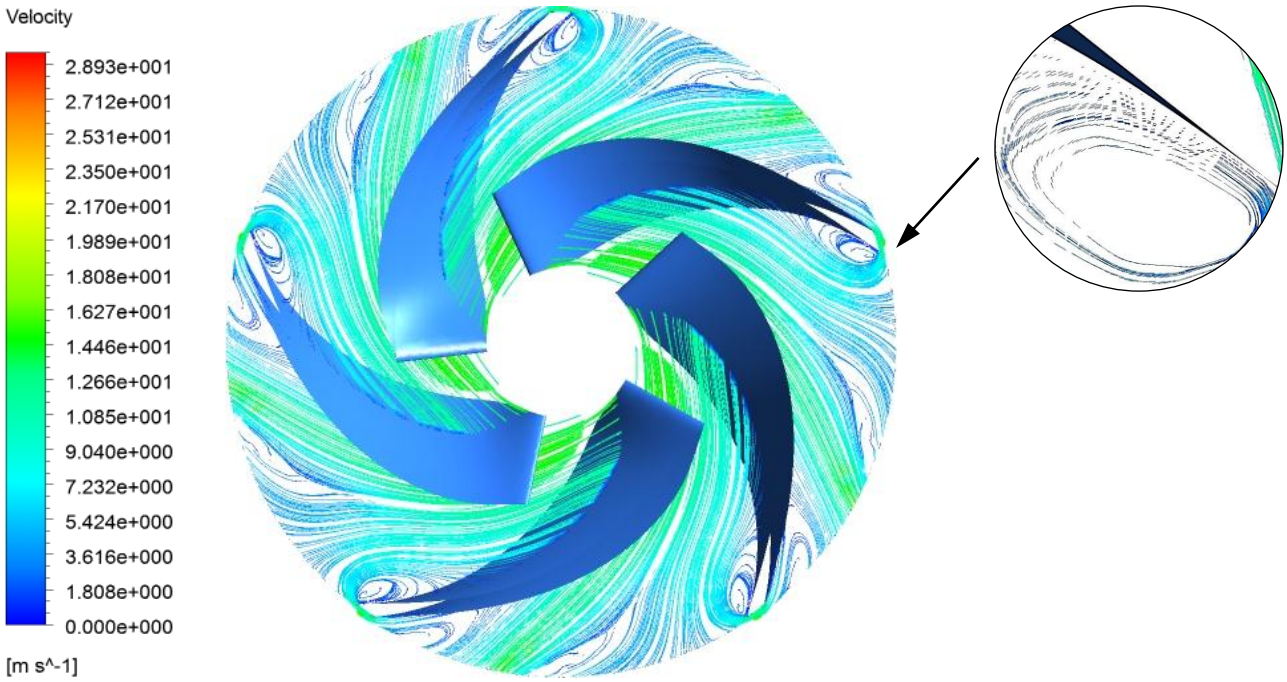

Figure 4-24: Relative velocity vector plot for trimmed tip impeller model at Q = 0.04 m^3/s

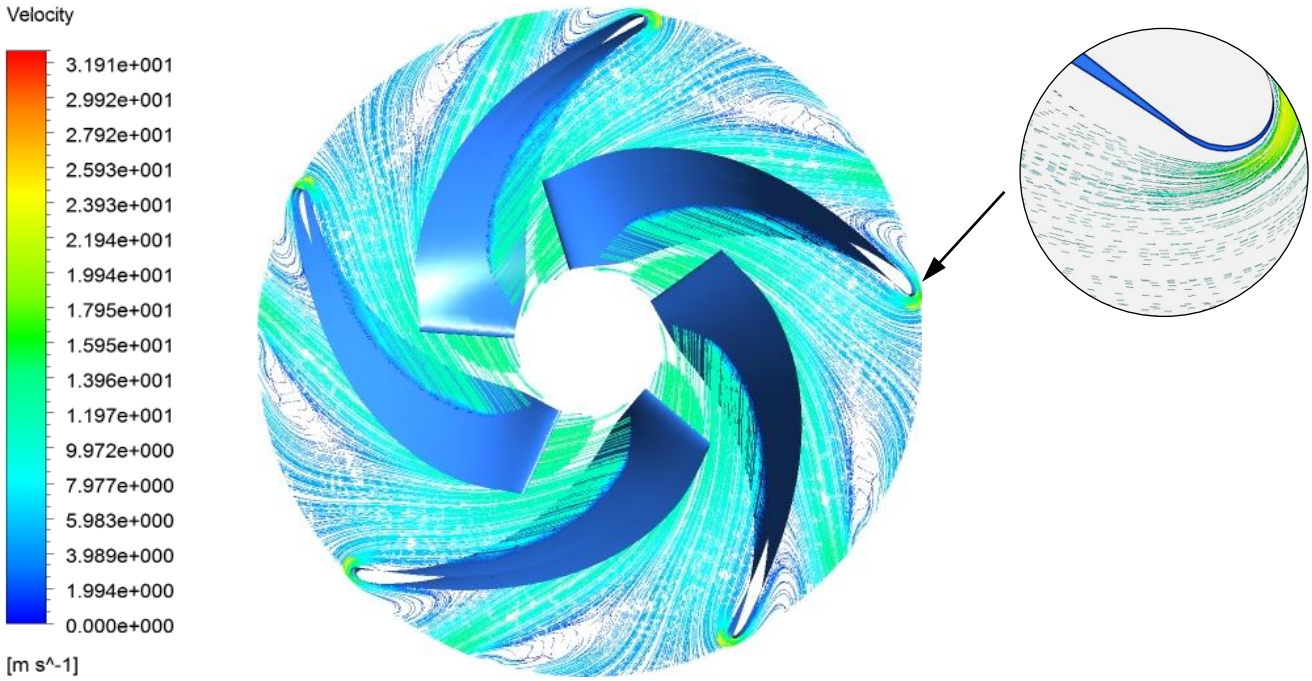

Figure 4-25: Relative velocity vector plot color for round tip impeller model at Q = 0.04 m^3/s

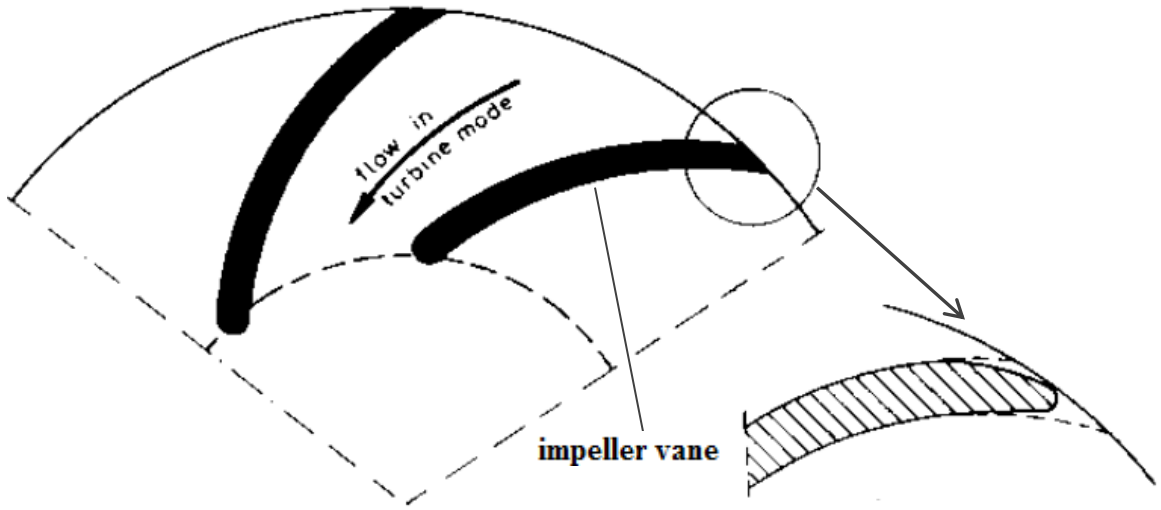

Figure 4-26: Details of under filled blade tip [6]

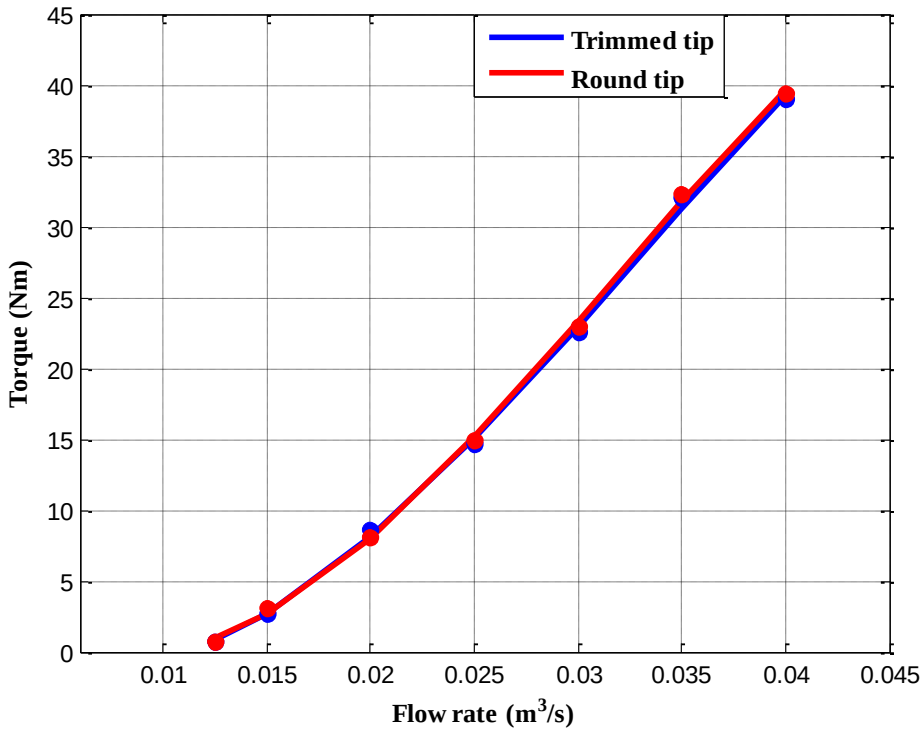

Figure 4-27: Variation of torque with flow rate of selected PAT with trimmed and round impeller tip

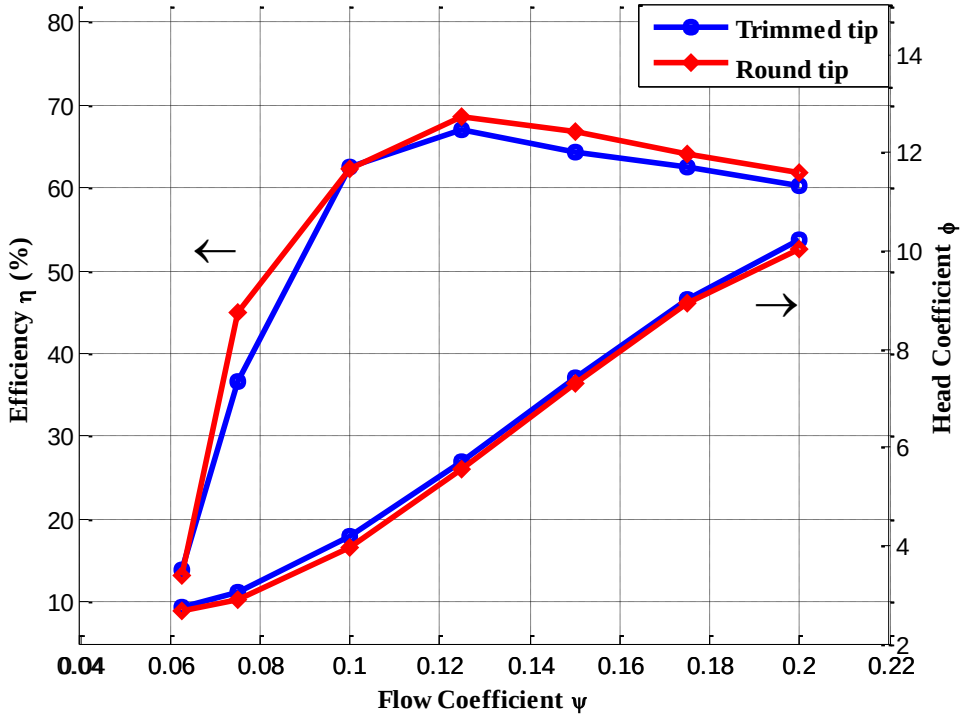

Figure 4-28: Variation of efficiency and head coefficient with flow coefficient of selected PAT with trimmed and round impeller tip

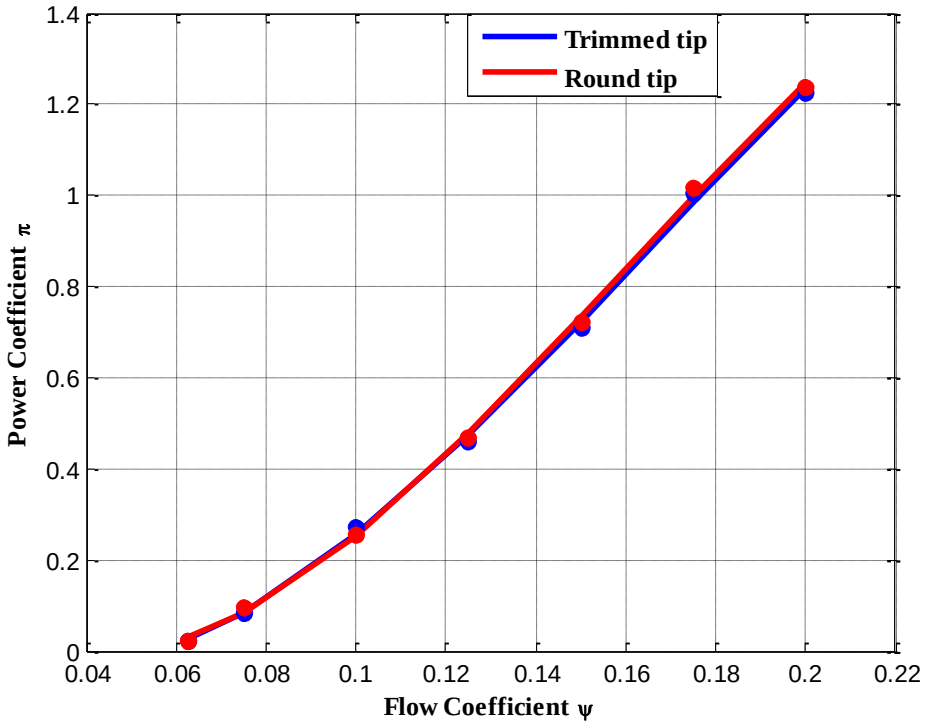

Figure 4-29: Power coefficient vs. flow coefficient characteristics of selected PAT with trimmed and round impeller tip

Table 4.6: Numerical output result of turbine mode performance of selected pump with round tip impeller

Flow rate, Q (m^3/sec)	Total pressure at Inlet, TP_{in} (pa)	Total pressure at Outlet, TP_{out} (pa)	Head (m) H $\frac{TP_{in} - TP_{out}}{\rho g}$	Water Power, P_{hy}(W) $= \rho gHQ$	Torque (Nm)	Brake Power, P_b(W) $T \times \omega$	Efficiency **η**	Head Coefficient, **ψ**	Flow Coefficient, **ϕ**	Power Coefficient **π**
0.0125	77150.5	11126.355	6.73029	825.301811	0.6889	108.21216	0.1311	2.641	0.0625	0.02164
0.015	85074.1	12798.631	7.36753	1084.13204	3.09981	486.91702	0.4491	2.891	0.075	0.0974
0.02	112422	10272.432	10.4128	2042.99136	8.09419	1271.4324	0.6223	4.086	0.1	0.2543
0.025	155068	18295.999	13.9421	3419.30003	14.9373	2346.3456	0.6862	5.471	0.125	0.4693
0.03	196238	16057.73	18.367	5405.4081	22.95	3604.9776	0.6669	7.207	0.15	0.721
0.035	252700	25923.211	23.1169	7937.18762	32.3583	5082.8299	0.6403	9.071	0.175	1.0166
0.04	291563	41521.796	25.4884	10001.6482	39.4351	6194.451	0.6193	10.002	0.2	1.239

4.7. Effect of Draft Tube

The main idea of a draft tube is to convert kinetic energy of water leaving the impeller to static pressure. If water that leaves the rotating impeller is at a high velocity, it would imply that the flow had much kinetic energy. Thus using a draft tube in this situation can be helpful to recover the kinetic energy of the water the impeller. A way of decreasing the speed of a flow in a pipe is to increase the cross sectional area of the pipe. So in this thesis, the effect of draft tube on PAT performance is analyzed using total required exhaust head (TREH) on Figure D-4 and the results from the simulation are plotted using dimensionless coefficients at constant speed of 1500 RPM (157.08 rad/s). These results compared with PAT. The numerical result for the PAT with draft tube model is tabulated in Table 4.7.

In Figure 4-11, it is clearly indicated that as the flow rate increases, the velocity of water coming out of the impeller increase, thus the water will have more kinetic energy.

Figure 4-32 shows stream line of flow of the water through the PAT and draft tube at different flow rate colored by velocity. It can be observed from the figure that the fluid velocity is reduced as the fluid flows through the diffuser section of the draft tube regardless of the flow rate. Figure 4-33 shows stream line colored by static pressure distribution of PAT with draft tube at different flow rate. The static pressure of the fluid increases with the expense of the reduced kinetic energy of the fluid.

In Figure 4-32 and 4-33, the flow is seen to be entering smoothly from the casing passing through the impeller and there is swirl phenomena present at the outlet of the PAT at most of the flows. Acceleration at leading edge combined with the movement of the impeller, results in a swirl at the impeller eye. At Q = 0.020 m^3/s, the swirl in the draft tube is in the direction of PAT rotation.And the swirl tends to change direction oppoiste to PAT rotation at higher flows at Q = 0.040 m^3/s. Despite the existence of swirl in all cases, the flow tends to stabilizes as the fluid continues flowing through draft tube.

To show the effect of draft tube on PAT, the numerical values obtained from the result in table 4.7 are used to construct the plot in Figure 4-30 and 4-31. Figure 4-30 shows the variation of flow coefficient with head coefficient and efficiency at N = 1500 RPM as a result of including draft tube in PAT system. It can be clearly seen that, as the result of adding draft tube to the PAT system, the head and head coefficient increases independent of the flow rate. But increasing the head has reduced the overall system efficiency since the hydraulic power increased without changing the power output of the PAT. The power coefficient in Figure 4-31 shows that in both cases the dimension-less number is almost the same for varying flow rate.

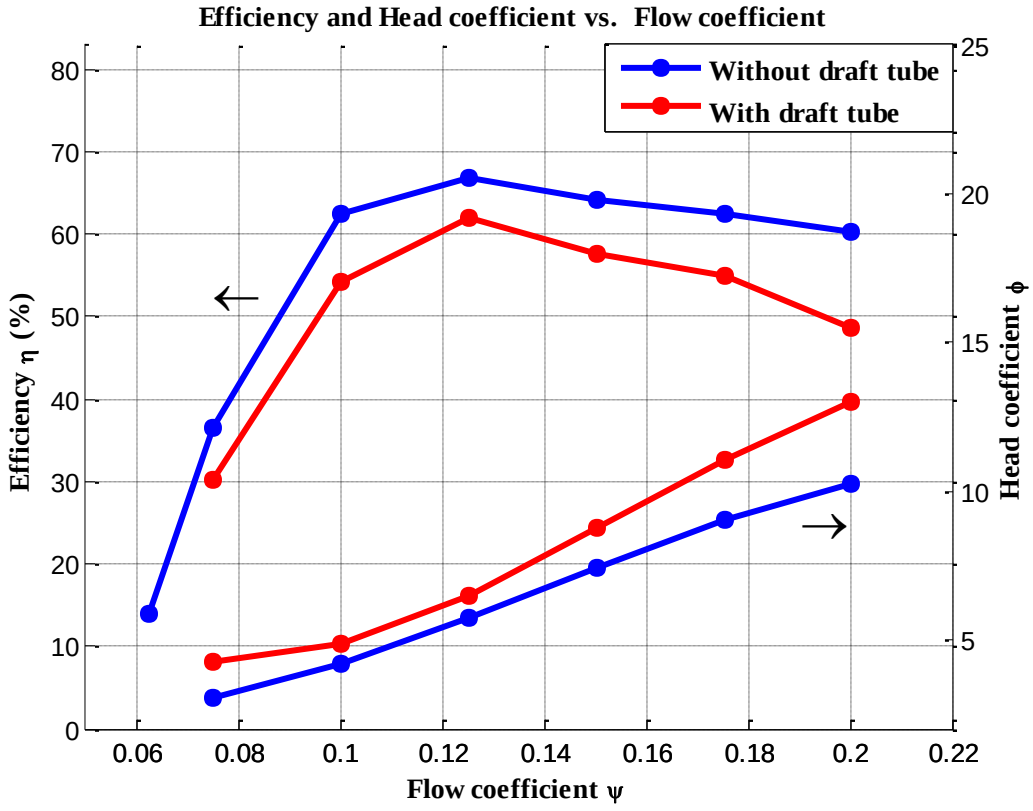

Figure 4-30: Comparsion of efficiency and head coefficient vs. flow coefficient for selected PAT with and without draft tube

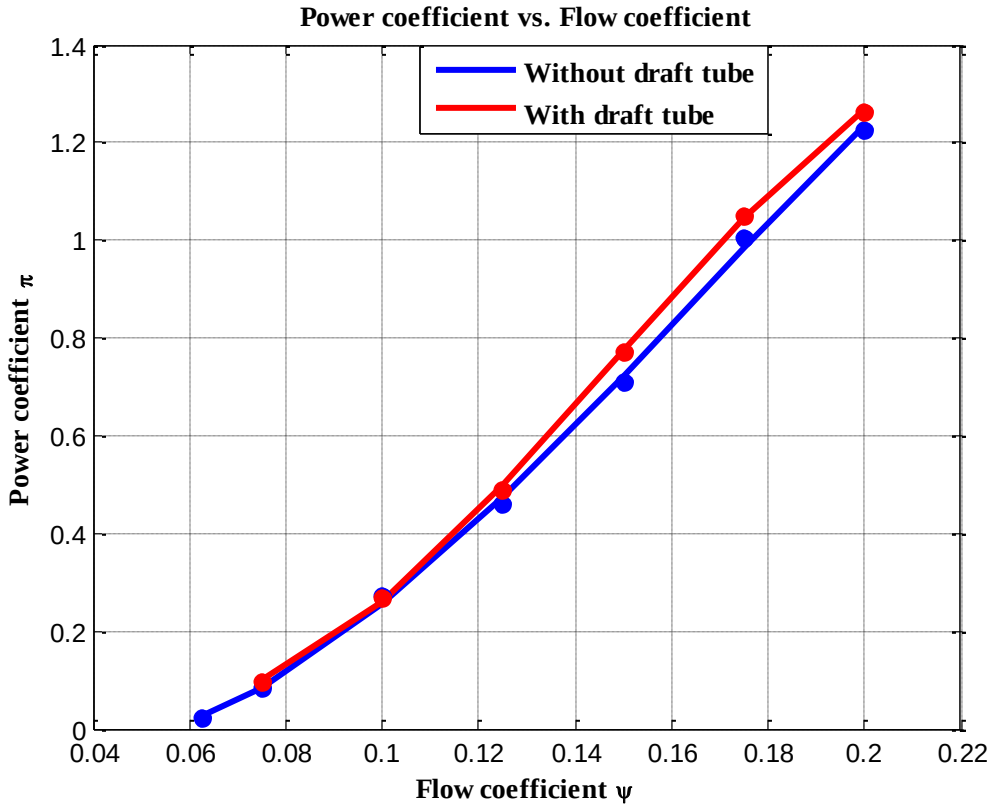

Figure 4-31: Power vs. flow coefficient for selected PAT with and without draft tube

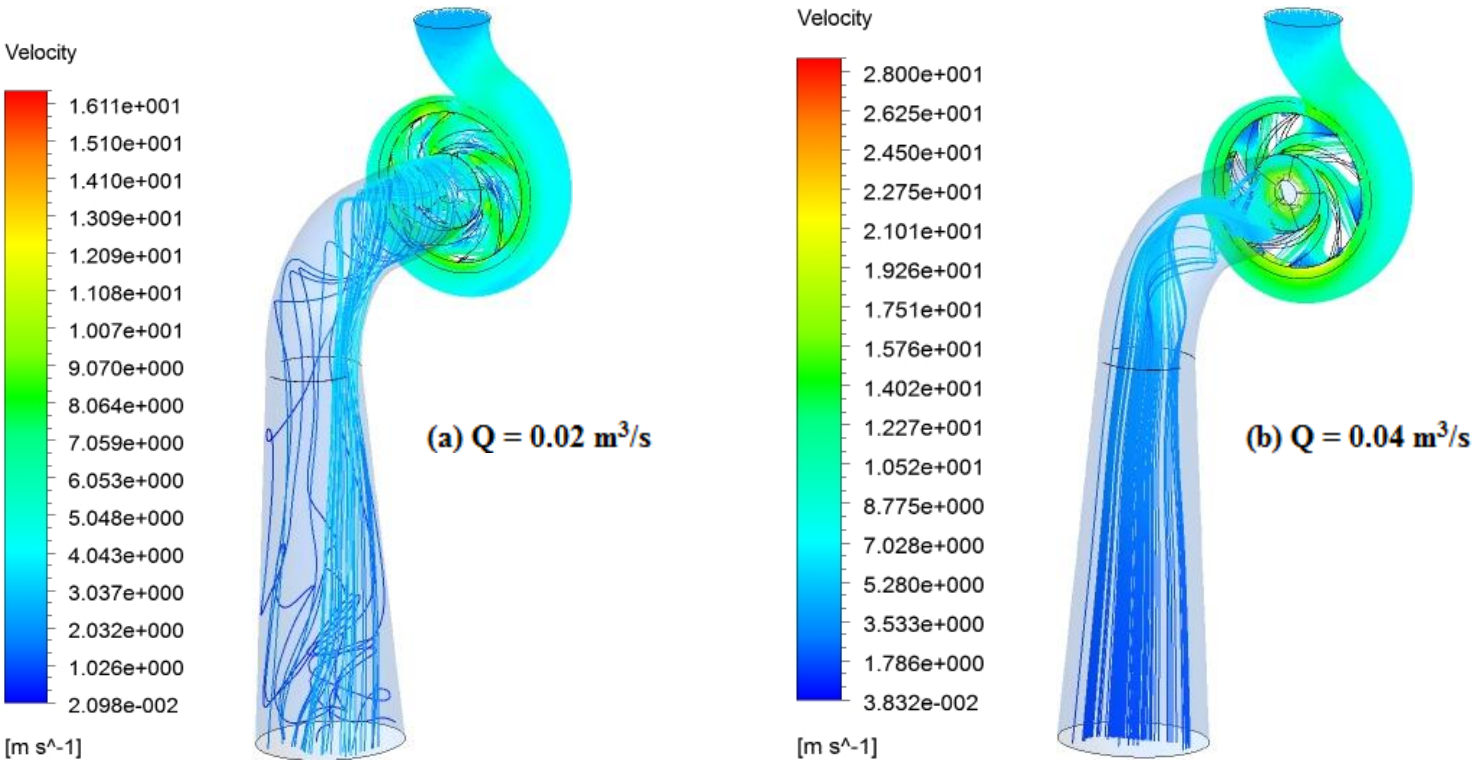

Figure 4-32: 3D streamline colored by relative velocity distribution of PAT with a draft tube model at different flow rate at N_t = 1500 RPM

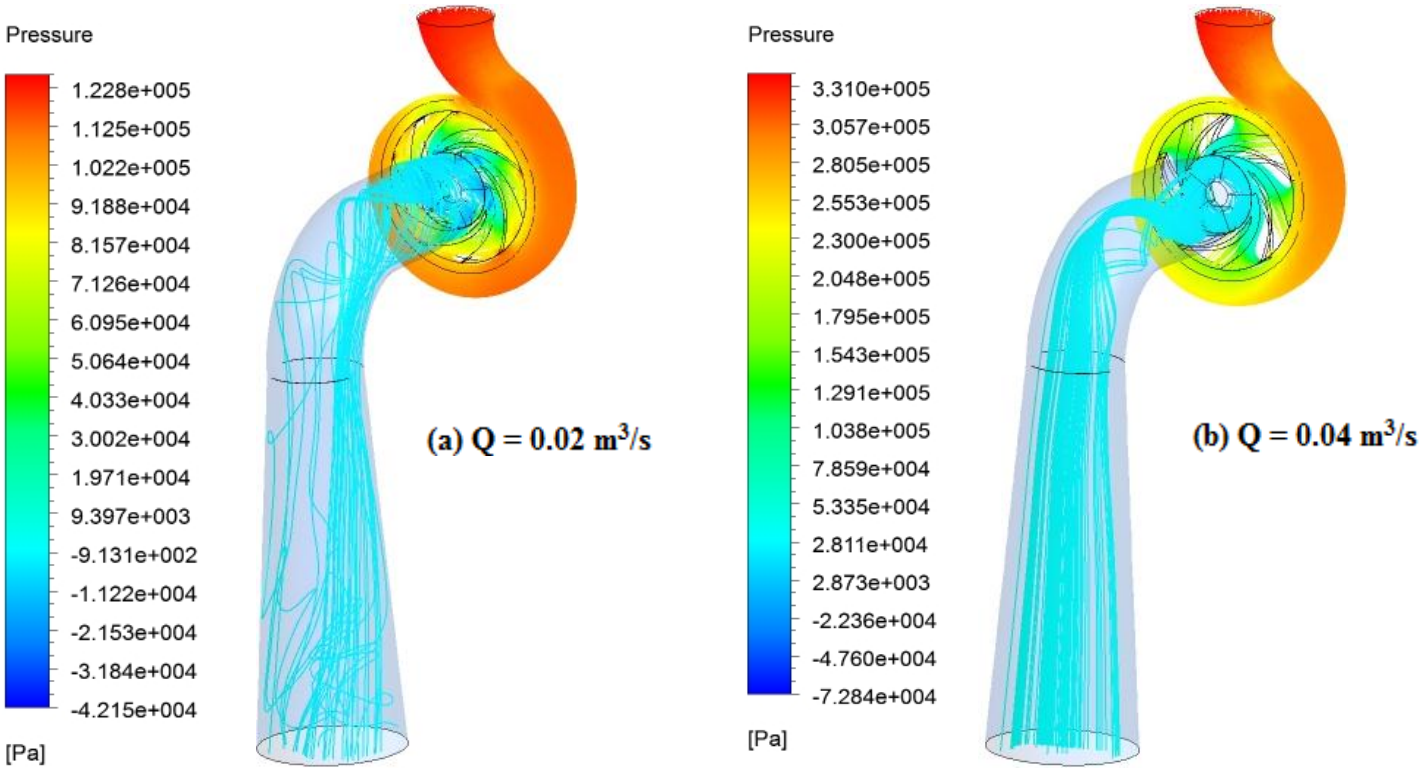

Figure 4-33: 3D streamline colored by static pressure (gauge) distribution of PAT with a draft tube model at different flow rate at N_t = 1500 RPM

Table 4.7: Numerical output result of selected PAT with draft tube model

Flow rate, Q (m^3/sec)	Total pressure at Inlet, TP_{in} (pa)	Total pressure at Outlet, TP_{out} (pa)	Head (m) H $\frac{TP_{in} - TP_{out}}{\rho g}$	Water Power, P_{hy}(W) $= \rho gHQ$	Torque (Nm)	Brake Power, P_b(W) $T \times \omega$	Efficiency **η**	Head Coefficient, **ψ**	Flow Coefficient, **ϕ**	Power Coefficient **π**
0.015	107343	469.917	10.894	1603.096	3.083	484.324	0.3021	4.275	0.075	0.0967
0.02	125347	2246.215	12.549	2462.016	8.509	1336.581	0.5429	4.924	0.1	0.2673
0.025	170386	12382.216	16.106	3950.095	15.573	2446.233	0.6193	6.3202	0.125	0.4892
0.03	236670	12566.436	22.844	6723.107	24.62	3867.222	0.5752	8.9641	0.15	0.7734
0.035	289807	16748.593	27.835	9557.044	33.401	5246.538	0.5490	10.922	0.175	1.0493
0.04	345824	20783.384	33.134	13001.625	40.231	6319.424	0.4860	13.002	0.2	1.2639

CHAPTER FIVE

Conclusion and Recommendation

5.1. Conclusion

Performance analysis of PAT using CFD code Ansys CFX is made on a centrifugal pump. A 3D geometric model for the selected centrifugal pump is used to compute the steady state solution in turbine mode. The results are presented using different graphical displays of pressure and velocity distribution of the PAT model. Numerical results are also obtained from the simulation to evaluate the performance characteristics of various models under consideration.

To check the consistency of the selected centrifugal pump with the model, the first simulation is made considering the original pump running in normal operating mode. The numerical result of the simulation in direct operating pump mode shows a good agreement with the experimental tested results. The turbine mode characteristic curves at angular velocity 1500 RPM are also prepared using the simulation result when the centrifugal pump operates in reverse mode. The PAT simulation results showed that when the PAT is made to operate from low to high head condition, the required flow rate at the site also increases. And the power output vs. flow rate characteristic curve of the PAT shows that when the PAT is installed at different hydro site with flow rate matching the available head based on the head – flow rate characteristic curve, the power output of the PAT increases. The maximum efficiency of the PAT is obtained when it operates at 0.025 m^3/sec flow rate and 14.01 m head. The head value at BEP, predicted by **Stephanoff [15]** method, has closer result with the CFD value.

The effect of round trailing edge is also simulated and compared with the original trimmed impeller tip. The results show that round trailing edge has caused lower head and higher efficiency value compared to the trimmed edge. PAT speed at constant head and flow rate is also considered to evaluate the effect on the PAT performance. The numerical result shows that as the impeller speed increases, both the power output and efficiency of the PAT increase until 1400 RPM. And the result also showed that the impeller torque decreases as the result of increasing the speed. Lastly, The effect of draft tube when added PAT is also analyzed and the result shows the draft tube causes the head to increase while the overall system efficiency get lower.

5.2. Recommendation

This research deals with numerical analysis of centrifugal pump when it operates in turbine mode. Graphical displays were used to view change of variables like pressure and velocity distribution as a result change of flow rate.

Keeping the original pump design with the exception of changing trailing edge, its effect is studied on the performance of PAT. Studies are also carried out to determine the effect draft tube and impeller speed on the operation of PAT. CFD being a reliable tool for investigating alternative design and operation of PAT, different performance parameters should be effectively examined and analyzed to ensure and obtain an efficient PATs performance characteristic.

For further evaluation and investigation of the performance of PATs using CFD, other researchers should focus on studying:

- The effect of blade thickness
- The effect of pump volute design
- Cavitation on PAT

Reference

[1]. "Water Sector Development Program", *Main Report*, vol. 1, 2002.

[2]. Dalelo A., "Rural Electrification in Ethiopia: Opportunities and Bottlenecks".

[3]. Meder K., "Application of Environment Assessment Related to GIZ ECO Micro Hydropower Plants in the Sidama Zone/Ethiopia", *MSc Thesis*, *Heidelberg University*, 2011.

[4]. "EEPCo Report", 2001.

[5]. Rama S. R. Gorla and Aijaz A. Khan, "Turbo Machinery Design and Theory", 2003.

[6]. Chapallaz J.M., Eichenberger P., Fischer G., "Manual on Pumps Used as Turbines",

Vieweg, Braunschweig, 1992.

[7]. Singh P., "Optimization of Internal Hydraulics and of System Design for Pumps as Turbines with Field Implementation and Evaluation", *Ph.D. Dissertation, University of Karlsruhe*, 2005.

[8]. Tilahun A., "Assessment of Micro Hydro Power Potential of Selected Ethiopian Rivers- A Case Study in the North-West Part of the Country", *MSc thesis, Addis Ababa Institute of Technology*, 2011.

[9]. Rawal S. & Kshirsagar J.T, "Numerical Simulation on a Pump Operating in a Turbine", *Proceedings of the Twenty – Third International Pump Users Symposium*, 2007, pp. 21-27.

[10]. Derakhshan S. & Nourbakhsh A., "Experimental Study of Characteristic Curves of centrifugal pumps working as turbines in different specific speeds", *Experimental Thermal and Fluid Science*, vol. 32, 2008, pp. 800–807.

[11]. Derakhshan S. & Nourbakhsh A., "Theoretical, Numerical and Experimental Investigation of Centrifugal Pumps in Reverse Operation", *Experimental Thermal and Fluid Science*, vol. 32, 2008, pp.1620 –1627.

[12]. Barrio R., Fernández J., Parrondo J. and Blanco E., "Performance Prediction of a Centrifugal Pump Working in Direct and Reverse Mode Using Computational Fluid Dynamics", *International Conference on Renewable Energies and Power Quality*, 2010.

[13]. Woo Oh H., "Applied Computational Fluid Dynamics", 2012.

[14]. "Reference Guide for Ansys CFX 14.5", 2012.

[15]. Claudio Alatorre-Frenk, "Cost Minimization in Micro-Hydro Systems Using Pumps as Turbines", *Ph.D. Dissertation, University of Warwick*, 1994.

[16]. Nautiya H., Varun, Kumar A. and Yadav S., "Experimental Investigation of Centrifugal Pump Working as Turbine for Small Hydropower Systems", *Energy Science and Technology*, vol. 1, no. 1, 2011, pp. 79-86.

[17]. Williams A., "Pumps as Turbine: A User's Guide", 1997.

[18]. Agarwal T., "Review of Pump as Turbine (PAT) for Micro-Hydropower", *International Journal of Emerging Technology and Advanced Engineering*, vol. 2, 2012, pp. 163-169.

[19]. "Laboratory Manual and Test Data", *Addis Ababa University, Mechanical Engineering Department*.

.

Appendix

A: Geometric modeling of PAT components

A.1.Impeller and Volute modeling using CFturbo

When the 3D impeller geometry is modeled, the main dimensions menu item is used to define main dimensions of the impeller. By clicking '**main dimension**' icon on toolbar, the main dimensions of the impeller like hub diameter, suction diameter, and impeller diameter are manually inserted in the box using the manual dimensioning mode. All these values are user-defined input values.

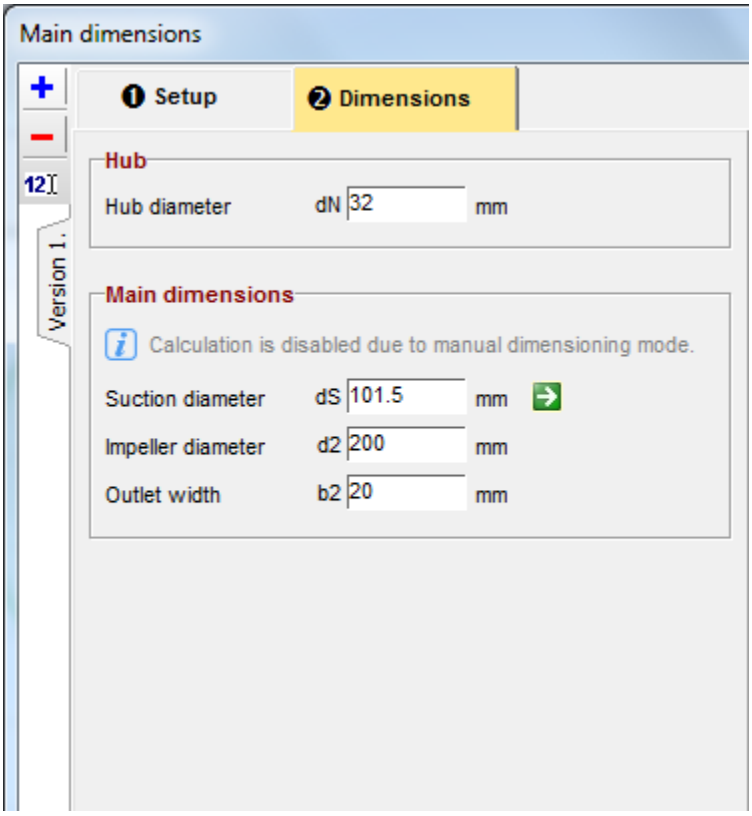

Figure A-1: Main dimension GUI in CFturbo

The meridional contour is the second important step to define the geometry of impeller. In this way the blade position between the hub and shroud can easily be created with a reasonable accuracy. In Meridional contour menu, Graphical elements can be manipulated by the computer

mouse per drag and drop .The final geometry of meridional of the meridional view looks like in Figure A-2. The trailing edge is fixed on meridional outlet.

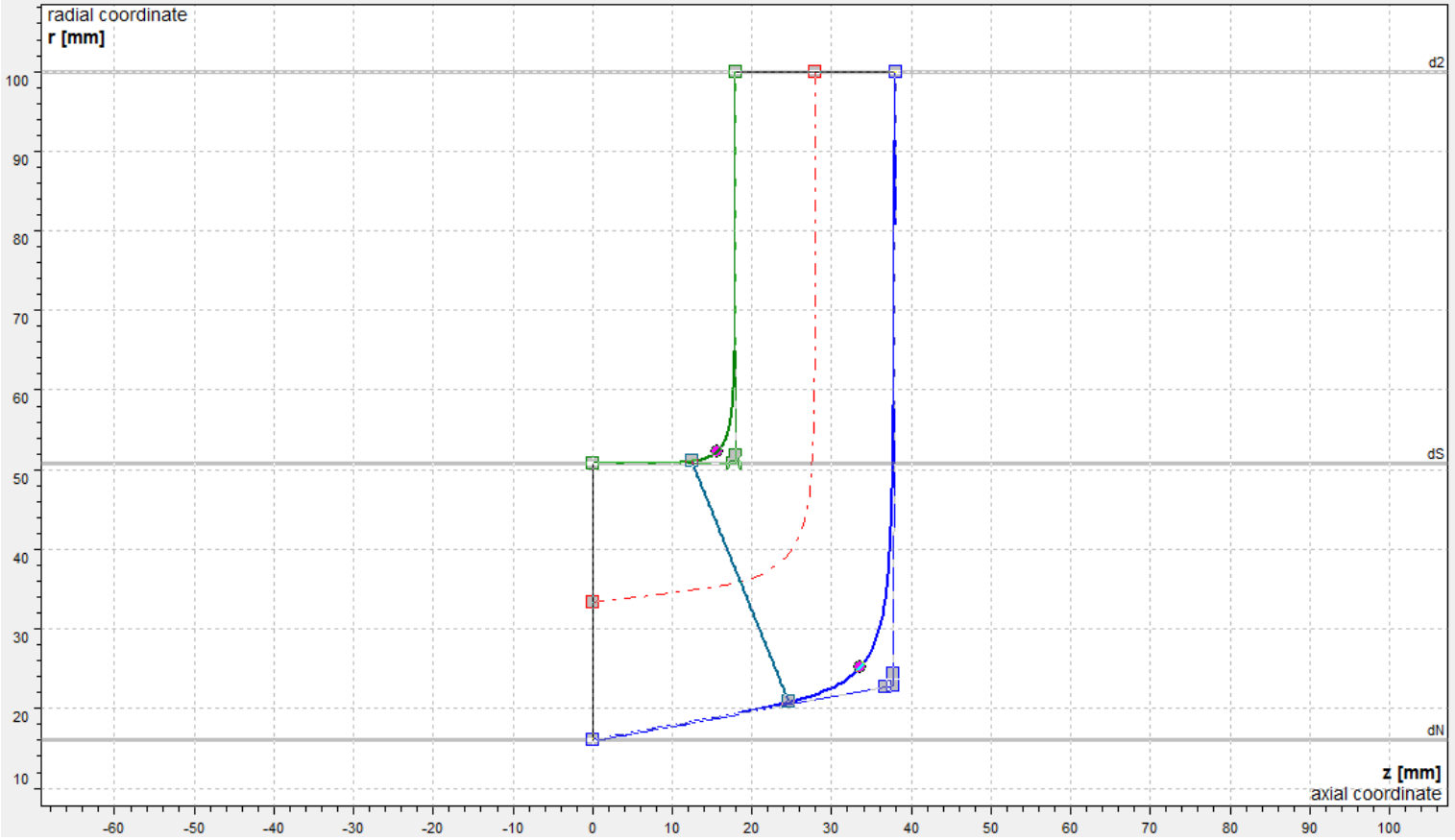

Figure A.2: Meridional view of the selected pump impeller

The next step is to define the blade thickness, blade angle and blade number using the '**blade property**' icon on the toolbar. Definition of blade properties is made in two steps; first the blade angle is defined in the '**blade angle**' tab while the blade number and blade thickness at the leading and trailing edge of the corresponding hub and shroud is defined in '**blade setup**' tab. Figure A-3 shows the dimensions set for the blade angles and blade thickness at the leading edge and trailing edge on the blade angel and blade setup tab respectively.

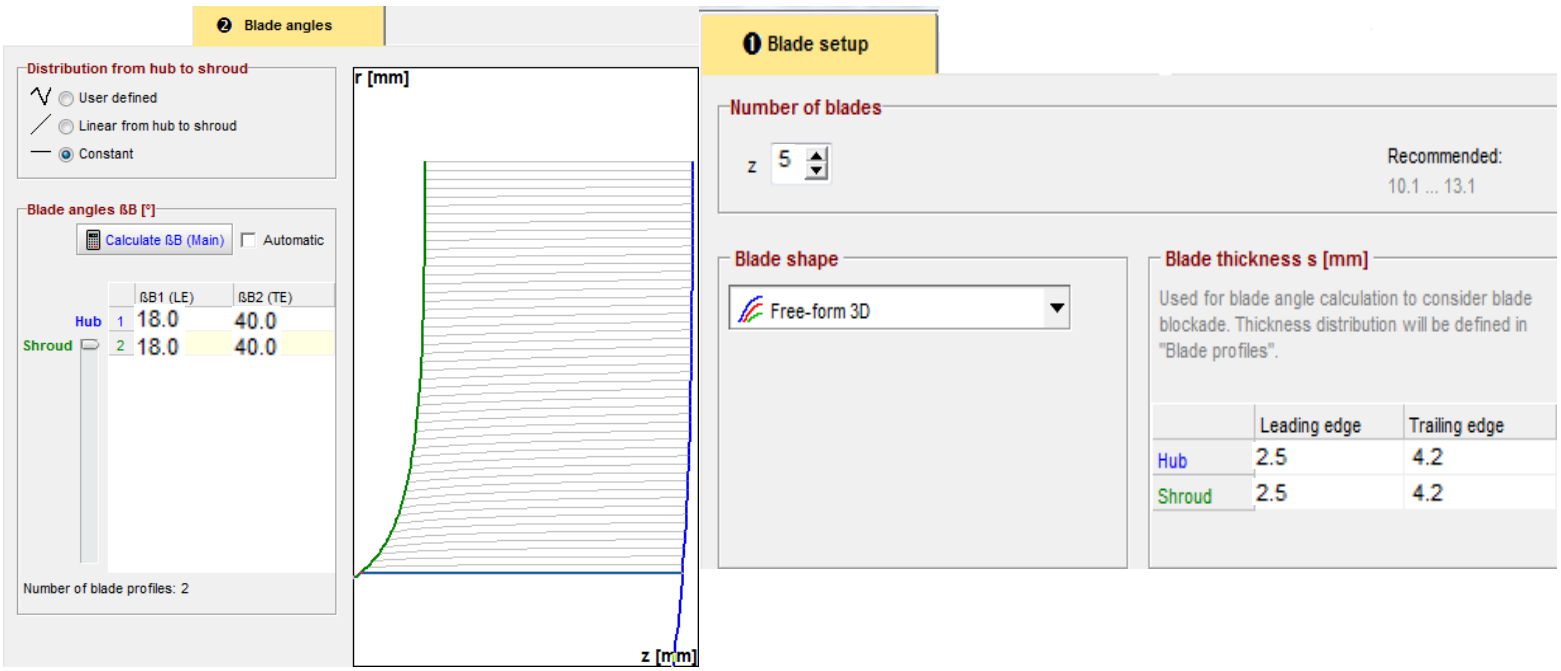

Figure A-3: Blade properties GUI in CFturbo

Then we proceed in defining the blade edge of the impeller at the leading and trailing edge. This is done by using the '**blade edge**' icon on the toolbar. The blade edge at the leading edge is created using elliptical element by specifying the ellipse axis ratio. Thus the leading edge is made into curved edge while trailing edge is provided with a trimmed or sharpened tip. The edge geometry at the leading edge is as described in Figure A-4.

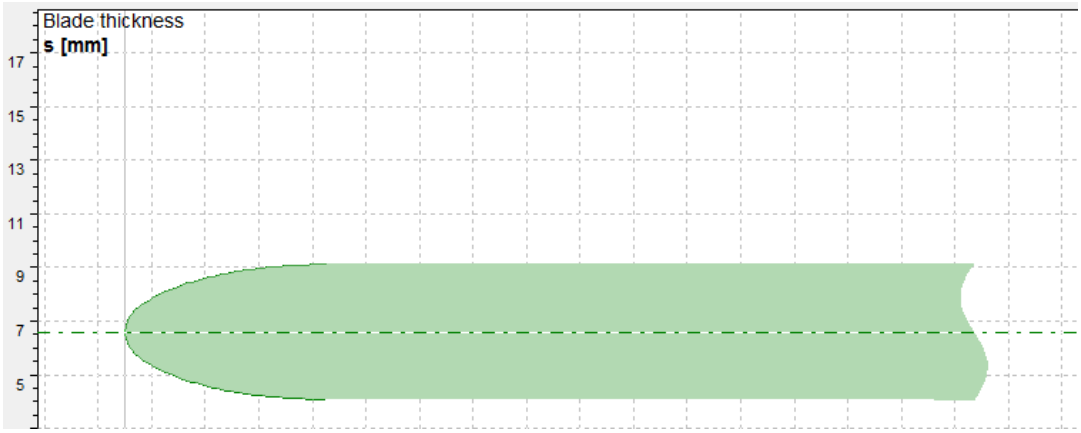

Figure A-4: Leading edge profile of impeller blade

Finally after all the necessary dimensions are fed, the complete geometry of the impeller is created. The final step is to add CFD setup extension to the Impeller. The extension defines the impeller-volute interface .The extension is added in meridional direction at the outlet. Figure A-5 represents the final modeled geometry and CFD fluid volume extracted from the impeller model.

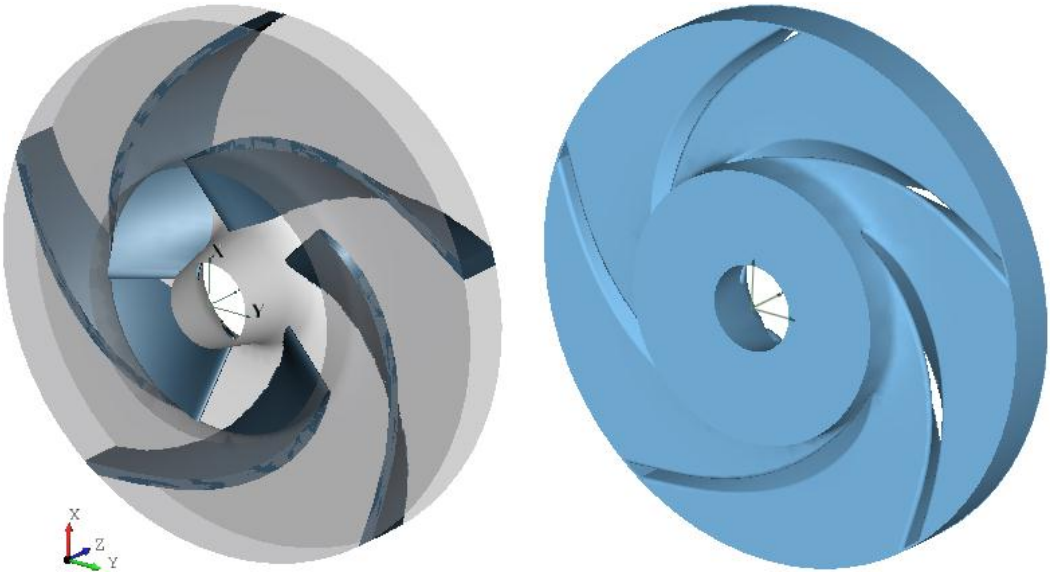

Figure A-5: 3D model of a centrifugal pump impeller and CFD fluid volume

The second component to be modeled is the volute casing. When the geometry of the volute is created, the cross section, spiral profile, cut water, and the diffuser should be provided to get the required geometry. By clicking '**Project**' tab on the main window menu and using '**add component**' button, the volute component is added

The first step to model the volute is to define the inlet side using the inlet definition icon. It consists of two steps: defining the details inlet interface is first specified on the '**Inlet' tab** page; this is done by manually putting the radial and z-axis coordinates of hub and shroud tips of the impeller. Defining the volute diameter and width of the spiral design is the second step is to be specified on the '**Volute**' tab; this is used to define the spiral inlet diameter and width. The GUI for the Inlet definition tab is show in Figure A-6.

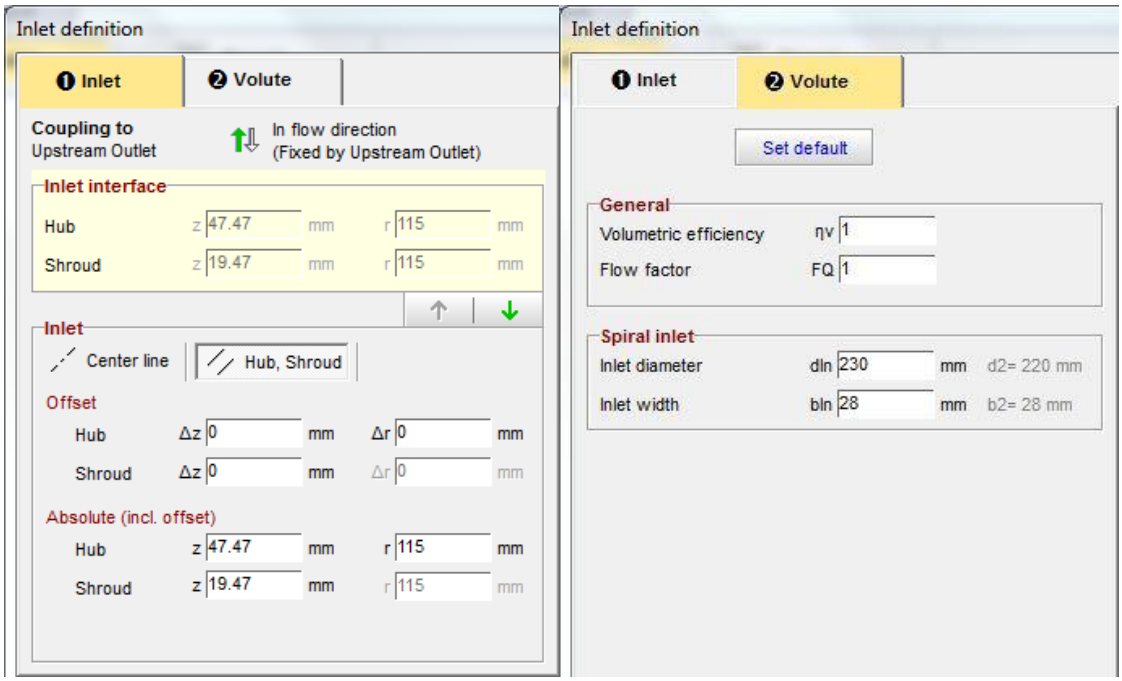

Figure A-6: Inlet and volute definition GUI of CF Turbo

Definition of the cross-section of the volute is the succeeding step in defining the volute. The shape of the cross-section can be selected using the '**cross-section'** icon on volute toolbar menu. The cross-section of the volute is made horseshoe shaped. Figure A-7 shows the cross-section of the volute casing. The shape of the horseshoe cross-section of the volute is created by selecting the '**Bezier - Trapezoid type'** from the cross-section type option at the right side. And under '**cone angle'** dialogue box, the opening angle of the horse shoe is set to 35^{o}.

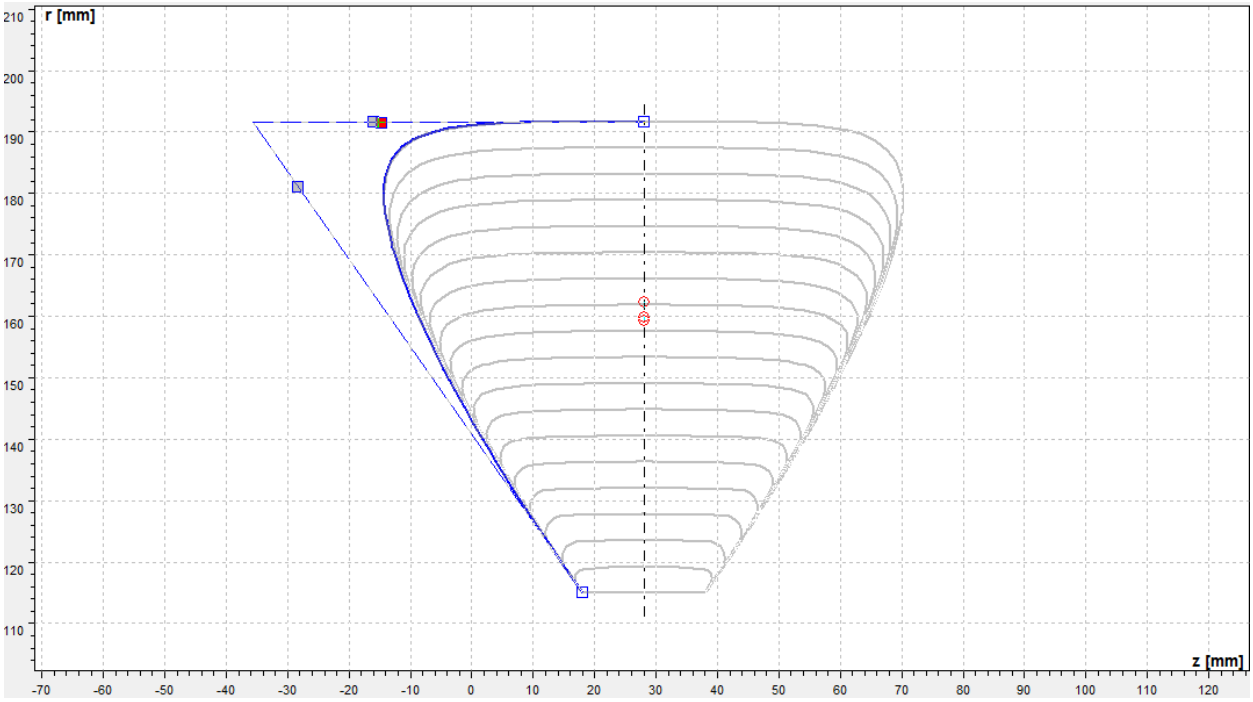

Figure A-7: Cross-section of the volute

The third step is to define the spiral profile of the volute. The '**spiral area'** icon is used to development spiral profile. In spiral development first the wrap angle is set in to 360°.The end cross- section of the spiral is defined by specifying the radius .Figure A-8 shows user defined values set within the dialogue box for the wrap angle and radius based end cross-section definition. Figure A-9 shows final spiral profile of the volute casing.

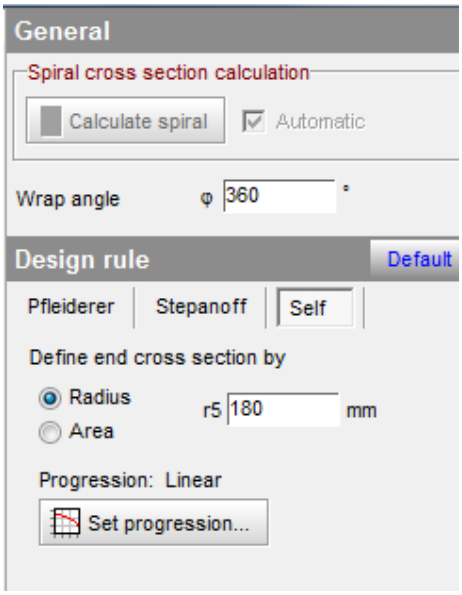

Figure A-8: Dialogue box to define wrap angle and spiral design

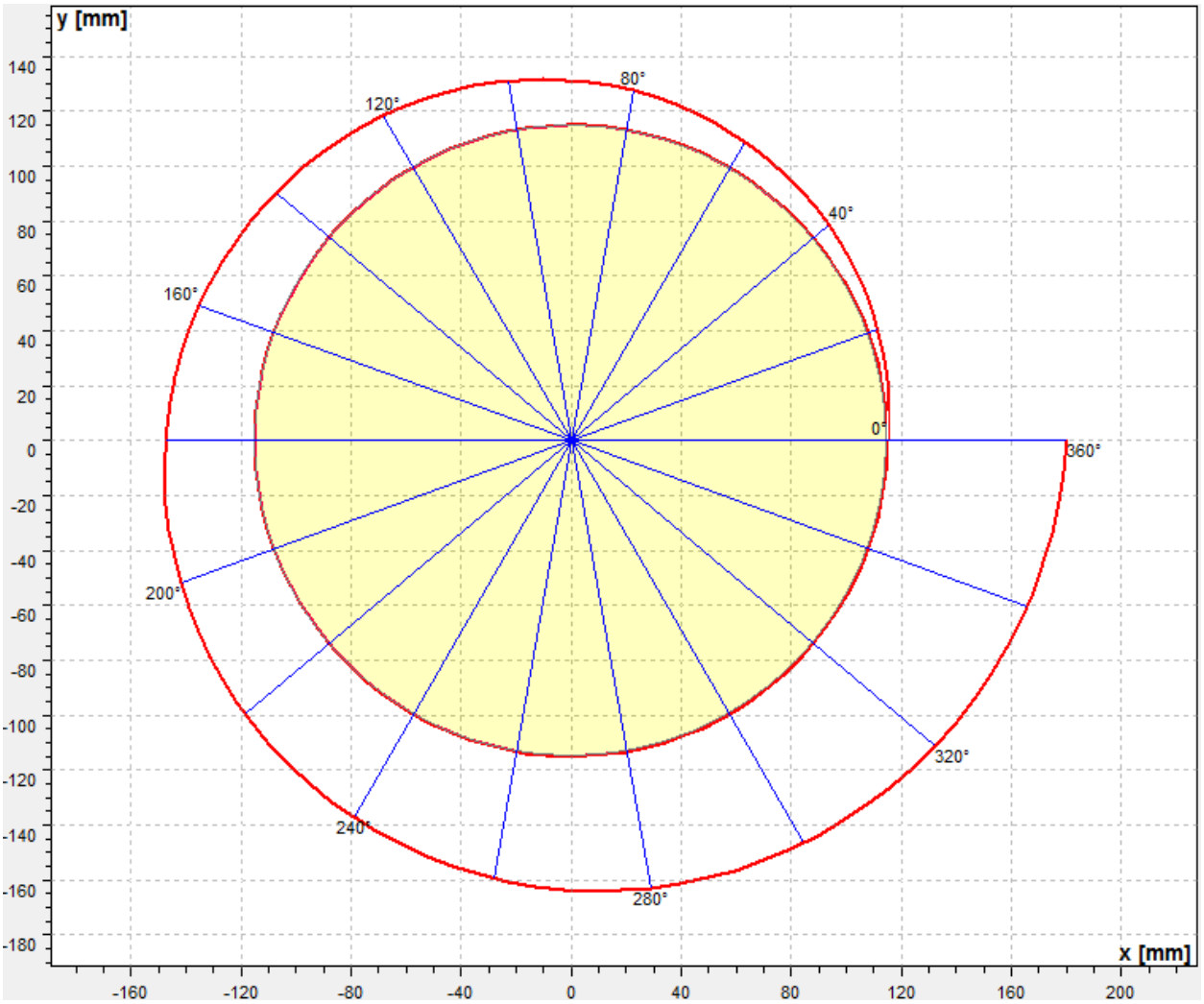

Figure A-9: Spiral profile of the volute

The fourth step is to model the diffuser of the pump using '**diffusor icon**' on the volute toolbar. The geometry of the outlet diffuser is made to extend radial direction. In the case of a radial diffuser, the angle between the outlet branch and the line connecting impeller-center and outlet branch center should be specified. The angle is made 90^{o} whereas the diameter of the diffuser is set to 180 mm from the center line of the pump and by making the diffuser outlet a circular cross section, diameter is set to 100 mm. The final step is to define the cut water by setting the fillet radius and the angular position .Figure A-10 shows the GUI used to insert the necessary dimension of the diffuser. The complete process of modeling of the volute ends when the fluid volume is extracted from the volute casing. Figure A-11 shows the fluid volume defined with the volute casing.

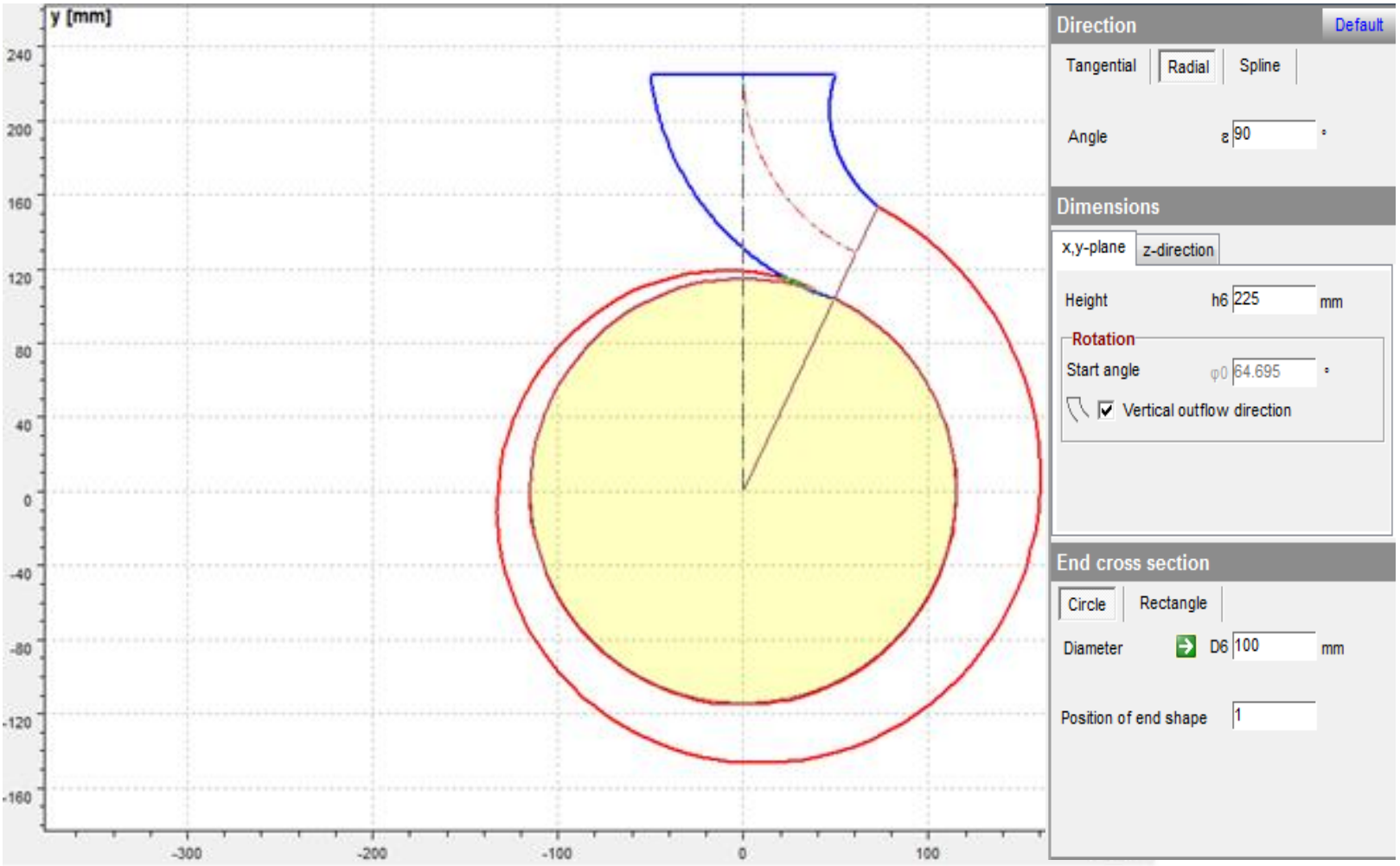

Figure A-10: GUI for defining pump diffuser

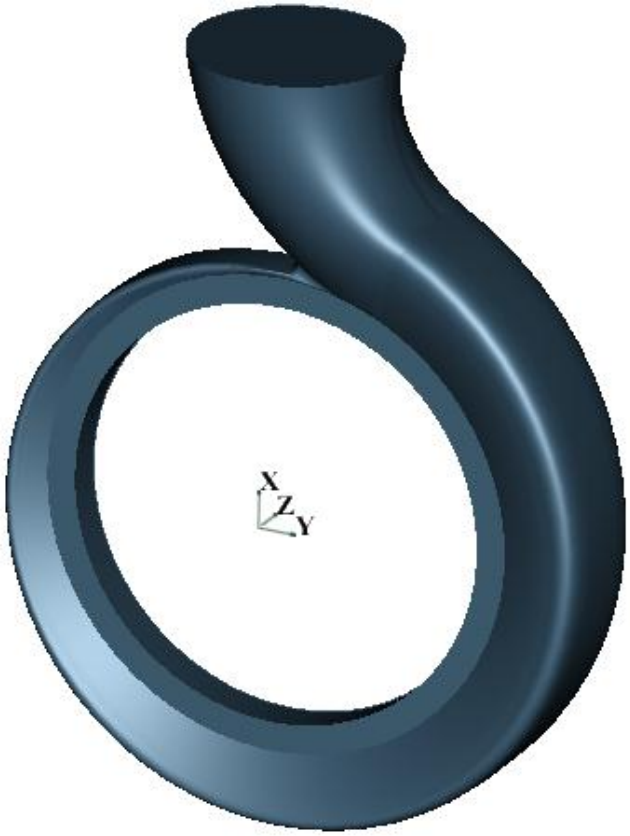

Figure A-11: Fluid volume of volute casing

A.2.Draft tube modeling using Catia

The geometry of the draft tube is defined using Catia. The first step is to define a circle with 125 mm diameter on XY plane and extrude the circle to 200 mm using the '**Pad**' icon on the right side toolbar.

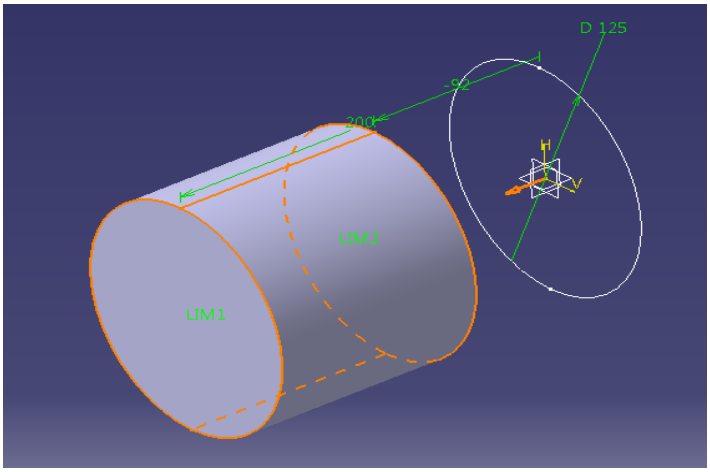

Figure A-12: Extruding operation

Then comes drawing another circle with the same diameter as the previous one by making the extruded end face as base plane. After that by selecting the ZX plane, drawing a quarter circle with diameter 300 with one end of the quarter circle coinciding the center line of the extruded circle.

This quarter circle is used as a guide so that the second circle can use this arc as path when rib operation is done. Using the '**Rib**' icon on the toolbar, the profile shown in Figure A-13 is made using the circle as a profile to make the rib and the quarter circle as a path.

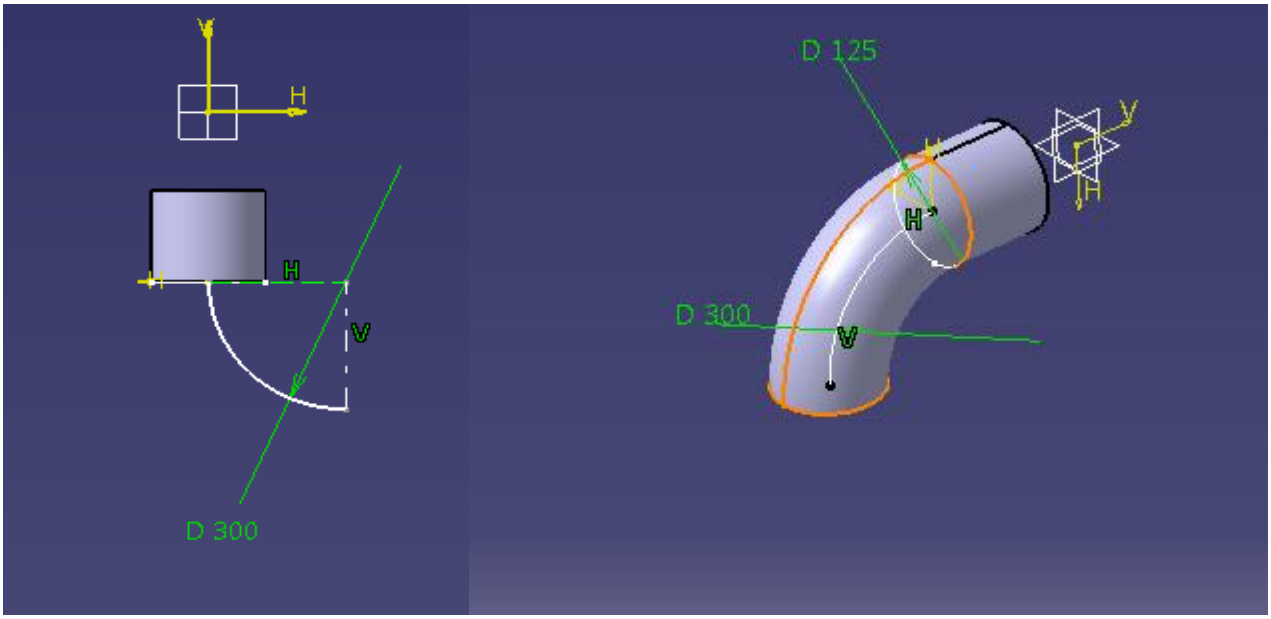

Figure A-13 : Rib operation for constructing elbow profile

Then a circle with diameter 125 mm is drawn for the third time at the end of the rib profile surface. Another circle with diameter 233 mm is drawn at the distance 500 mm apart from the end surface rib profile shown in Figure A-13. Then lastly, by using the '**multi section sections**' icon, the draft tube profile is made as shown in Figure A-14

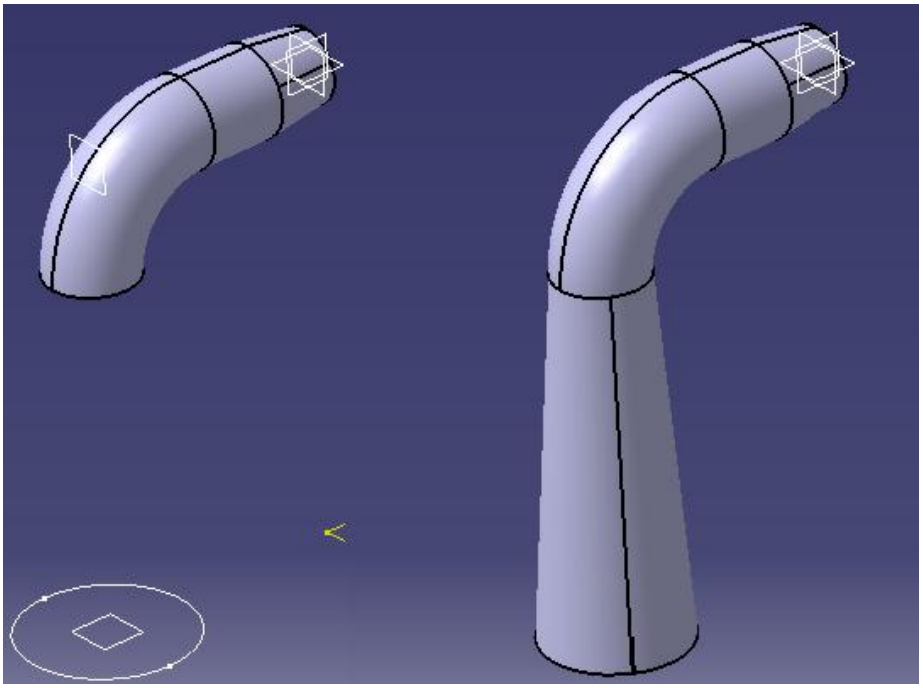

Figure A-14: Before and after multiple section solid operation respectively

C: Matlab Codes for selecting a pump to be used as turbine

C.1. Pump Selection Procedure proposed by Chapallaz [6]

```
clear all
clc
g=9.81;                     %Gravitational acceleration m/s^2
rho=1000;                   %Density of water in kg/m^3
Qnt=0.025;                  %Nominal turbine flow rate in m^3/s
Hnt=17;                     %Available site head in m
Nt=1500;                    %selected nominal PAT speed in RPM
%specific speed of PAT
nst=(Nt*(Qnt^0.5))/(Hnt^0.75);
%Pump mode specific speed
nsp=nst/0.89;
%%%%%%%%%%%%%%%%%%%%%%%%%%%%%%%%%%%%%%%%%%%%%%%%%%%%%%%%%%%%%%%%%%%%%%%%%%%%
%Efficiency determination
%knowing the pump mode flow rate and the pump mode specific speed, the
%efficiency can be determined from Figure D1
Qnp1=Qnt/1.3;               %Pump mode flow rate
Etap=0.73;                  %Maximum pump efficiency from Figure D3
%%%%%%%%%%%%%%%%%%%%%%%%%%%%%%%%%%%%%%%%%%%%%%%%%%%%%%%%%%%%%%%%%%%%%%%%%%%%
%Converting Turbine design condition to Pump design using specific speed and
%efficiency of pump
%The conversion factor for head and flow are obtained using Figure D2 and D3
%respectively
Ch=1.44;                     %Conversion factor for head using Figure D2
Cq=1.32;                     %Conversion factor for flow rate using D3

Hnp=Hnt/Ch;                  %Pump mode nominal head
Qnp=Qnt/Cq;                  %Pump mode nominal flow rate
%%%%%%%%%%%%%%%%%%%%%%%%%%%%%%%%%%%%%%%%%%%%%%%%%%%%%%%%%%%%%%%%%%%%%%%%%%%%
%Converting pump design condition at turbine nominal speed to pump nominal
%speed
Np=3000;                     %Selected pump rated speed in RPM
Hp=Hnp*((Np/Nt)^2);          %Nominal head at pump rated speed 3000 RPM
Qp=Qnp*(Np/Nt);              %Nominal flow at pump rated speed 3000 RPM
%%%%%%%%%%%%%%%%%%%%%%%%%%%%%%%%%%%%%%%%%%%%%%%%%%%%%%%%%%%%%%%%%%%%%%%%%%%%
fprintf('rated Flow rate of pump in (m^3/s) is %0.2f \n\n ',Qp)
fprintf('rated Head of the pump in (m) is %0.2f \n\n ',Hp)
%%%%%%%%%%%%%%%%%%%%%%%%%%%%%%%%%%%%%%%%%%%%%%%%%%%%%%%%%%%%%%%%%%%%%%%%%%%%
```

C.2. Procedure presented to choose a proper centrifugal PAT by Shahram Derakhshan and Ahmad Nourbakhsh [10].

```
clc
clear all
g=9.81;                              %Gravitational Acceleration in m/s^2
rho=1000;                            %Density of water in kg/m^3
Nt=1500;                             %Selected PAT speed in PRM

%%%%%%%%%%%%%%%%%%%%%%%%%%%%%%%%
Np=3000;                             %Selected Pump speed in RPM
%Site Information
H=17.0;                              %Available site head in m
Q=0.025;                             %Site flow rate in m^3/s
P=2.7;                               %Estimated power of site power in Kw
%%%%%%%%%%%%%%%%%%%%%%%%%%%%%%%%%%%%%%%%%%%%%%%%%%%%%%%%%%%%
%Step1: The pump specific speed in its rated point, Nsp can be calculated
%as
Nst=(Nt*(P^0.5))/(H^1.25);            %Turbine Specific speed in(Kw,m)
Nsp= 0.3705*Nst+ 5.083;               %Pump Specific speed in(m,m^3/s)
%step2
alphap=Nsp/(g^0.75);
%step3
zeta=0.0233*alphap+0.6464;
%step4
a=Nt/Np;
h=(zeta/a)^(-2);
Hp=H/h;                               %Pump Head in m
%step5
Qp=((Nsp*(Hp^0.75))/Np)^2 ;           %Pump flow rate in m^3/s

fprintf('Available site Head in (m) is %0.2f \n\n ',H)
fprintf('Estimated power output of Turbine in (Kw)is %0.2f \n\n ',P)
fprintf('Estimated PAT specific Speed in (Kw,m)is %0.2f \n\n ',Nst)
fprintf('Estimated pump specific Speed in (m,m^3/s)is %0.2f \n\n ',Nsp)
fprintf('Pump Head in (m)is %0.2f \n\n ',Hp)
fprintf('Pump Flow rate in (m^3/s) is %0.2f \n\n ',Qp)
```

D: Diagrams used for determining turbine mode performance [6]

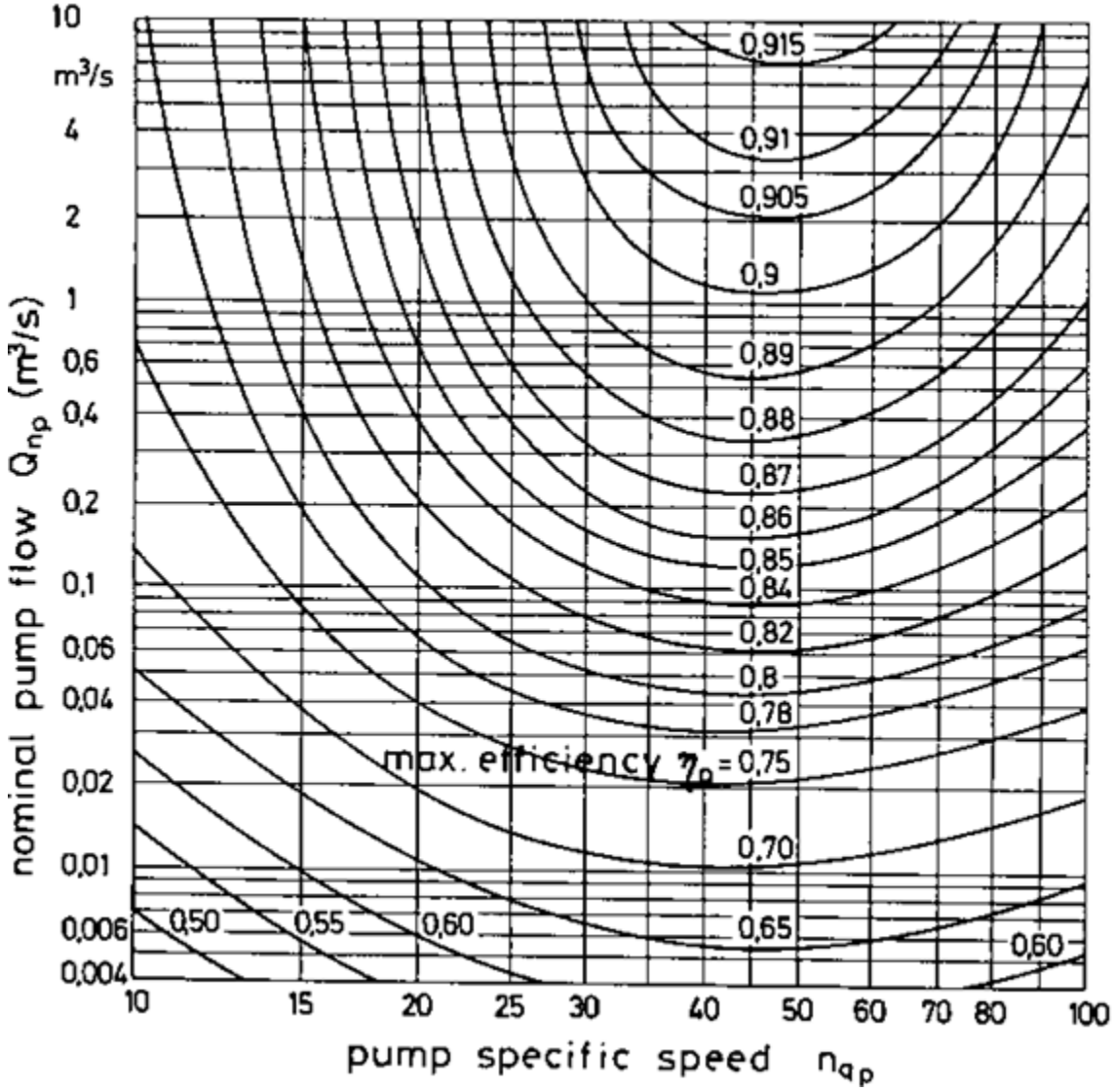

Figure D-1: Maximum pump efficiency as function of specific speed and flow

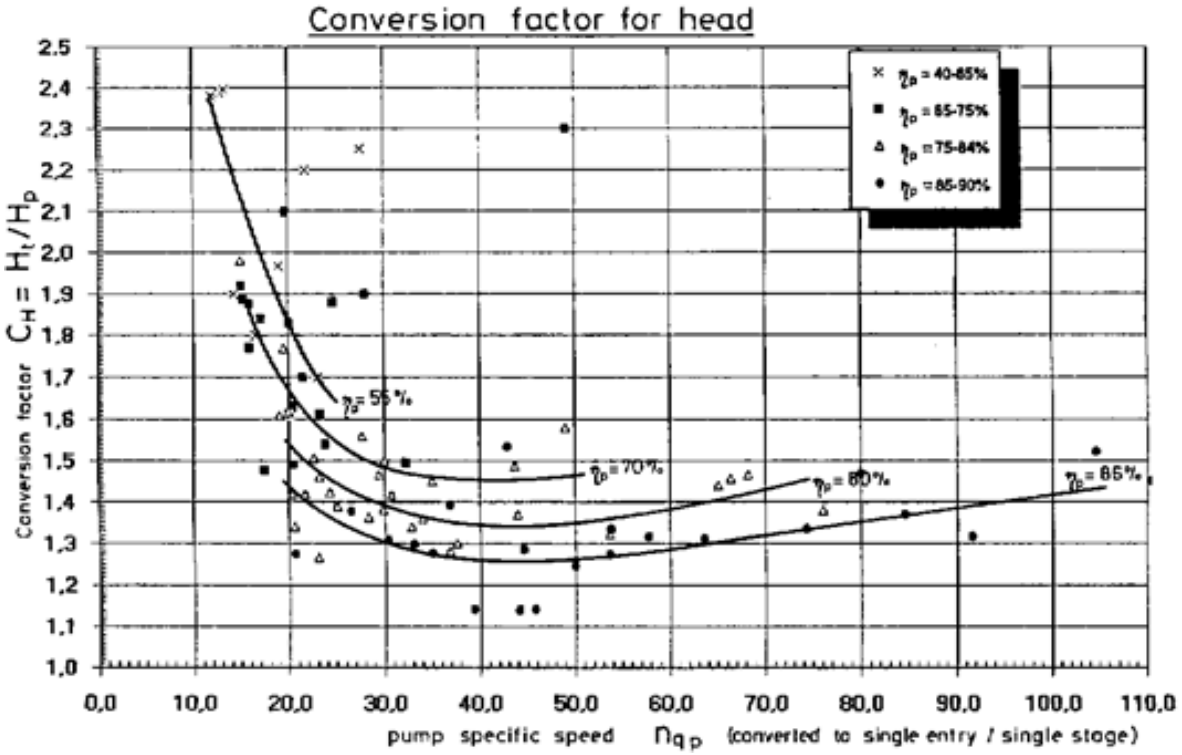

Figure D-2: Factors for the conversion of pump head into turbine design condition

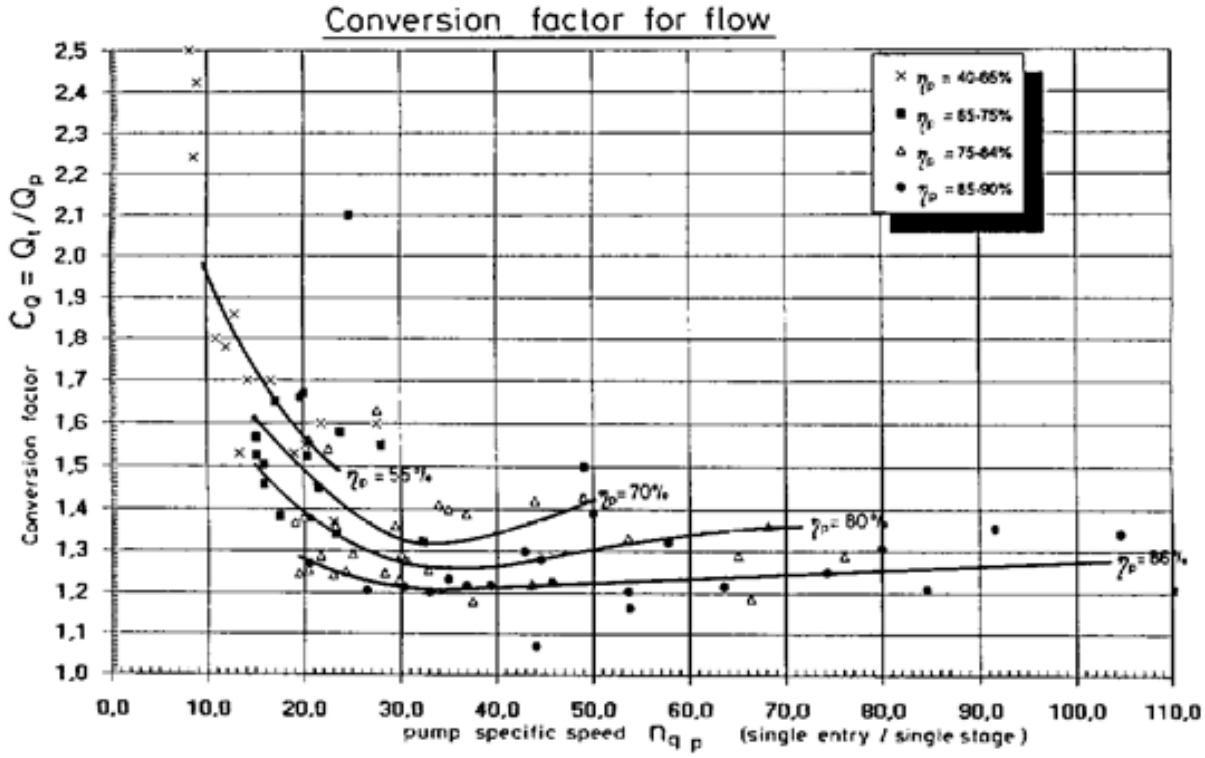

Figure D-3: Factors for the conversion of pump nominal flow rate into turbine design condition

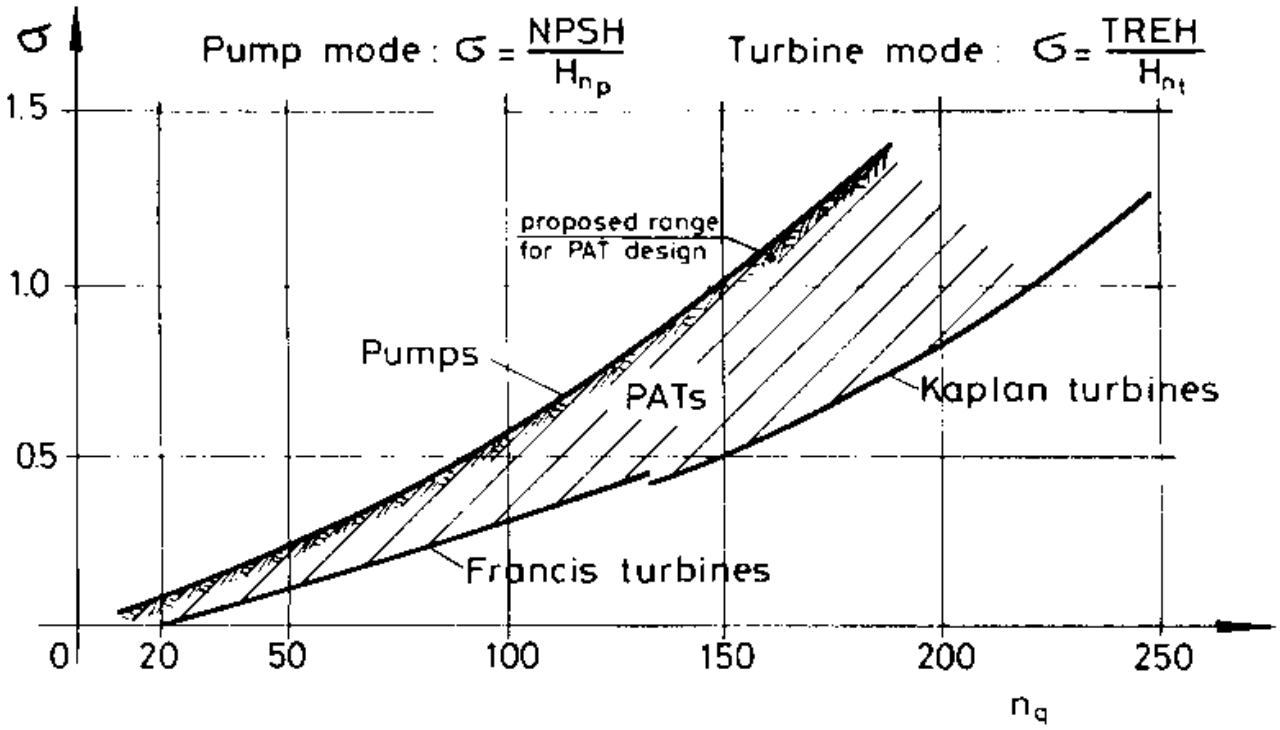

Figure D-4: Cavitation for pumps, turbines and PATs expressed by the Thoma number Sigma versus specific speed nq (only valid if operated at BEP) (source: R.K. Turton: Principles of Turbomachninery)

For selected pump with specific speed is 25.5, Thoma number, σ ranges from 0.1- 0.14

Selecting Thoma number, $\sigma = 0.12$

Total required exhaust head (TREH) is given as

$= \sigma * H_{nt}$

$= 0.12 * 14.01\ m$

TREH = 1.681 m